University of Oklahoma

Graduate College

Synthesis and Characterization of Stimuli-Responsive Polymers with Aqueous Atom Transfer Radical Polymerization

A Dissertation

Submitted to the Graduate Faculty

In Partial Fulfillment of the Requirements for the

Degree of

Doctor of Philosophy

in Chemical Engineering

By

Collin N. Britten

Norman, Oklahoma

2021

Synthesis and Characterization of Stimuli-Responsive Polymers with Aqueous Atom Transfer Radical Polymerization

A Dissertation Approved for the School of Chemical, Biological, and Materials Engineering

By the Committee Consisting of

Dr. Keisha B. Walters, Chair

Dr. Jeffrey H. Harwell

Dr. Lance Lobban

Dr. Edgar A. O'Rear III

Dr. Charles Rice

Name: Collin Britten

Date of Defense: September 23, 2021

Institution: University of Oklahoma

Major Field: Chemical Engineering

Major Professor: Dr. Keisha B. Walters

Title of Study: Synthesis and Characterization of Stimuli-Responsive Polymers with Aqueous

Atom Transfer Radical Polymerization

Pages in Study: 172

Candidate for Degree of Doctor of Philosophy

In this study the synthesis of hydrophilic, stimuli-responsive polymers is approached with the goal to optimize their synthesis in terms of quality of product as well as overall user-friendliness of the polymerization scheme. Though many reversible deactivation radical polymerization (RDRP) schemes have been described, many to date require either extensive degassing and polymerization under very tightly control oxygen-free conditions, prohibitively long reaction times, or harsh reagents/conditions to drive the polymerization to completion. Through careful optimization, the use of aqueous Cu^0-mediated atom transfer radical polymerization is demonstrated as a polymerization technique with relatively rapid kinetics (99% conversion in $t = 3$ hr vs $t > 8$ hr for non-aqueous systems), well-defined control over final molecular weight distributions (polydispersity index $Đ < 1.2$), and a high tolerance to oxygen. This system eliminates the need for the extensive degassing protocols often associated with RDRP reactions, with no detrimental effect observed on the final molecular weight distributions. This eliminates a

tedious step in reaction preparation and presents a significant step towards a robust reaction system that can be readily implemented beyond the laboratory scale.

This system is also demonstrated to apply well to acidic monomers in the form of phosphate-laden hydrogels. Exchange of the activating/reducing agent for the catalyst system from copper metal to ascorbic acid enables the direct synthesis of phosphate-pendant hydrogels with greater phosphate content than previously reported, using an internal diene impurity in the commercially sourced monomer as its own crosslinker. Careful optimization reveals this route to yield hydrogels with high swellability (water uptake > 6,000% w/w) despite higher crosslinker concentration than is typically thought feasible for the synthesis of well-defined hydrogels (ca. 16 mol%). These conditions establish the groundwork for synthesizing these hydrogels under the most extreme condition, establishing a toolset to slowly dilute with secondary monomers for targeting specific mechanical properties in response to changes in *pH*, ionic strength, and cation structure.

Finally, the *pH-* and temperature-responsive behavior of poly(2-[dimethylamino]ethyl methacrylate) (PDMAEMA) are considered, with emphasis on understanding the role of individual variables that have often been convoluted in prior studies. Careful assessment suggests a large enthalpy of protonation (ΔH = -89 kJ/mol) that drives the dissociation of the polymer pendant groups as solutions are heated, heavily coupling the temperature and *pH* responsiveness. Preliminary results suggest this relationship between temperature and protonation may be a more predictive tool for interpreting the temperature responsiveness of PDMAEMA. These results provide a theoretical basis to establish this connection across additional conditions and other polymers, improving the understanding the fundamental thermodynamic processes that drive this equilibrium.

DEDICATION

To my wife, Brennah, and my parents Michelle and Russell. Words do not exist to give you all

the thanks you deserve; your constant love and support will never be forgotten.

ACKNOWLEDGEMENTS

TABLE OF CONTENTS

xiii

LIST OF FIGURES

xv

LIST OF ABBREVIATIONS

SRP:	stimuli responsive polymer
RDRP:	reversible deactivation radical polymerization
ATRP:	atom transfer radical polymerization
MWD:	molecular weight distribution
SARA-ATRP:	supplemental activator and reducing agent ATRP
ARGET-ATRP:	activation by reducing agent ATRP
SET-LRP:	single-electron transfer living radical polymerization
DMAEMA:	2-(dimethylamino)ethyl methacrylate
DEAEMA:	2-(diethylamino)ethyl methacrylate
DEAEMA:	2-(diethylamino)ethyl methacrylate
DPAEMA:	2-(diisopropylamino)ethyl methacrylate
LCST:	lower critical solution temperature
MOEP:	2-(methacryloyloxy)ethyl phosphate
SPMA:	3-sulfopropyl methacrylate
NIPAM:	N-isopropylacrylamide
2Bpy:	2-2'-bipyridyl
TPMA:	tris-(2-pyridylmethyl)amine
PMDETA:	N,N,N',N'',N''-pentamethylethylenetriamine
Me$_6$TREN:	tris(2-[dimethylamino]ethyl)amine
GPC:	gel permeation chromatography
NMR:	nuclear magnetic resonance
MBPA:	methyl α-bromophenylacetate
MBP:	methyl 2-bromoproprionate
BPAA:	α-bromophenylacetic acid
M_N:	number-average molecular weight
$Đ$:	polydispersity index
BiBA:	α-bromoisobutyric acid

CHAPTER I: INTRODUCTION

1.1 Background and Motivation

In recent years, stimuli-responsive polymers (SRPs) have been a topic of significant interest for a wide range of technologies, including targeted drug delivery, advanced separations, and chemical sensors.[1,2] These materials are designed in such a way that changes to local conditions such as pH, temperature, light exposure, or redox state – among others – induce changes in the physical or chemical structure of the polymeric backbone. Dependent on specific chemistries, these changes can cause spontaneous demixing and precipitation of the polymer from solution as a polymer transitions from its solvated random-coil structure to a tightly coiled condensed structure (Figure I-1).[3] This responsive behavior allows for the targeted design of so-called "smart" materials, whereby material properties can be tuned on the fly by modulating the desired environmental stimuli. In general, these are solution-phase behaviors, modulating between a soluble and insoluble state, often observed as a transition between optically transparent (soluble) and opaque (insoluble) solutions. However, this behavior may be leveraged into more complex materials by integration into more complex polymer architectures, such as block copolymers and
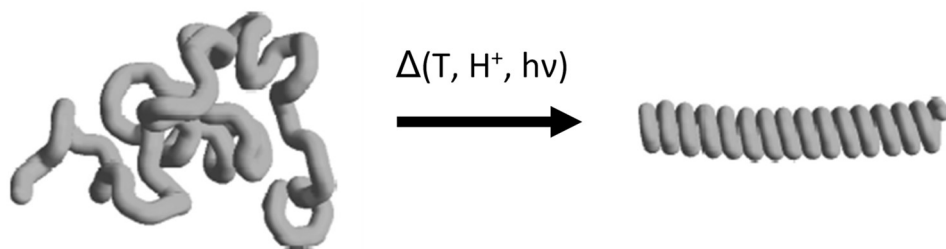
Figure I-1: Configurational change for SRPs, from solvated random coil configuration (left) to tightly coiled configuration (right).

hyperbranched polymers, or by grafting SRPs to the surface of various substrates, such as physical surface coatings on both macroscopic materials and micro- or nanoscopic materials.[4-10]

In solution, this responsive behavior has been utilized as a mechanism for the triggering either formation or collapse of micelles and other complex secondary or tertiary structures, as well as modulating solubility of additive components. This is especially true when more complex polymer architectures are considered, where the SRP moiety comprises only one portion of the overall molecular structure. For example, inclusion of SRPs in block copolymers allows for the synthesis of self-assembling structures, accomplishing either stimuli-induced assembly or stimuli-induced disassembly based on the material design.[5,7,11] These materials rely on a switch between relative hydrophobicity of the component blocks of the material to induce this assembly or disassembly. SRPs provide a mechanism to trigger assembly of micellar structures by switching one block to the hyper-coiled state, but also a means to trigger micellar collapse by returning to the random coil state. This behavior may be further extended through the inclusion of tertiary blocks, with hydrophilic-hydrophobic-hydrophilic block copolymers able to assemble into hollow-sphere structures, often termed as polymersomes. These structures may be pre-assembled in the presence of a deliverable molecule – such as a therapeutic drug – to trap the molecule on the interior of the polymersome. The polymersome may then be forced to disassemble later in response to internal or external stimuli, collapsing the polymer structure and releasing the cargo molecule.[10,11]

SRPs may also be leveraged as surface coatings or modifiers for the tunability of surface wettability or swelling of membranes and hydrogels.[9,12-21] These phenomena are often accomplished by chemically grafting the polymer on the surface of the substrate of interest. This may be approached with a strategy of grafting-to or grafting-from. Grafting-to relies on attachment

of pre-synthesized polymer to a chemical moiety on the surface of the substrate. The grafting-from approach instead attaches a polymer precursor to the substrate surface, which may then be polymerized *in-situ* to extend the polymer from the surface. Grafting-from often allows for a higher grafting density, yielding a thicker coverage of polymer brushes. However, this approach requires the substrate of interest to tolerate the conditions needed for the polymerization, as well as limit side reactions introduced by the surface chemistry of the substrate. In either case, surface-grafted polymer brushes retain the stimuli responsive behaviors of their free solution analogues, with the transition between the random coil and hyper-coiled configuration corresponding to the expansion and collapse of the polymer brushes. The expansion and contraction of these polymer brushes can be used to tune surface wettability, due to the hydrophobic nature of the hyper-coiled configuration. This behavior can also be used to open and close access to microscopic pores below the substrate surface, blocking diffusion of small molecules through the pores until the SRP behavior is triggered. This has been leveraged in the context of targeted drug delivery to load porous nanoparticles with a therapeutic drug under the hyper-coiled brush state, with brush expanding to plug the pores after loading. The SRP behavior may then be re-triggered at the desired localization, releasing the loaded therapeutic with higher specificity and lower off-target dosing.[4]

In some applications, the required response must fit within a narrow window of environmental conditions to elicit the desired behavior, as is often the case for products designed for use in biological systems. This requirement may restrict the available synthetic routes, as the responses of many SRPs depend on molecular weight due to the inherent balance between hydrophobicity of the polymer backbone and hydrophilicity of the responsive pendant groups.[22,23] The use of

reversible deactivation radical polymerization (RDRP) techniques has thus shown significant promise for many SRP applications, to synthesize polymers with narrow and highly reproduceable molecular weight distributions (MWDs). These techniques include atom transfer radical polymerization (ATRP), reversible addition-fragmentation chain transfer polymerization (RAFT) and ring-opening metathesis polymerization (ROMP), among others. While each method has its own merits and shortcomings, ATRP has continued to show promise as a versatile synthetic tool for a wide range of monomers, with advances in recent years for more functional monomers including those with acidic and basic pendant groups.[24]

1.2   Atom Transfer Radical Polymerization (ATRP)

In ATRP, the polymerization control is maintained by a reversible halide transfer to promote growing polymer chains from a deactivated state to an active radical, using a transition metal catalyst complex (Figure I-2). This catalyst relies on complexation between multidentate tertiary amines and the transition metal ion. By promoting the transition metal center to a higher oxidation state, this catalyst can homolytically cleave the carbon-halide bond, generating a halide anion and a carbon radical. As such, the oxidation state of the metal must be precisely maintained, meaning all ATRP reactions should be conducted in an oxygen-free environment to prevent oxidation of the catalyst to the inactive higher oxidation state. The activity of this catalyst can be fine-tuned by altering the ligand structure; when the inactive alkyl halide state is favored, the effective concentration of radicals is reduced.[25] Because termination by radical-radical coupling is second order with respect to radical concentration, this equilibrium serves to limit the rate of termination, allowing continuous growth of polymer chains at a steady rate. Ultimately, ATRP kinetics thus

boil down to the fine-tuning of the equilibrium between active and dormant chains, with a well-controlled polymerization running under a steady-state equilibrium between these two states.

$$P_n - X + L - Cu^{I}X = P_n \cdot + L - Cu^{II}X_2 \qquad \rightarrow \text{Activation}$$

$$P_n \cdot + M = P_{n+1} \qquad \rightarrow \text{Propagation}$$

$$P_n \cdot + P_m \cdot = P_{n+m} \qquad \rightarrow \text{Termination}$$

$$P_n \cdot + L - Cu^{II}X_2 = P_n - X + L - Cu^{I}X \qquad \rightarrow \text{Deactivation}$$

$$\text{L-Cu}^{I}\text{X} + \text{P}_n\text{-X} \rightleftarrows \text{L-Cu}^{II}\text{X}_2 + \text{P}_n{}^\bullet \circlearrowleft M$$
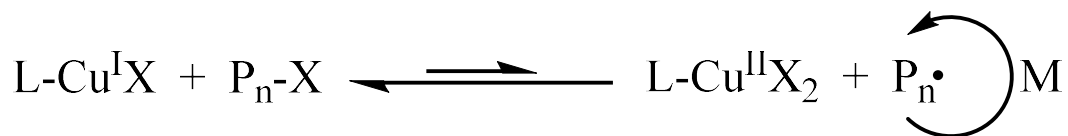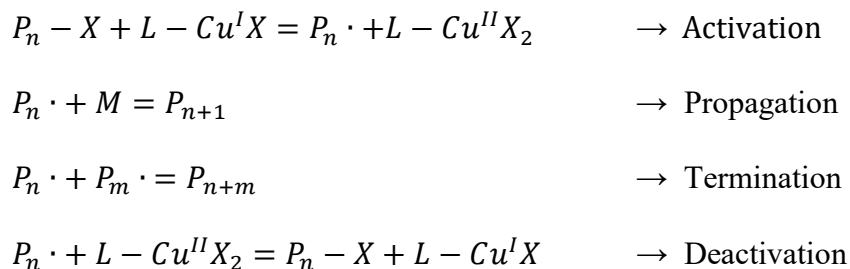
Figure I-2: Overall chemical equilibrium for ATRP.

While in-depth kinetic studies do exist for a wide range of ligands, by and large these studies are restricted to a very small window of monomer-solvent pairings.[26] While these results are useful for informing initial synthesis conditions, the complex nature of the ATRP equilibrium means that each new monomer-solvent pairing will require optimization to find the best catalyst to maintain adequate control. Small disruptions – such as solvation effects in a new monomer or solvent system – lead to a loss of control, yielding an increase in radical concentration and subsequently chain-chain termination. This is especially true when transitioning from nonpolar to polar or aprotic to protic solvents – under such conditions, the equilibrium between the catalyst complex and the growing polymer chains is often drastically different, even to the point that polymerizations may fail altogether if no further adjustments are made. Protic solvents, for

example, often require a means of regenerating the activator species for the catalyst. Without this addition, the solvent will promote oxidation of the transition metal center to its inactive state and the catalyst cannot activate the alkyl halides.[24,25,27]

Furthermore, changes to the general monomer structure adjacent to the alkene impact the substitution of the polymer backbone. This in turn changes the substituent groups present for radical stabilization during the polymerization, further altering the equilibrium between different classes of monomers. These are not always easily predicted, with pendant group substitution serving to further alter the stabilization of radicals and overall rates of propagation.[28,29] In general, conditions must be carefully adjusted between different classes of monomers to correct for the impact of varied radical stabilization and steric hinderance around the propagating radical and alkene of the monomer.
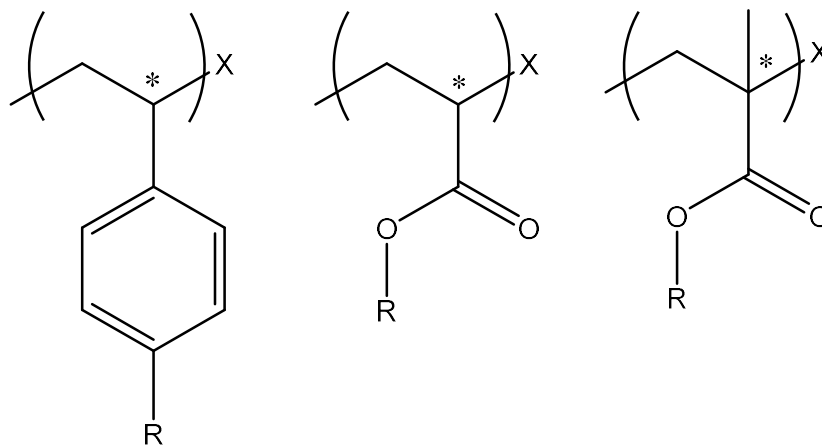
Figure I-3: Generalized chemical structures for polymers based on styrenic derivatives (left), acrylic derivatives (center), and methacrylic derivatives (right). Carbons marked by asterisk (*) represent the position of radicals in activated chains during polymerization.

Aqueous ATRP presents a particularly unique – if challenging – opportunity for optimizing polymerizations. As a protic solvent, it heavily alters the equilibrium between Cu^I and Cu^{II} that describes traditional ATRP kinetics.[30,31] Even for those cases where successful ATRP in aqueous conditions is reported, a close examination of kinetic plots demonstrates that MWD remain initially narrow but broaden over time, suggesting a continual loss of chain functionality over the course of the reaction.[32] While acceptable for some applications, these results preclude such synthetic routes from the development of multifunctional block copolymers as some portion of the polymer chains will be unable to initiate growth of the secondary block. Furthermore, the strong dissociating power of water can abstract halides from the catalyst complex, leading to an accumulation of inactive Cu^{II} salts that halts polymerization.[31,33] The discovery of alternative methodologies such as supplemental activator and reducing agent (SARA-ATRP) and activator regenerated by electron transfer (ARGET-ATRP) introduced a means to mitigate the difficulties of aqueous ATRP. Under these conditions, reducing agents are added to regenerate active Cu^I species *in-situ*. These can either be homogeneous additives, such as ascorbic acid or Sn(II) 2-ethylhexanoate, or heterogeneous as in the case of added zero valent metals [34,35]. Frustratingly, however, details to inform decisions on optimal Cu^0 addition are difficult to parse from results presented in the literature. Results are sometimes presented without clear description of the zero valent metal size or available surface area – the most glaring of these being examples that simply describe the added concentration of copper filings or microparticles, with no characterization of surface area or surface activity.[36] In fact, one may postulate that this disconnect may be a main contributor to the lengthy debate over the mechanism between SARA-ATRP and single electron transfer living radical polymerization (SET-LRP), an alternative proposed mechanism for highly

active ligand systems in aqueous conditions, as failure to properly qualify Cu^0 surface area generated by the rapid disproportionation of Cu^I salts leads to invalid comparisons between systems with different activities. Furthermore, Cu^0 is not the only zero valent metal that has been examined for SARA or ARGET-ATRP of methacrylic monomers, with studies demonstrating Fe^0 and Ag^0 for generating active copper species.[37,38] Once again, studies comparing the effects of different metals on overall kinetics are few and far between, with published studies only examining one small subset of conditions.

ATRP equilibrium is also heavily influenced by the choice of halide, with the strength of the alkyl halide bond increasing as one moves down the halide group. This is due to the weakening of alkyl halide bonds with decreasing electronegativity, as the bonding electrons are held further from the halide nucleus. This trend holds true for all halides but introduces a narrow window of feasible syntheses; for alkyl fluorides, the electronegativity of the F center is sufficiently high that the copper-ligand cleavage necessary for ATRP is generally not observed. Conversely, in the case of alkyl iodides, the low electronegativity of the I center leads to poor control over polymerization, as the activity is shifted far towards active chains, effectively proceeding as a free radical polymerization for all but the lowest activity monomers.

Despite the growing popularity of these systems, many monomers have not been fully characterized under these growth conditions. Often, slower reaction systems utilizing low concentrations of water in alcohol mixtures are utilized, to favor slower kinetics and increased control over final MWDs.[37] However, it has been shown for systems such as N-isopropylacrylamide that near quantitative conversion can be obtained in as little as 30 minutes under aqueous conditions while maintaining a low polydispersity index ($Đ$).[30] Exploration of

fully aqueous systems may lead to the discovery of similarly such active catalysts for other monomers, providing access to robust and rapid synthesis routes for a wide range of monomers.

1.3   Tertiary amines – Dual pH and Temperature SRPs
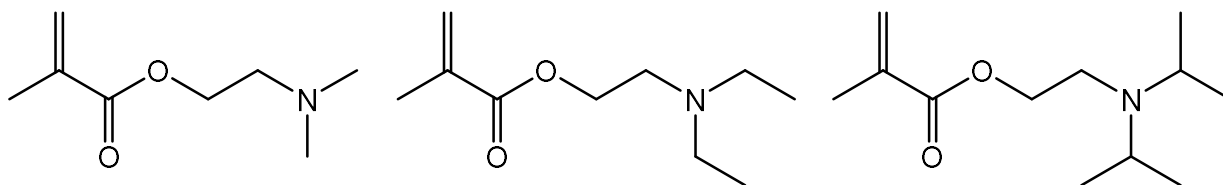
Figure I-4: Chemical structure for 2-(dimethylamino)ethyl methacrylate (left), 2-(diethylamino)ethyl methacrylate (middle), and 2-(diisopropylamino)ethyl methacrylate (right).

2-(dimethylamino)ethyl methacrylate (DMAEMA) is a stimuli responsive monomer, containing a weakly basic tertiary amine.   As a polymer, this functionality introduces responsiveness to changes in both temperature and pH, with a lower critical solution temperature (LCST) between 30 °C and 50 °C, dependent on molecular weight, solution *pH*, and solution ionic strength.[22,39,40]   However, this amine functionality should be expected to imitate the ligand structures necessary to facilitate ATRP. Indeed, despite previously reported synthetic conditions that show rapid and controlled results for many methacrylic monomers, synthesis of PDMAEMA under aqueous conditions has generally been shown to require less active aromatic amines.[32,41] While catalyst disruption has been noted for this monomer in previous studies, to the author's knowledge no in-depth studies have compared the effects of ligand structure to examine the full effect on reaction kinetics under aqueous conditions.[37,41] Successful optimization of conditions to synthesize PDMAEMA should also be considered for extension to the higher alkane content

equivalents, 2-(diethylamino)ethyl methacrylate (DEAEMA) and 2-(diisopropylamino)ethyl methacrylate (DPAEMA). Polymers of these moieties yield similar behavior, with a dual *pH* and temperature responsive behavior, but with the hydrophilic/hydrophobic balance shifted by the increasing hydrophobicity of the amino groups.[42,43] A well-defined polymerization scheme for these monomers should be designed to successfully polymerize each of these moieties, with a suite that may target a wide range of *pH* and temperature responsive behaviors.

1.4 Phosphate/sulfonate – pH and Cation Responsive SRPs
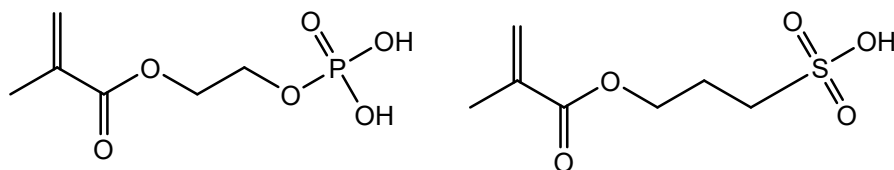
Figure I-5: Chemical structures for 2-(methacryloyloxy)ethyl phosphate (left) and 3-sulfopropylmethacrylate (right).

In addition to cationic SRPs, anionic moieties may also be demonstrated to induce a *pH* responsive behavior by modulating protonation of the anion. Typically, these are found in the form of carboxylic acids, such as methacrylic acid or acrylic acid. Historically, these monomers have been difficult to synthesize under acidic conditions, due to the high degree of catalyst disruption by the deprotonated species and the highly acidic conditions needed to polymerize in the protonated form. Polymerization schemes have thus relied on protecting groups to shield the acidic moieties, with deprotection of the groups post-polymerization.[9] However, recent advances in ATRP have demonstrated that syntheses under acidic conditions may be maintained with well-

defined MWDs if the proper ligand complex is selected. To date, this has generally been restricted to methacrylic acid and its derivatives as proof-of-concept studies, but this system should extend well to other acidic moieties, such as phosphates and sulfonates.

These polymers should also be expected to demonstrate changes in their solution properties based on the presence and concentration of multivalent cations. Phosphates are known to demonstrate strong chelation of multivalent metals such as calcium and magnesium, showing some promise for the development of *in vivo* calcification models.[19,44,45] Sulfonates have been demonstrated to have chelating properties for heavy metals, presenting a potential avenue for advanced separations in traditionally difficult water treatment techniques.[13] Successful extension of ATRP to these moieties would thus yield access to a complex combination of polymer architectures, with tunable charge density and stimuli responsive behavior.

1.5   Research Objectives and Summary

Through this body of work, synthesis routes are designed from the mindset of user-friendliness; that is, polymerization schemes should be versatile across the different classes of stimuli responsive monomers discussed, easily approachable for the user, and scalable beyond the laboratory. The polymerization of stimuli-responsive materials represents a powerful tool for the design of novel polymeric materials, but many existing ATRP protocols are fundamentally limited in scalability which prevents the implementation of these fascinating materials beyond the lab scale. The chief limitation for these protocols is sensitivity to oxygen, which disrupts the redox cycle that drives ATRP; solutions to this sensitivity have historically utilized extensive degassing protocols that both i) require extensive training and practice to master and ii) are difficult to scale

beyond the laboratory. This presents a significant barrier to entry for both researchers and industrial interests and is a key consideration to pushing these materials beyond the scope of the test tube, and into proper applications development.

In Chapter II, efforts are devoted to the optimization of reaction conditions for the synthesis of well-defined polymers of tertiary amine-pendant monomers. These efforts highlight the key polymerization variables for aqueous ATRP, with results yielding a narrow MWD polymer at near-quantitative conversion in under five hours. In addition to maintaining a well-defined and narrow MWD, this system is demonstrated to show no deleterious effects upon eliminating degassing protocols, afforded by the inclusion of zero-valent copper to continue driving the ATRP equilibrium in the presence of dissolved oxygen in the starting reaction mixture. This approach yields easily approachable and scalable syntheses for translation beyond the lab scale.

In Chapter III, efforts are devoted to the improvement of end group fidelity for synthesis of tertiary amine-pendant monomers to access block copolymers and other complex polymer architectures. Consideration of the likely mechanisms for end group loss are considered, with pH adjustment to reduce hydroxide concentration yielding excellent results for the sequential chain extension of PDMAMEA. The oxygen tolerance of this system is retained, with chain extensions requiring no degassing prior to addition. This approach simultaneously serves to expand the accessibility of higher hydrophobicity tertiary amines DEAEMA and DPAEMA by protonating the pendant groups to solubilize the hydrophobic amine group. Successful polymerization of 3-sulfopropyl methacrylate (SPMA) is also demonstrated, with successful block copolymerization of PDMAEMA-b-SPMA demonstrated by a facile one-pot method. By improving end group

retention, research efforts are focused on the development of complex and multi-functional materials for use across a wide range of potential systems.

In Chapter IV, the results from Chapters II and III are used to inform translation to ATRP using *in situ*-generated Cu^0 powder, by the disproportionation of Me$_6$TREN and Cu^I halides. This system has been previously demonstrated to yield rapid conversion of NiPAM and other hydrophilic monomers, but extension to tertiary amines such as DMAEMA has not been demonstrated. Efforts demonstrate poor performance at the acidic conditions needed for optimized conditions of TPMA-mediated ATRP, indicating limited performance for the higher activity Me$_6$TREN system, and highlighting the resilience of TPMA for the synthesis of a wide range of monomers. Though this system does not reveal the same access to block copolymers and other complex architectures, moderately well-defined homopolymerizations of PDMAEMA are still attainable, with near quantitative conversion in only one hour.

In Chapter V, efforts are devoted to the extension of this reaction system to phosphate-pendant monomers. The presence of a diene impurity in commercially available 2-(methacryloyloxy)ethyl phosphate (MOEP) leads to extensive crosslinking of polymer chains, eliminating the access to narrow MWDs. As such, efforts are instead positioned towards the extension of this polymerization system to synthesize functional hydrogels. Synthesis of phosphate-rich hydrogels is demonstrated, with both Cu^0 and ARGET ATRP considered. Though restricted to commercially available monomers in the body of this work, extension to novel phosphate and phosphonate moieties is expected to be readily approachable.

In Chapter VI, discussions explore the temperature and *pH* responsive behavior of PDMAEMA as a model for the tertiary amine class of polymers. Responsiveness is considered as a function of

pH and salt content, with varied salt structures used to probe the effects of charge neutralization on the LCST transition. These results illustrate the interconnected responsiveness between temperature and *pH*, establishing the dissociation of protonated DMAEMA pendant groups as a key component in the LCST phenomenon. Efforts also highlight a dependence of temperature responsiveness on storage conditions, with storage under refrigerated conditions demonstrating a clear shift in LCST in a matter of days, with little to no shift in LCST observed for the same solutions stored at room temperature for $t > 1$ month. This anomalous shift is not fully understood and highlights the need for further investigation to understand the complexation effects that may be occurring.

1.6   References

1.   Boyer, C., Corrigan, N.A., Jung, K., Nguyen, D., Nguyen, T.K., Adnan, N.N., Oliver, S., Shanmugam, S., and Yeow, J., *Copper-Mediated Living Radical Polymerization (Atom Transfer Radical Polymerization and Copper(0) Mediated Polymerization): From Fundamentals to Bioapplications.* Chem. Rev., 2016. **116**(4): p. 1803-949. DOI: 10.1021/acs.chemrev.5b00396.
2.   Wei, M., Gao, Y., Li, X., and Serpe, M.J., *Stimuli-responsive polymers and their applications.* Polym. Chem., 2017. **8**(1): p. 127-143. DOI: 10.1039/c6py01585a.
3.   Zhang, Q., Weber, C., Schubert, U.S., and Hoogenboom, R., *Thermoresponsive polymers with lower critical solution temperature: from fundamental aspects and measuring techniques to recommended turbidimetry conditions.* Materials Horizons, 2017. **4**(2): p. 109-116. DOI: 10.1039/c7mh00016b.
4.   Frickenstein, A.N., Hagood, J.M., Britten, C.N., Abbott, B.S., McNally, M.W., Vopat, C.A., Patterson, E.G., MacCuaig, W.M., Jain, A., Walters, K.B., and McNally, L.R., *Mesoporous Silica Nanoparticles: Properties and Strategies for Enhancing Clinical Effect.* Pharmaceutics, 2021. **13**(4). DOI: 10.3390/pharmaceutics13040570.
5.   Ahmadkhani, L., Abbasian, M., and Akbarzadeh, A., *Synthesis of sharply thermo and PH responsive PMA-b-PNIPAM-b-PEG-b-PNIPAM-b-PMA by RAFT radical polymerization and its schizophrenic micellization in aqueous solutions.* Des Monomers Polym., 2017. **20**(1): p. 406-418. DOI: 10.1080/15685551.2017.1314654.
6.   Benten, H., Mori, D., Ohkita, H., and Ito, S., *Recent research progress of polymer donor/polymer acceptor blend solar cells.* J. Mater. Chem. A, 2016. **4**(15): p. 5340-5365. DOI: 10.1039/c5ta10759h.

7. Chen, D., Huang, Y., Xu, S., Jiang, H., Wu, J., Jin, X., and Zhu, X., *Self-Assembled Polyprodrug Amphiphile for Subcutaneous Xenograft Tumor Inhibition with Prolonged Acting Time In Vivo.* Macromol Biosci, 2017. **17**(11). DOI: 10.1002/mabi.201700174.

8. Zou, H. and Yuan, W., *CO2- and thermo-responsive vesicles: from expansion–contraction transformation to vesicles-micelles transition.* Polymer Chemistry, 2015. **6**(13): p. 2457-2465. DOI: 10.1039/C5PY00024F.

9. Huang, T., Liu, H., Liu, P., Liu, P., Li, L., and Shen, J., *Zwitterionic copolymers bearing phosphonate or phosphonic motifs as novel metal-anchorable anti-fouling coatings.* J. Mater. Chem. B, 2017. **5**(27): p. 5380-5389. DOI: 10.1039/c7tb01017f.

10. Mason, A.F. and Thordarson, P., *Polymersomes with Asymmetric Membranes Based on Readily Accessible Di- and Triblock Copolymers Synthesized via SET-LRP.* ACS Macro Letters, 2016. **5**(10): p. 1172-1175. DOI: 10.1021/acsmacrolett.6b00747.

11. Zhao, Y., Li, X., Zhao, X., Yang, Y., Li, H., Zhou, X., and Yuan, W., *Asymmetrical Polymer Vesicles for Drug delivery and Other Applications.* Front Pharmacol, 2017. **8**: p. 374. DOI: 10.3389/fphar.2017.00374.

12. Chabrol, V., Léonard, D., Zorn, M., Reck, B., D'Agosto, F., and Charleux, B., *Efficient Copper-Mediated Surface-Initiated Polymerization from Raw Polymer Latex in Water.* Macromolecules, 2012. **45**(7): p. 2972-2980. DOI: 10.1021/ma300236r.

13. Gu, J., Yuan, S., Shu, W., Jiang, W., Tang, S., Liang, B., and Pehkonen, S.O., *PVBC microspheres tethered with poly(3-sulfopropyl methacrylate) brushes for effective removal of Pb(II) ions from aqueous solution.* Colloids and Surfaces A: Physicochemical and Engineering Aspects, 2016. **498**: p. 218-230. DOI: https://doi.org/10.1016/j.colsurfa.2016.03.062.

14. Kizhakkedathu, J.N., Norris-Jones, R., and Brooks, D.E., *Synthesis of Well-Defined Environmentally Responsive Polymer Brushes by Aqueous ATRP.* Macromolecules, 2004. **37**(3): p. 734-743. DOI: 10.1021/ma034934u.

15. Kobayashi, M., Terada, M., Terayama, Y., Kikuchi, M., and Takahara, A., *Direct Synthesis of Well-Defined Poly[{2-(methacryloyloxy)ethyl}trimethylammonium chloride] Brush via Surface-Initiated Atom Transfer Radical Polymerization in Fluoroalcohol.* Macromolecules, 2010. **43**(20): p. 8409-8415. DOI: 10.1021/ma1014897.

16. Kotsuchibashi, Y., Faghihnejad, A., Zeng, H., and Narain, R., *Construction of 'smart' surfaces with polymer functionalized silica nanoparticles.* Polym. Chem., 2013. **4**(4): p. 1038-1047. DOI: 10.1039/c2py20845h.

17. Ramstedt, M., Ekstrand-Hammarstrom, B., Shchukarev, A.V., Bucht, A., Osterlund, L., Welch, M., and Huck, W.T., *Bacterial and mammalian cell response to poly(3-sulfopropyl methacrylate) brushes loaded with silver halide salts.* Biomaterials, 2009. **30**(8): p. 1524-31. DOI: 10.1016/j.biomaterials.2008.12.008.

18. Sankhe, A.Y., Husson, S.M., and Kilbey, S.M., *Direct polymerization of surface-tethered polyelectrolyte layers in aqueous solution via surface-confined atom transfer radical polymerization.* J. Polym. Sci., Part A: Polym. Chem., 2007. **45**(4): p. 566-575. DOI: 10.1002/pola.21817.

19. Stancu, I.C., Filmon, R., Cincu, C., Marculescu, B., Zaharia, C., Tourmen, Y., Basle, M.F., and Chappard, D., *Synthesis of methacryloyloxyethyl phosphate copolymers and in*

vitro calcification capacity. Biomaterials, 2004. **25**(2): p. 205-13. DOI: 10.1016/s0142-9612(03)00485-x.

20.   Venault, A., Hsu, K.J., Yeh, L.C., Chinnathambi, A., Ho, H.T., and Chang, Y., *Surface charge-bias impact of amine-contained pseudozwitterionic biointerfaces on the human blood compatibility.* Colloids Surf B Biointerfaces, 2017. **151**: p. 372-383. DOI: 10.1016/j.colsurfb.2016.12.040.

21.   Yan, W., Dadashi-Silab, S., Matyjaszewski, K., Spencer, N.D., and Benetti, E.M., *Surface-Initiated Photoinduced ATRP: Mechanism, Oxygen Tolerance, and Temporal Control during the Synthesis of Polymer Brushes.* Macromolecules, 2020. **53**(8): p. 2801-2810. DOI: 10.1021/acs.macromol.0c00333.

22.   Mohammadi, M., Salami-Kalajahi, M., Roghani-Mamaqani, H., and Golshan, M., *Effect of molecular weight and polymer concentration on the triple temperature/pH/ionic strength-sensitive behavior of poly(2-(dimethylamino)ethyl methacrylate).* Int. J. Polym. Mater. Polym. Biomater., 2017. **66**(9): p. 455-461. DOI: 10.1080/00914037.2016.1236340.

23.   Plunkett, K.N., Zhu, X., Moore, J.S., and Leckband, D.E., *PNIPAM chain collapse depends on the molecular weight and grafting density.* Langmuir, 2006. **22**(9): p. 4259-66. DOI: 10.1021/la0531502.

24.   Fantin, M., Isse, A.A., Venzo, A., Gennaro, A., and Matyjaszewski, K., *Atom Transfer Radical Polymerization of Methacrylic Acid: A Won Challenge.* J. Am. Chem. Soc., 2016. **138**(23): p. 7216-9. DOI: 10.1021/jacs.6b01935.

25.   Matyjaszewski, K., *Atom Transfer Radical Polymerization (ATRP): Current Status and Future Perspectives.* Macromolecules, 2012. **45**(10): p. 4015-4039. DOI: 10.1021/ma3001719.

26.   Tang, W. and Matyjaszewski, K., *Effect of Ligand Structure on Activation Rate Constants in ATRP.* Macromolecules, 2006. **39**(15): p. 4953-4959. DOI: 10.1021/ma0609634.

27.   Konkolewicz, D., Wang, Y., Zhong, M., Krys, P., Isse, A.A., Gennaro, A., and Matyjaszewski, K., *Reversible-Deactivation Radical Polymerization in the Presence of Metallic Copper. A Critical Assessment of the SARA ATRP and SET-LRP Mechanisms.* Macromolecules, 2013. **46**(22): p. 8749-8772. DOI: 10.1021/ma401243k.

28.   Mendonça, P.V., Serra, A.C., Coelho, J.F.J., Popov, A.V., and Guliashvili, T., *Ambient temperature rapid ATRP of methyl acrylate, methyl methacrylate and styrene in polar solvents with mixed transition metal catalyst system.* European Polymer Journal, 2011. **47**(7): p. 1460-1466. DOI: https://doi.org/10.1016/j.eurpolymj.2011.03.014.

29.   Pirman, T., Ocepek, M., and Likozar, B., *Radical Polymerization of Acrylates, Methacrylates, and Styrene: Biobased Approaches, Mechanism, Kinetics, Secondary Reactions, and Modeling.* Industrial & Engineering Chemistry Research, 2021. **60**(26): p. 9347-9367. DOI: 10.1021/acs.iecr.1c01649.

30.   Zhang, Q., Wilson, P., Li, Z., McHale, R., Godfrey, J., Anastasaki, A., Waldron, C., and Haddleton, D.M., *Aqueous copper-mediated living polymerization: exploiting rapid disproportionation of CuBr with Me6TREN.* J. Am. Chem. Soc., 2013. **135**(19): p. 7355-63. DOI: 10.1021/ja4026402.

31.	Fantin, M., Isse, A.A., Gennaro, A., and Matyjaszewski, K., *Understanding the Fundamentals of Aqueous ATRP and Defining Conditions for Better Control.* Macromolecules, 2015. **48**(19): p. 6862-6875. DOI: 10.1021/acs.macromol.5b01454.

32.	Zeng, F., Shen, Y., Zhu, S., and Pelton, R., *Atom transfer radical polymerization of 2-(dimethylamino)ethyl methacrylate in aqueous media.* J. Polym. Sci., Part A: Polym. Chem., 2000. **38**(20): p. 3821-3827. DOI: 10.1002/1099-0518(20001015)38:20<3821::Aid-pola130>3.0.Co;2-g.

33.	Tsarevsky, N.V., Pintauer, T., and Matyjaszewski, K., *Deactivation Efficiency and Degree of Control over Polymerization in ATRP in Protic Solvents.* Macromolecules, 2004. **37**(26): p. 9768-9778. DOI: 10.1021/ma048438x.

34.	Chan, N., Cunningham, M.F., and Hutchinson, R.A., *ARGET ATRP of Methacrylates and Acrylates with Stoichiometric Ratios of Ligand to Copper.* Macromolecular Chemistry and Physics, 2008. **209**(17): p. 1797-1805. DOI: 10.1002/macp.200800328.

35.	Jones, G.R., Whitfield, R., Anastasaki, A., Risangud, N., Simula, A., Keddie, D.J., and Haddleton, D.M., *Cu(0)-RDRP of methacrylates in DMSO: importance of the initiator.* Polym. Chem., 2018. **9**(18): p. 2382-2388. DOI: 10.1039/c7py01196b.

36.	Tom, J., Hornby, B., West, A., Harrisson, S., and Perrier, S., *Copper(0)-mediated living radical polymerization of styrene.* Polym. Chem., 2010. **1**(4): p. 420-422. DOI: 10.1039/b9py00382g.

37.	Cordeiro, R.A., Rocha, N., Mendes, J.P., Matyjaszewski, K., Guliashvili, T., Serra, A.C., and Coelho, J.F.J., *Synthesis of well-defined poly(2-(dimethylamino)ethyl methacrylate) under mild conditions and its co-polymers with cholesterol and PEG using Fe(0)/Cu(ii) based SARA ATRP.* Polym. Chem., 2013. **4**(10). DOI: 10.1039/c3py00190c.

38.	Williams, V.A., Ribelli, T.G., Chmielarz, P., Park, S., and Matyjaszewski, K., *A silver bullet: elemental silver as an efficient reducing agent for atom transfer radical polymerization of acrylates.* J. Am. Chem. Soc., 2015. **137**(4): p. 1428-31. DOI: 10.1021/ja512519j.

39.	Zheng, J.Y., Tan, M.J., Thoniyot, P., and Loh, X.J., *Unusual thermogelling behaviour of poly[2-(dimethylamino)ethyl methacrylate] (PDMAEMA)-based polymers polymerized in bulk.* RSC Advances, 2015. **5**(76): p. 62314-62318. DOI: 10.1039/c5ra12816a.

40.	de Souza, J.C.P., Naves, A.F., and Florenzano, F.H., *Specific thermoresponsiveness of PMMA-block-PDMAEMA to selected ions and other factors in aqueous solution.* Colloid and Polymer Science, 2012. **290**(13): p. 1285-1291. DOI: 10.1007/s00396-012-2651-9.

41.	Dong, H. and Matyjaszewski, K., *ARGET ATRP of 2-(Dimethylamino)ethyl Methacrylate as an Intrinsic Reducing Agent.* Macromolecules, 2008. **41**(19): p. 6868-6870. DOI: 10.1021/ma8017553.

42.	Wang, G. and Zhang, L., *Synthesis, self-assembly and pH sensitivity of PDEAEMA–PEG–PDEAEMA triblock copolymer micelles for drug delivery.* Reactive and Functional Polymers, 2016. **107**: p. 1-10. DOI: 10.1016/j.reactfunctpolym.2016.08.001.

43.	Jin, N., Morin, E.A., Henn, D.M., Cao, Y., Woodcock, J.W., Tang, S., He, W., and Zhao, B., *Agarose hydrogels embedded with pH-responsive diblock copolymer micelles for triggered release of substances.* Biomacromolecules, 2013. **14**(8): p. 2713-23. DOI: 10.1021/bm4005639.

44.   Monge, S., Canniccioni, B., Graillot, A., and Robin, J.J., *Phosphorus-containing polymers: a great opportunity for the biomedical field.* Biomacromolecules, 2011. **12**(6): p. 1973-82. DOI: 10.1021/bm2004803.
45.   Suzuki, S., Whittaker, M.R., Grondahl, L., Monteiro, M.J., and Wentrup-Byrne, E., *Synthesis of soluble phosphate polymers by RAFT and their in vitro mineralization.* Biomacromolecules, 2006. **7**(11): p. 3178-87. DOI: 10.1021/bm060583q.

CHAPTER II: Aqueous Cu⁰-Mediated ATRP for the Synthesis of Tertiary Amine-Pendant Polymers

2.1   Abstract

Poly([2-dimethylamino]ethyl methacrylate) (PDMAEMA) is explored as a model polymer for the extension Cu⁰-mediated ATRP in aqueous media to tertiary amine-pendant methacrylate polymers.   By increasing concentration of deactivating Cu^{II} species, reducing reaction temperature, and increasing supporting halide concentration to 1 M, polymers with well-defined MWDs are achieved in under four hours. MWDs show good agreement with theoretical values, with $Đ$ as low as 1.14.   Furthermore, this reaction system shows a remarkable tolerance to dissolved oxygen, with little to no deleterious effects observed for polymerizations run without degassing prior to initiation. However, chain extensions demonstrate a limited retention of active terminal halides, attributed to the high *pH* of the reaction mixture (9.6). Though this limits the accessibility of block copolymers and other complex architecture, this work presents a new aqueous method for the rapid and facile synthesis of tertiary amine-pendant homopolymers with well-defined MWDs.

2.2   Introduction

In recent years, stimuli-responsive polymers (SRPs) have been a topic of significant interest for a wide range of applications, including targeted drug delivery, advanced separations, and chemical sensors.[1,2]   SRPs are designed so that changes to local conditions such as *pH*, temperature, light exposure, or redox state—among others—induce reversible chemical or

physical conformation changes in the polymer. Often, these changes result in spontaneous demixing and precipitation of the polymer from solution through transition from a solvated random-coil structure to a tightly coiled condensed structure.[3] For many SRPs this behavior depends on molecular weight and molecular weight distribution (MWD).[4,5] Requirements on the stimulus type and range, response rate, and desired SRP property change may thus restrict the options for viable synthetic routes, with broad MWDs from free radical polymerizations yielding broad and poorly-defined response windows. Consequently, reversible deactivation radical polymerization (RDRP) techniques have shown significant promise for many SRP applications, allowing for the synthesis of polymers with reproducible and linear polymerization kinetics and narrow MWDs. RDRP techniques include atom transfer radical polymerization (ATRP), reversible addition-fragmentation chain transfer polymerization (RAFT), ring-opening metathesis polymerization (ROMP), and others. While each RDRP method has its own merits and limitations, ATRP has continued to show promise as a versatile synthetic tool for a wide range of monomers.[6-8] Advances in ATRP methods in recent years have allowed for its application to more functional monomers, including those with acidic and basic pendant groups.[9]

In ATRP, polymerization control is maintained by a reversible halide transfer to promote growing polymer chains from a deactivated state to an active radical, that is mediated by a transition metal catalyst complex. This catalyst relies on complexation between multidentate tertiary amines and a transition metal ion. By promoting the transition metal to a higher oxidation state, this catalyst can reversibly and homolytically cleave the alkyl halide at the terminus of a deactivated polymer molecule, generating the active radical and enabling propagation. The

20

equilibrium between active and inactive chains can then be tuned by modulating ligand structure, solvent, and catalyst metal.[10,11]

Aqueous ATRP presents a particularly unique, if challenging, opportunity for optimizing polymerizations. As a protic solvent, water heavily alters the equilibrium between the Cu^I and Cu^{II} species that are part of traditional ATRP kinetics.[12,13] As a result, the ATRP equilibrium coefficient (K_{ATRP}) is three orders of magnitude higher under aqueous conditions than in most aprotic solvents.[8] The accelerated kinetics of this system—when leveraged properly—have been shown to reduce reaction times from hours or days to as little as 30 min for full conversion, while still maintaining a narrow MWD.[12] Despite the growing popularity of aqueous ATRP systems, many monomers have not been fully characterized under these reaction conditions. Often, reaction systems utilize low concentrations of water in alcohol mixtures to favor slower reaction kinetics and increased control over final MWDs.[14] Studies of aqueous ATRP with acidic or basic monomers, which can disrupt the catalyst equilibrium, have been avoided. Instead, those reactions have been designed to either be carried out in the aforementioned alcohol-water mixtures or acidic or basic moieties have been protected during polymerization with labile functional groups that may be removed post-polymerization.[14,15] While these reaction systems yield well-defined final products, they suffer from the added cost and time of a longer overall synthetic route.

One potential system that has shown promise for extending ATRP to these historically difficult monomers is Cu^0-mediated ATRP. Though the specific mechanism for this system is still contested between supplemental activator and reducing agent ATRP (SARA-ATRP) and single electron transfer living radical polymerization (SET-LRP), the versatility of the catalyst system has continued to grow in recent years.[11,12,16,17] In this study, we report the synthesis of poly(2-

21

[dimethylamino]ethyl methacrylate) (PDMAEMA) under fully aqueous conditions, using Cu^0-mediated ATRP. The 2-(dimethylamino)ethyl methacrylate (DMAEMA) monomer used in this study serves as a model to examine complex interactions between the catalyst and monomer, due to the tertiary amine functional group. DMAEMA has the potential to disrupt the catalyst-ligand complex, as has been previously noted in the literature.[18] MWDs and conversion are compared across a wide range of synthesis conditions, exploring the effect of initiator structure, ionic strength, copper surface area, and Cu^{II} loading. Reaction conditions are optimized to target conditions which yield i) narrow MWDs ($Đ$ < 1.2); ii) high conversion (>90% initial monomer); and iii) rapid kinetics compared to traditional ATRP (t < 6 hr). Results demonstrate a synthesis method using basic tertiary amine monomers in water that is rapid (t < 4 hr for 95% conversion), yields polymers up to 100 kDa, and with polydispersity indices ($Đ$) of 1.2 or lower attainable.

2.3   Materials and Methods

2.3.1   Materials

Toluene (CAS 108-88-3; 99.5%) was purchased from Fisher Scientific. α-bromophenylacetic acid (BPAA, CAS 4870-65-9; 98%), 2,2'-bipyridine (2Bpy, CAS 366-18-7; >99%), copper(II) chloride (CAS 7447-39-4; 98%), glacial acetic acid (CAS 64-19-7; 99%), methyl 2-bromoproprionate (MBP, CAS 5445-17-0; 98%), methyl α-bromophenylacetate (MBPA, CAS 3042-81-7; 97%), N,N,N',N'',N''-pentamethyldiethylenetriamine (PMDETA, CAS 3030-47-5; 99%), PDMAEMA (M_N = 10 kDa, $Đ$ ≤ 1.4), sodium hydroxide (CAS 1310-73-2; 97%), and triethylamine (CAS 121-44-8; 99.7%) were purchased from Sigma-Aldrich. Poly(ethylene glycol) (PEG, CAS 25322-68-3) standards for gel permeation chromatography were purchased from

Scientific Polymer Products. 2-(dimethylamino)ethyl methacrylate (DMAEMA, CAS 2867-47-2; 98%) was purchased from TCI America. Hydrochloric acid (CAS 7647-01-0; 36.5%), methanol (CAS 67-56-1; 99.8%), sodium chloride (CAS 7647-14-5; 98%), tris(2-dimethylaminoethyl)amine (Me$_6$TREN, CAS 33527-91-2; 98%), and tris(2-pyridylmethyl)amine (TPMA, CAS 16858-01-8; 98%) were purchased from VWR. Type I ultrapure water (18.2 MΩ) was generated using a Millipore Synergy UV Water Purification System. Copper wire (d = 0.4 mm) was provided by the University of Oklahoma. DMAEMA was passed over activated poly(styrene-co-divinyl benzene) resin (CAS 9003-70-7) before use to remove MEHQ inhibitors. All other reagents were used as received.
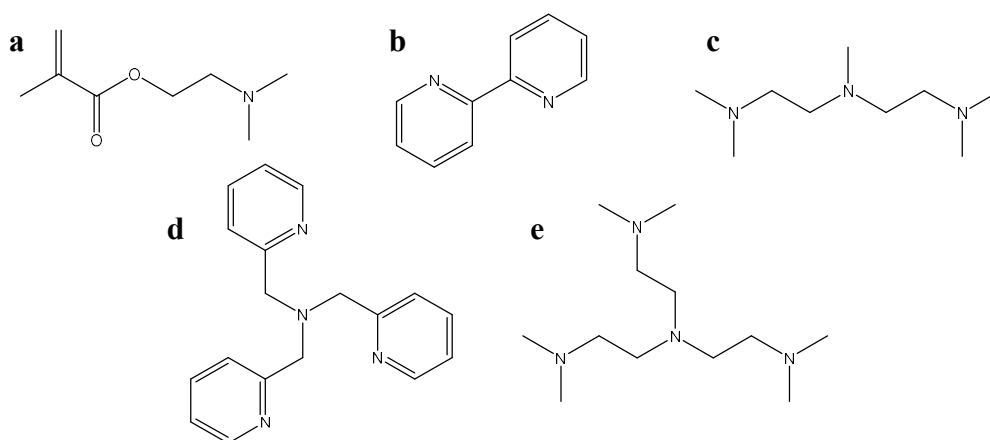
Figure II-1: Chemical structures for: a) DMAEMA; b) 2Bpy; c) PMDETA; d) TPMA; e) Me$_6$TREN

2.3.2   Characterization

2.3.2.1   Gel Permeation Chromatography

Gel permeation chromatography (GPC) was conducted on a Shimadzu Prominence HPLC with an Agilent Aquagel-OH Mixed H and Aquagel-OH 30 column bank. All analyses use a 0.3 M sodium acetate buffer (pH = 4.0) as the mobile phase, modified from conditions established in a

previous study.[19] The buffer solution was also modified to include 0.15 M triethylamine, to suppress adsorption of the polymer to the stationary phase. Chromatograms were collected with a Waters R410 differential refractometer and a Wyatt DAWN F light scattering detector. The light scattering detector was calibrated to the Rayleigh ratio of toluene. Refractometer response was calibrated using low polydispersity PEG standards. The incremental refractive index (*dn/dc*) for PDMAEMA was taken to be 0.20 mL/g as previously described in literature.[19] All chromatograms were collected using an eluent flow rate of 1 mL/min. Additional details for molecular weight calibration are discussed in Appendix A.3. Peak fitting was conducted using Fityk curve fitting software (v. 1.3.1), assuming an exponentially modified Gaussian distribution for all peaks to capture any tailing towards low molecular weight.

2.3.2.2   Nuclear Magnetic Resonance

Nuclear magnetic resonance (NMR) spectra were collected using a Varian VNMRS 500 MHz spectrometer and analyzed using MestReNova software (v. 12.0.2). All NMR samples were dissolved in 10% D_2O-90% H_2O. Spectra were collected with H_2O solvent suppression using a total of 8 scans. A relaxation delay of 40 seconds was used to allow alkene peaks of unreacted monomer to relax between acquisitions. Chemical shifts were assigned according to values previously reported in literature.[20] Conversion is calculated based on the ratio of monomer C=C-H peak area (δ = 5.5-6 ppm) to the area of peaks corresponding to monomer -CH_3 and polymer -CH_2- (δ = 1.4-2 ppm). The overall conversion is calculated as follows, with additional details provided Appendix A.1.

$$Conv.\% = \frac{\delta_{1.4-2} - 3(\delta_6 + \delta_{5.5})}{\delta_{1.4-2} - \delta_6 - \delta_{5.5}}$$

24

2.3.3   Synthesis of PDMAEMA

Syntheses of PDMAEMA were carried out at room temperature or 2 °C in 10 mL test tubes. Exploratory polymerizations were conducted with [DMAEMA]:[Initiator]:[Ligand] = 100:1:0.4. Reactions were carried out with a 2:1 v/v% water to monomer ratio, corresponding to a starting concentration of 2 M. NaCl was added as supplemental halide, preventing dissociation of the ligand-catalyst complex.[13] Copper wire was added with a calculated surface area to volume ratio of 0.1-0.5 cm^2 mL^{-1} of solution, and this surface area to volume ratio was varied as part of the study to probe the efficacy of different synthesis conditions. A representative synthesis is summarized as follows: 8.0 mg (59 μmol) of $CuCl_2$, 17.2 mg (59 μmol) of TPMA, 31.9 mg of BPAA (148 μmol), and 124.6 mg (2.1 mmol) of NaCl were added to a dry test tube. 5 mL of Type I ultrapure water and 2.5 mL (14.8 mmol) of DMAEMA were added to the same test tube. The test tube was then capped with a rubber septum and the reaction mixture dispersed using a vortex mixer. The reaction mixture was then subjected to three freeze-thaw cycles to displace any dissolved oxygen with an inert nitrogen atmosphere, with additional vortexing between each cycle to ensure proper mixing. While the reaction mixture is being subjected to freeze-thaw cycles, a 6.5 cm length of copper wire (d = 0.4 mm; surface area/volume = 0.1 cm^2 mL^{-1}) was added to a separate test tube, and a 1:1 mixture of 35% HCl and methanol was added to fully reduce the copper surface. After 10-15 minutes, the HCl-methanol mixture was decanted, and then the copper was rinsed repeatedly with methanol and dried under N_2. The reaction mixture was transferred to the test tube containing the cleaned copper wire by cannula. The reaction mixture was continuously sparged with N_2 during the reaction to maintain the inert atmosphere and agitate the reaction mixture. Aliquots of 100 μL were withdrawn at regular time points to track conversion

and MWD over the course of the reaction. Aliquots were diluted to a total volume of 1.5 mL using Type I ultrapure water. To quench the reactions, reaction vessels were uncapped and decanted from the copper wire into clean and dry vials and stored in a refrigerator overnight before further processing. Polymer products were purified by precipitation with heating above the lower critical solution temperature (LCST). After purification, polymers were dried in vacuo and stored until further characterization.

2.4 Results and Discussion

2.4.1 Ligand Selection for PDMAEMA Synthesis

A set of initial syntheses were conducted to probe the effects of ligand structure on overall control during the polymerization. To interrogate both the effects of ligand denticity and aromaticity, 2Bpy, TPMA, PMDETA, and Me$_6$TREN were selected as ligands for these experiments, allowing for a comparison between aromatic and alkyl ligands with denticity ranging from two to four. Indeed, TPMA and 2Bpy have been previously utilized for ATRP polymerizations of DMAEMA, although exploration in fully aqueous conditions has been limited any many fully aqueous systems showing $Ð > 1.4$.[18,21] All polymerizations were conducted using methyl α-bromophenylacetate (MBPA) as the initiator and with [DMAEMA]:[MBPA]:[Ligand]:[CuCl$_2$] set as 100:1:0.4:0.1. MBPA was selected as the initiator due to prior demonstration of narrow $Ð$ for methacrylic polymers.[22] These initial syntheses for ligand evaluation were conducted at room temperature, using sodium chloride as a supporting electrolyte at 0.3 M to prevent disassociation of the catalyst complex.[13] Sodium chloride was chosen to induce a halide exchange, allowing for a rapid initiation step for the brominated initiator

before the alkyl bromide terminal groups were displaced with less-active alkyl chlorides to slow propagation and maintain a well-controlled polymerization.[23,24]

Results for these syntheses are summarized in Table II-1. Aromatic amine ligands show improved control over the final MWD. Both 2Bpy and TPMA resulted in moderately narrow distributions—and $Đ = 1.60$ and 1.41, respectively—and number-average molecular weights (M_N) close to the 15.7 kDa target molecular weight. An additional comparison which may help validate overall behavior for the polymerization is initiator efficiency (I_{eff}), which is defined as the ratio of measured M_N to theoretical M_N ($M_{N,theo}$). Comparing the two aromatic ligands, 2Bpy demonstrated a moderate I_{eff} at 73% while TPMA gave a much lower efficiency (26%). The combination of lower I_{eff} and lower final $Đ$ for TPMA suggests that the higher activity ligand complex induces rapid initiation. Rapid initiation leads to a narrower initial MWD at the cost of rapid termination of a large fraction of the available initiator species and, therefore, a lower concentration of growing chains. While this limited the conversion to 36%, using TPMA did result in the lowest $Đ$ of the four ligands examined. With 2Bpy this termination effect is reduced, but as a result the initiation is slower and yields a broader final molecular weight distribution.

Table II-1: Reaction conditions for Cu^0-mediated ATRP of DMAEMA in water using various ligands.[a]

Ligand	Conversion[b] (%)	$M_{N,theo}$ (kDa)	M_N[c] (kDa)	Đ[c]	I_{eff}[d] (%)
PMDETA	48	7.5	124	2.74	6
Me₆TREN	9	1.4	52.3	2.01	3
2Bpy	88	13.8	18.9	1.60	73
TPMA	36	5.7	21.5	1.41	26

[a]: All polymerizations conducted with [DMAEMA]:[MBPA]:[Ligand]:[CuCl₂] = 100:1:0.4:0.1, [DMAEMA]$_0$ = 2 M, [NaCl] = 0.3 M, T = RT, and t = 4 hr. [b]: measured by NMR. [c]: measured by aqueous GPC. [d]: I_{eff} = $M_{N,theo}/M_N$.

Alkyl ligands, on the other hand, displayed markedly poor control over the reaction. The use of PMDETA resulted in broad molecular weight distributions (Đ > 2.5) and the resultant M_N were a full order of magnitude larger than the target M_N, with I_{eff} of only 8%. Though PMDETA has previously been demonstrated to yield well-defined ATRP under mixed solvent systems, these results indicate widespread termination events and poorly controlled polymerizations under fully aqueous conditions.[14] While Me₆TREN does achieve a M_N of 52.3 kDa, the broad dispersity (Đ > 2) and a measured conversion of only 9% also indicate a poorly controlled polymerization. The results of this initial set of syntheses suggest aromatic amine ligands will be required to provide a controlled synthesis that can yield a well-defined tertiary amine-pendant polymer in a fully aqueous Cu^0 system. This is likely a result of high pH, which was measured at 9.6 for this system. Previous studies have indicated poor control for electrochemically-mediated ATRP using PMDETA and Me₆TREN at pH > 8, with PDI > 1.8 observed at pH 10.[13] These results indicate a similarly poor control for Cu^0-mediated ATRP at high pH, due to the destabilizing effect of

hydroxide ions. While increasing denticity appears to aid in narrowing the final MWD, it is at the cost of decreased I_{eff}. From this initial synthesis data, TPMA was determined as the best ligand to pursue for further optimizations targeting narrow MWDs in polymers with pendant tertiary amine groups.

2.4.2   Synthesis Optimization for PDMAEMA

2.4.2.1   Initiator Structure

Initiator structure was investigated as a potential means of narrowing MWDs, with the goal of improving initiation efficiency to reduce the early termination of active chains. In addition to the MBPA initiator used for ligand screening experiments, two additional initiators were examined under similar reaction conditions: methyl 2-bromoproprionate (MBP) and α-bromophenylacetic acid (BPAA). MBP is a far less active ATRP initiator than MBPA, with the difference in activation rates between MBP and MBPA demonstrated to be on the order of 10^4 due the radical stabilization provided by the phenyl group adjacent to the alkyl bromide.[10] For methacrylic monomers, the radical stabilization provided for propagating chains by the two pendant groups has been demonstrated to improve MWD. However, these observations were established using DMSO as the solvent, which has an ATRP equilibrium constant (K_{ATRP}) approximately 10^3 times smaller than water.[8] MBP was included as a comparison to validate that the higher K_{ATRP} does not lead to unnecessary loss of initiator. A summary of these reaction conditions and the resultant polymer properties is presented in Entries 1 and 2 of Table II-2. Most notably, polymerization with MBP demonstrates a slight narrowing of the MWD ($Đ$ = 1.34), though the observed I_{eff} is still limited (21%). This is a surprising result, given the substantial difference in initiator activity. MBP has

been previously shown to demonstrate broad MWD for methacrylic polymers when using higher denticity ligands, with $Đ > 2$ observed in many cases.[10] On the other hand, MBP has yielded moderately narrow MWD for traditional ATRP of PDMAEMA in aqueous media ($Đ > 1.4$), but MWDs were notably larger for higher activity initiators such as ethyl α-bromoisobutyrate (EBiB).[21] The relative invariance observed for this system is attributed to the pairing of the brominated initiator with the chloride supporting salt, generating an accelerated halide exchange. This mechanism has been used previously to force a more rapid initiation using alkyl bromide initiators, then which are converted to alkyl chlorides using a copper chloride catalyst. The alkyl chloride has a lower activation rate, shifting the ATRP equilibrium towards the inactive state to maintain adequate control over the MWD during propagation.[23,24] However, these studies often rely on the chloride solely from added Cu^{I} and Cu^{II} species, with chloride concentrations on the same order of magnitude as those for the initiator species.
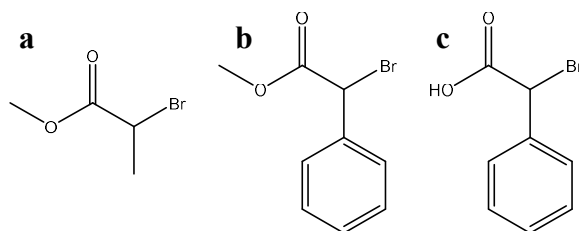
Figure II-2: Initiator structures explored during optimization. a) MBP; b) MBPA; c) BPAA

The conditions in the present study utilize a relatively high concentration of sodium chloride (0.3 M) to ensure a high efficiency of conversion to the alkyl chloride for propagating chains. This introduces an effective bottleneck to growing polymer chains, suppressing the effect of initiator activity on final MWD. While the benefit of this method towards MWD optimization appears

limited, this does present an interesting avenue for cost optimization. This approach would eliminate the need for higher activity initiators in methacrylic systems, allowing use of more widely used and lower cost initiators such as MBP and EBiB. This mechanism should be investigated further, to validate this relative invariance and its extension to additional initiators.

MBPA was notably difficult to dissolve under aqueous conditions. Extensive vortexing was required to fully disperse MBPA, and the MBPA would not completely dissolve until the addition of the monomer to act as a cosolvent. Proper measurements of the true solubility limits for MBPA in water are limited if they exist at all, but it should be expected that the free carboxylic acid, BPAA, will show greater solubility than MBPA. As shown in Entry 3 of Table II-2, use of BPAA as the initiator resulted in a reduction in $Đ$ similar to MBP, although with a slight improvement in I_{eff} (34%). This data indicates that improved solubility limits loss of initiator. Initiator adsorption has been demonstrated as a key step in the activation of the initial alkyl halide bonds under non-aqueous systems.[16] If solubility limitations shift the initiator towards preferential adsorption to the Cu^0 surface, it stands to reason that the activation kinetics will be altered. Therefore, it is important to consider that BPAA ($pK_a = 4.3$ for non-brominated analogue[25]) will be deprotonated under the reaction conditions (measured pH of 9.6). The carboxylate anion is then free to adsorb to the surface of the copper wire. While this study was restricted to commercially available initiators, the result suggests there may be benefit to exploring other solubilizing esters, such as hydroxyethyl or glycerol esters as previously described.[12]

Table II-2: Conditions and molecular weight distributions for syntheses of PDMAEMA. [a]

Entry	Initiator	T (°C)	[NaCl] (M)	[Cu^{II}]:[TPMA]	SA_{Cu}/V (cm^2 mL^{-1})	Target D_P	t (hr)	Conv.[b] (%)	$M_{N,theo}$ (kDa)	M_N[c] (kDa)	$Đ$[c]	I_{eff}[d] (%)
1	MBPA	RT	0.3	0.25	0.1	100	4	36	5.7	21.5	1.41	26
2	MBP	RT	0.3	0.25	0.1	100	4	27	4.2	20.3	1.34	21
3	BPAA	RT	0.3	0.25	0.1	100	4	38	6.0	17.5	1.36	34
4	BPAA	2	0.3	0.25	0.1	100	5	56	8.8	20.8	1.26	42
5	BPAA	2	0.3	1	0.1	100	5	82	12.9	22.4	1.18	57
6	BPAA	2	0.3	0.125	0.1	100	5	71	11.1	32.6	1.50	34
7	BPAA	2	0.3	2	0.1	100	5	3	0.5	n.d.	n.d.	-
8	BPAA	2	1	1	0.1	100	5	84	13.2	19.7	1.15	67
9	BPAA	RT	1	1	0.1	100	5	82	12.9	22.9	1.25	56
10	BPAA	2	1	1	0.5	100	4	95	14.9	21.6	1.14	63
11	BPAA	2	1	1	0.5	200	5	91	28.6	38.0	1.25	75
12	BPAA	2	1	1	0.5	500	5	81	63.6	106	1.43	60
13	BPAA	2	1	1	0.5	1000	5	60	94.2	122	1.45	77
14[e]	BPAA	2	1	1	0.5	100	4	94	14.8	21.1	1.15	70

[a]. All polymerizations were conducted with [DMAEMA]:[Initiator]:[TPMA] = 100:1:0.4 and [DMAEMA]$_0$ = 2 M. [b]. as measured by NMR. [c]. as measured by GPC. [d]. $I_{eff} = M_{N,theo}/M_N$. [e]. no freeze/thaw or degassing prior to polymerization.

2.4.2.2   Reaction Temperature

Experiments were next conducted at reduced temperature (2 °C), which has previously been shown to yield decreased $Đ$ for acrylamides and methacrylates under aqueous conditions.[12,26] This decrease in $Đ$ at lower reaction temperatures is generally attributed to two key factors. First, decreased K_{ATRP} shifts the activation equilibrium to favor the inactive polymer state and slow the overall rate of reaction. Second, and of key importance in aqueous systems, decreasing temperature slows the rate of end group hydrolysis, improving the retention of active alkyl halide end groups over the full course of the polymerization. An immersion chiller and stir bar were added to a water bath, which was then placed on a magnetic stir plate. The water bath was cooled to thermal equilibrium before adding the reaction vessels, measured at 2 °C. Polymerizations were extended an additional hour (5-hour total reaction time) to account for slowed kinetics at the reduced temperature. Entry 4 in Table II-2 shows this temperature reduction generates additional improvement in I_{eff} (42%), as well as a reduction of the MWD ($Đ = 1.26$). These results are in good agreement with prior studies, suggesting the reduced K_{ATRP} helps to mitigate the rapid termination at the onset of the reaction, as well as limit any further termination over the course of the reaction. However, despite the relatively narrow MWD the efficiency is still remarkably low, limiting conversion to 56% for the M_N attained (20.8 kDa). These polymerization results suggest that reduced temperature alone is insufficient to provide proper control for the fully aqueous Cu^0-mediated ATRP polymerization of tertiary amine polymers.

2.4.2.3   Copper(II) Content

Experiments were designed to increase initial Cu^{II} loading, to prevent rapid and uncontrolled polymerization immediately following initiation. The initial 1:4 loading of Cu^{II} relative to the ligand selected was guided by data in the literature utilizing Cu^0-mediated ATRP;[22,27] however, successful fully aqueous systems, such as the Cu^I/Me$_6$TREN catalyst previously demonstrated for N-isopropylacrylamide (NiPAM) and other hydrophilic monomers, utilize an effective 1:1 loading of Cu^{II} relative to the ligand.[12,26] Inclusion of equimolar CuCl$_2$ relative to TPMA (Table II-2, Entry 5) reduces $Đ$ for this system to 1.18, with I_{eff} of 56%. This data suggests that lower Cu^{II} concentrations are insufficient to suppress the period of rapid growth following initiation. A reduction in initial CuCl$_2$ loading to 1:8 relative to TPMA (Table II-2, Entry 6) confirms this behavior with the MWD broadening further ($Đ = 1.50$) and a precipitous drop in I_{eff} to 34%— indicating a large portion of chains are lost to termination at the onset of the reaction. It should also be noted there is a limit to increasing the Cu^{II} loading relative to the ligand. Increasing the concentration of CuCl$_2$ to 2:1 relative to TPMA resulted in only 3% conversion in 5 hours (Table II-2, Entry 7). GPC analysis for this sample showed no polymer elution, within the instrumental resolution limit (ca. 1 kDa). The reaction mixture for the 2:1 Cu^{II} to TPMA loading was a much darker shade of blue, which may signal the onset of Cu(OH)$_x$ formation. Prior studies have demonstrated that Cu(OH)$_x$ formation can disrupt catalyst equilibrium at high *pH*, with deactivating species displaced by inactive Cu^{II}L(OH) species under electrochemically-mediated ATRP.[13] Furthermore, the native *pH* for reaction mixture is measured at 9.6, which is higher than the *pH* limit of 8.5 previously cited for TPMA in the same study. These findings then suggest the

34

versatility of TPMA as a ligand capable of supporting well-controlled Cu^0-mediated ATRP even up to ca. *pH* 10.

2.4.2.4   Supplemental Halide

For some aqueous systems it has been noted that higher salt concentrations are required to maintain narrow MWDs, though generally these have been zwitterionic or charged monomers where charge balancing of the monomer introduces competition for the halide species.[28] Under native conditions, the 2 M reaction mixture has a 9.6 *pH*. The *pK$_a$* of monomeric DMAEMA is 8.4, with the polymer *pK$_a$* decreasing as molecular weight increases. All polymers synthesized in this study are expected to demonstrate a *pK$_a$* between 7.8 and 7.5.[29] Therefore, at the reaction *pH*, there will be ca. 12% protonation of the initial monomer which support the potential for disruption of the deactivating Cu^{II} catalyst by competitively binding free chloride ions in solution. Indeed, at onset of the polymerization a 12% monomer protonation would yield 0.24 M of charged monomer species, leaving only 0.06 M excess chloride. To probe this effect a reaction was designed using 1 M sodium chloride. Under these conditions, the polymerization dispersity was further reduced ($Đ = 1.15$), representing excellent control for the overall reaction (Table II-2, Entry 8). Additionally, these reaction conditions resulted in a molecular weight of 22.4 kDa at 82% conversion, indicating improved initiation efficiency of 68%. It should be noted that the higher halide concentration does necessitate cooling the reaction below room temperature. When this reaction was repeated at room temperature (Table II-2, Entry 9), rapid precipitation of the polymer was observed within the first hour of reaction due to suppression of the LCST below room temperature by the high salt concentration. While this room temperature reaction demonstrated

meaningful conversion and a relatively well-defined $Đ$ of 1.25, the polymer precipitation makes this system impractical for scaling up beyond test tube scale.

2.4.2.5   Copper Wire Surface Area

The initial experimental design utilizing 0.1 cm^2 of copper wire per mL of solution was reduced from a value of 0.5 cm^2/mL previously demonstrated for DMSO.[22] This reduction was added as an initial precaution to account for the larger K_{ATRP} in aqueous systems, as increasing Cu^0 surface area is known to correlate to increased catalyst activity.[16]   However, it has been previously demonstrated that longer reaction times lead to accumulation of hydrolyzed chain ends under aqueous conditions, providing impetus to reduce reaction time further if possible. Polymerization was repeated under the optimized synthesis conditions ([DMAEMA]:[TPMA]:[BPAA]:[CuCl$_2$] = 100:1:0.4:0.4, [NaCl] = 1 M, $T = 2$ °C), but instead utilizing a 0.5 cm^2/mL copper loading (Table II-2, Entry 10).   Under these conditions, the polymerization demonstrates 95% conversion in four hours while maintaining a narrow MWD ($Đ = 1.14$).   A slight reduction in I_{eff} was observed (63%), suggesting that higher activity does have a minor negative effect on the early polymerization stages.   However, this negative impact is insignificant with regards to the final $Đ$; overall the polymerization was pushed to near quantitative conversion while maintaining a narrow, well-defined molecular weight distribution.

Intermediate reaction time aliquots were analyzed to examine the reaction kinetics, as presented in Figure II-3. The polymerization demonstrates well-defined first order kinetics, with an apparent rate constant k_{app} of 0.83 hr^{-1} for 0.5 cm^2 mL^{-1} Cu^0, increased from 0.39 hr^{-1} for 0.1 cm^2 mL^{-1} Cu^0. This indicates a dependence of $k_{app} \propto (SA_{Cu}/V)^{0.47}$, in good agreement with the

theoretical prediction of $(SA_{Cu}/V)^{0.5}$ as previously reported in non-aqueous and semi-aqueous systems.[16,30] This dependency is due to the complex equilibrium between activating and deactivating species, with Cu^0 participating in the polymerization reaction through multiple mechanisms. Cu^0 can act as both a direct activator of alkyl halides, with surface Cu^0 atoms oxidized to Cu^I to cleave the C-X bond.[16] Simultaneously, Cu^0 can act with Cu^I/Cu^{II} species in solution to promote comproportionation or disproportionation, with relative contributions of these mechanisms known to be ligand dependent.[11,30] Furthermore, utilizing the typically cited value of 10^{15} atoms cm^{-2} for surface density of copper and a combined concentration of 28 mM for initiator and ligand at the beginning of polymerization, the number of ligand and alkyl halide molecules outnumber the number of surface copper atoms by ca. 10^4-fold.[16] This ratio is even greater if the adsorption of monomer is considered, with another 10^2-fold increase in adsorbates relative to the surface availability. The final ATRP equilibrium is thus a complex balance between adsorption of dormant chains, adsorption of Cu-ligand complexes, and the continuous redox reactions that activate and deactivate propagating polymer chains.

Overall, though this does suggest further increasing the copper loading could further accelerate reaction kinetics, the observed decrease in initiator efficiency is likely detrimental to the synthesis of well-defined polymers, as final M_N will deviate further from the designed conditions. As such, further reaction optimizations were designed to utilize a SA_{Cu}/V of 0.5 cm^2 mL^{-1}.
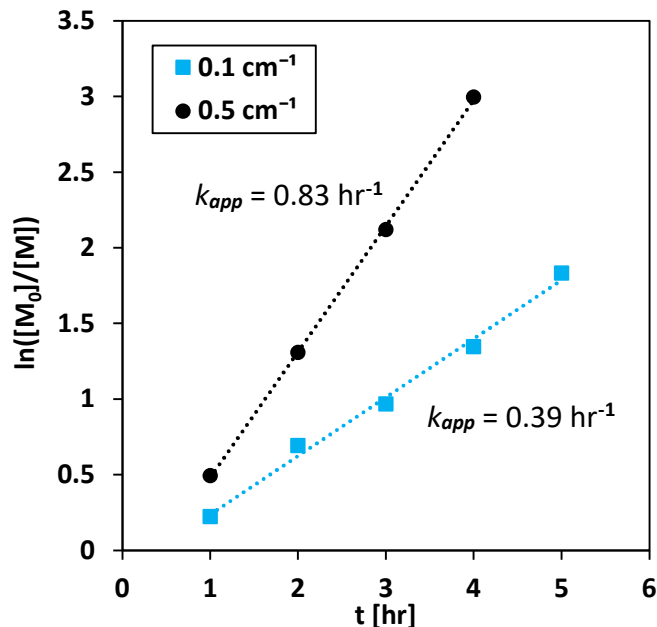
Figure II-3: First-order polymerization kinetic plot for optimized synthesis conditions: [DMAEMA]:[TPMA]:[BPAA]:[CuCl₂] = 100:1:0.4:0.4, [NaCl] = 1M, T = 2 °C.

The trends of molecular weight and Đ versus conversion do show a slight deviation from the ideal linear behavior as conversion increases above 90% with an increase in M_N of only ca. 600 Da between 88% and 95% conversion. This drop-off in conversion is accompanied by a slight increase in Đ from 1.12 to 1.14, marking a slight loss of control towards high conversions. Interestingly, this is not a clear indicator of direct radical coupling, which would be expected to present as a sharp increase in molecular weight growth versus conversion as individual radicals terminate together. Rather, this termination indicates the gradual accumulation of low molecular weight species. Indeed, repeated syntheses with additional low-conversion sampling highlight a gradual decrease in the rate of growth vs conversion (Figure II-4), signaling a small accumulation

of lower molecular weight chains. The narrow MWD for final polymers suggests this effect is small but does highlight the need to investigate end group retention.
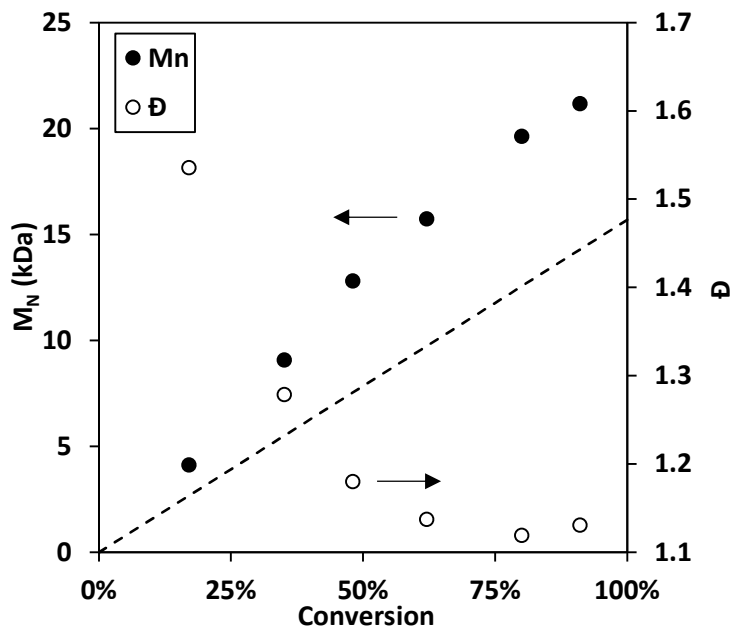
Figure II-4: Molecular weight distribution evolution with additional data points at low conversion. Dashed line represents theoretical M_N.

Overall, this anomalous observation is not well-understood and may indicate a need to halt syntheses near 90% conversion to retain the narrowest overall MWD. If these design targets are considered, polymerizations may be completed within three hours, which is a drastic reduction from the reaction times required for organic or mixed-solvent systems.

2.4.2.6   Homopolymer Chain Extensions

To evaluate the retention of active C-Cl end groups, homopolymer chain extensions were conducted for polymer syntheses at high conversion. For optimized conditions this corresponds

to a primary polymerization of 4 hours, at which point reaction mixtures were uncapped and spiked with an aliquot of fresh monomer. Monomer was added equimolar to the starting concentration, corresponding to a total target D_P of 200. This one-pot approach is the most facile approach to the eventual synthesis of block copolymers, circumventing the time-consuming processes of polymer purification and reinitiation. Results for the chain extension are presented in Figure II-5. While there is a clear shift toward higher molecular weight, the GPC traces demonstrate a clear shoulder that overlaps with the original MWD, indicating a non-negligible portion of chains that have lost their active end groups. This phenomenon has been observed before, with previous efforts for ATRP in isopropanol-water mixtures demonstrating <65% retention of active end group above 80% conversion.[14]
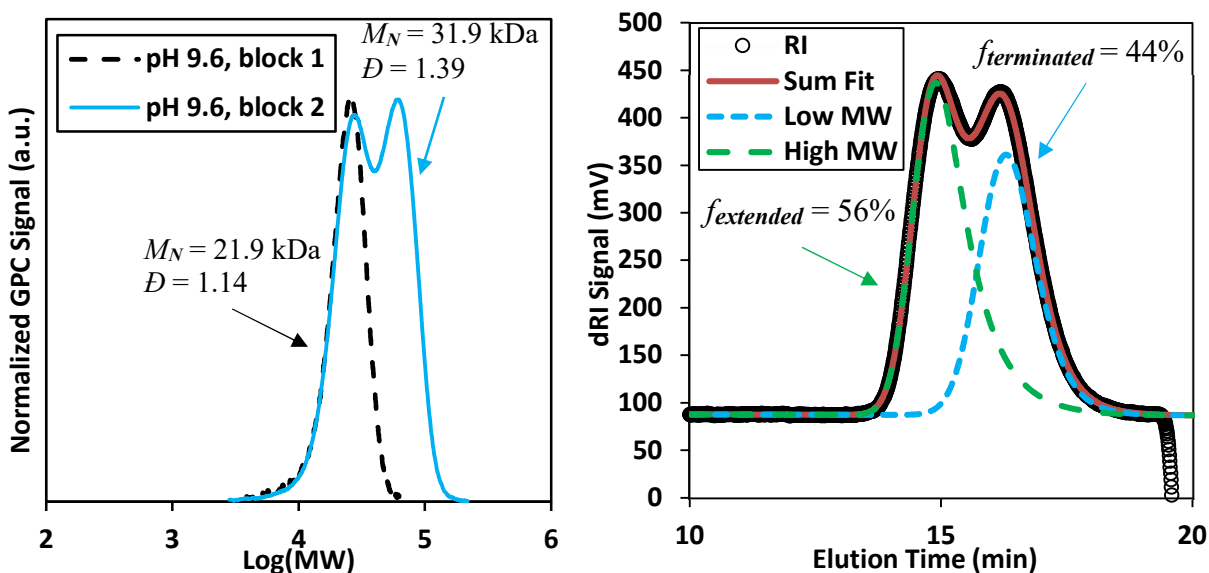
Figure II-5: Homopolymer chain extension for PDMAEMA under optimized conditions (left), with peak fitting for deconvolution (right).

There are multiple mechanisms that can lead to the loss of active halide end groups. Results can largely rule out radical-radical coupling; this mechanism would be accompanied by a doubling of molecular weight as active chains are coupled together, which would be apparent as a high molecular weight shoulder in the primary polymerization MWD. End group loss has also been demonstrated by a radical-mediated elimination pathway in ATRP, yielding the formation of a terminal alkene.[31] Finally, hydrolysis could drive both elimination and substitution reactions, generating either terminal alkenes or hydroxyl groups (Figure II-6). With a native *pH* of 9.6, the high [OH⁻] could contribute to both mechanisms; however, the reduced temperature of the optimized reaction conditions is likely to favor substitution over elimination. Indeed, matrix-assisted laser desorption/ionization coupled time-of-flight mass spectrometry (MALDI-TOF) studies for aqueous syntheses of PNIPAM have demonstrated that inactive chains are predominantly hydroxyl-terminated for the more labile alkyl bromide, though these reactions should be expected to be near neutral *pH*.[12] Though prior works in aqueous or semi-aqueous systems for PDMAEMA do not generally cite the observed *pH* for their systems, the monomer would be expected to increase *pH* through the protonation of the amine groups, likely contributing to the poor end group retention observed here and in prior studies. Exploration of solution *pH* thus represents a promising route for improving the retention of active end groups in this system. MALDI-TOF studies were not pursued, as MALDI-TOF is not available in the University of Oklahoma system, but future studies may benefit from this technique to assess the major contributor to end group loss.
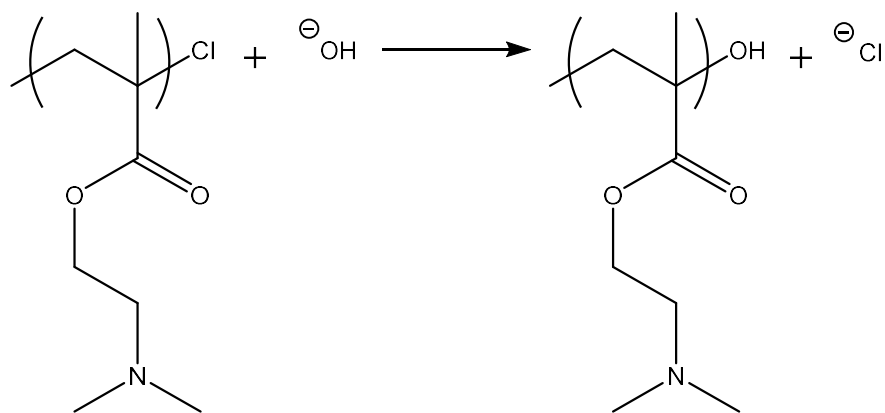
Figure II-6: Hydroxide-mediated termination of active polymers in ATRP.

The included peak fitting demonstrates the relative contribution of the component peaks in the overall molecular weight distribution. Peak deconvolution is conducted with Fityk software using exponentially modified Gaussian peaks. This peak type has been used for GPC peak deconvolution to resolve the theoretical Gaussian peak shape with the tailing often observed for experimentally observed MWDs. Peak parameters are then varied to minimize square residuals from the experimental chromatogram. The peak fitting here reveals a broader tailing effect in the high molecular weight component. Comparison of peak areas reveals a relative ratio of 56% of chains that successfully chain extend, leaving 44% of all chains inactive. This overall data suggests these optimized conditions yield well-defined homopolymers but have limited feasibility for the synthesis of block copolymers and other complex architectures.

2.4.2.7   Polymerizations at Higher Molecular Weights

Further experiments were designed to extend these optimized conditions to higher molecular weights (Table II-2, Entries 11-13). These reactions were allowed to proceed for the full 5 hours

to account for the lowered concentration of initiator and catalyst species. A gradual broadening of each MWD is observed as the targeted degree of polymerization increases. Polymerizations targeting D_P of 200 (Table II-2, Entry 11) still demonstrate good control over final MWD, with M_N of 38 kDa and Đ of 1.25. Polymerizations targeting a degree of polymerization of 500 (Table II-2, Entry 12) yield polymer with M_N of 106 kDa and Đ of 1.43. However, these reactions still show moderate control for relatively high molecular weights, showing potential for this system to extend to large molecular weight polymers if slightly broadened MWDs are acceptable for the final product. However, increasing the target degree of polymerization further to 1000 yields a broadening of Đ to 1.45 and a decrease in conversion to 60% over the same 5-hour time frame. This result is attributed to increased viscosity of the high molecular weight solution which due to continuous N_2 sparging during the reaction results in bubbly flow, with solution rising higher up the test tube walls. This allows for solids to form along the walls of the reaction vessel, slowly decreasing both the mobility of individual chains as well as effective contact with the copper surface. This system displays the ability to maintain moderately narrow MWDs (Đ < 1.5) for polymers up to ca. 100 kDa.

2.4.2.8   Oxygen Tolerance

In keeping with traditional understanding of ATRP techniques, reaction mixtures were extensively deoxygenated prior to initiation to ensure proper equilibrium for the catalyst system. However, the inclusion of copper wire to provide and generate activating Cu^0 and Cu^I species in situ should provide a mechanism for abstracting dissolved oxygen that would normally disrupt the activating catalyst species. To probe this effect, a positive control was designed at the optimized

reaction conditions, adding the copper wire directly to the reaction mixture without any freeze/thaw cycling to remove dissolved oxygen (Table II-2, Entry 14). This reaction was conducted with magnetic stirring under a N_2 headspace, to ensure the sparge was not the mechanism for oxygen compensation. Interestingly, even this positive control—where oxygen is present—showed similar results, with a well-defined MWD in excellent agreement with that observed with full degassing protocols (Table II-2, Entry 8). Under these conditions, the reaction yields a final polymer with M_N of 21.1 kDa and $Đ$ of 1.15. This reaction system thus represents a tremendous resilience to oxygen, like that described for user-friendly ARGET-ATRP systems.[18,32] However, the heterogeneous nature of this catalyst ensures that the reaction can be easily deactivated at any desired end point by simply removing the copper wire. The increased flexibility and ease of use for this approach allows for targeting intermediate conversions, as well as limiting the potential for chain-chain termination in sealed containers after polymerization.

2.5   Conclusions

Utilizing aromatic ligands, such as TPMA, the Cu^0-mediated ATRP synthesis of well-defined poly([2-dimethylamino]ethyl methacrylate) (PDMAEMA) is achievable under fully aqueous conditions within four hours with $Đ < 1.2$. Using TPMA and $CuCl_2$ at equimolar ratios, this facile synthesis is achievable with near quantitative conversion without detriment to the final MWD. This approach marks not only an improvement in MWD control from previously described aqueous ATRP approaches ($Đ > 1.4$) but also a significant reduction in reaction time, as $t > 8$ hr are often required for mixed solvent systems. Although MWDs do gradually broaden as target molecular weights increases, narrow MWDs ($Đ < 1.3$) are maintained below ca. 50 kDa, with M_N

up to 100 kDa still attainable with only moderate broadening of final MWDs ($Đ < 1.5$). This system displays a relative insensitivity to initiator choice by inducing a halide exchange, introducing a means to eliminate this variable as a design consideration for dictating control over the MWD of the final product; future efforts should further explore and confirm the mechanism for this behavior. Finally, this system exhibits a significant resilience to dissolved oxygen, with syntheses without prior degassing showing little to no effect on the breadth of the final MWD. This tolerance is retained even upon addition of secondary or tertiary aliquots of monomers for chain extensions, providing easily accessible methods for the synthesis of hydrophilic block copolymers. The oxygen insensitivity for this method provides a particularly attractive option for eliminating degassing protocols in larger scale reactions such as would be needed for commercial applications. Though low end group retention at high conversion limits the accessibility of block copolymers and other more complex architectures, these optimized reaction conditions result in a robust method to synthesize well-defined PDMAEMA, with the potential for scale-up to larger batch sizes and extension to other tertiary amine methacrylate monomers.

In particular, the systematic evaluation of the ligand, initiator, Cu^{II} concentration, reaction temperature, and supporting halide concentration allowed for an understanding of the critical reaction parameters for controlled Cu^0-mediated ATRP reactions using water as the solvent:

- Ligand: Aromatic amine ligands demonstrate greater control over the ATRP equilibrium, yielding narrower MWDs and higher I_{eff}.

- Initiator: Reactions demonstrate a relatively low sensitivity to initiator structure compared to previous ATRP systems, though initiator solubility does limit I_{eff} for more hydrophobic initiators.

45

- Temperature: Reactions at 2 °C demonstrate narrower MWDs and higher conversion than those at room temperature, with higher I_{eff} confirming an improved retention of active chains during polymerization.

- Cu^{II}: Increasing Cu^{II} loading to equimolar relative to ligand decreases Đ and increases I_{eff} compared to 1:4 loading previously described in literature for other monomers.

- Supporting halide: Increasing [Cl$^-$] from 0.3M to 1M decreases Đ and increases I_{eff}, attributed to the charge neutralization of DMAEMA.

- Cu^{0}: Increasing Cu^{0} surface area accelerates the reaction (ca. ½ reaction order) by providing additional catalyst surface area, yielding 95% conversion in 4 hours with little detriment to I_{eff} or Đ.

This work has been submitted and accepted in part for publication in Macromolecules, DOI 10.1021/acs.macromol.1c01234.

2.6   References

1.   Boyer, C., Corrigan, N.A., Jung, K., Nguyen, D., Nguyen, T.K., Adnan, N.N., Oliver, S., Shanmugam, S., and Yeow, J., *Copper-Mediated Living Radical Polymerization (Atom Transfer Radical Polymerization and Copper(0) Mediated Polymerization): From Fundamentals to Bioapplications.* Chem. Rev., 2016. **116**(4): p. 1803-949. DOI: 10.1021/acs.chemrev.5b00396.
2.   Wei, M., Gao, Y., Li, X., and Serpe, M.J., *Stimuli-responsive polymers and their applications.* Polym. Chem., 2017. **8**(1): p. 127-143. DOI: 10.1039/c6py01585a.
3.   Zhang, Q., Weber, C., Schubert, U.S., and Hoogenboom, R., *Thermoresponsive polymers with lower critical solution temperature: from fundamental aspects and measuring techniques to recommended turbidimetry conditions.* Materials Horizons, 2017. **4**(2): p. 109-116. DOI: 10.1039/c7mh00016b.

4.	Mohammadi, M., Salami-Kalajahi, M., Roghani-Mamaqani, H., and Golshan, M., *Effect of molecular weight and polymer concentration on the triple temperature/pH/ionic strength-sensitive behavior of poly(2-(dimethylamino)ethyl methacrylate).* Int. J. Polym. Mater. Polym. Biomater., 2017. **66**(9): p. 455-461. DOI: 10.1080/00914037.2016.1236340.

5.	Plunkett, K.N., Zhu, X., Moore, J.S., and Leckband, D.E., *PNIPAM chain collapse depends on the molecular weight and grafting density.* Langmuir, 2006. **22**(9): p. 4259-66. DOI: 10.1021/la0531502.

6.	Pan, X., Fantin, M., Yuan, F., and Matyjaszewski, K., *Externally controlled atom transfer radical polymerization.* Chemical Society Reviews, 2018. **47**(14): p. 5457-5490. DOI: 10.1039/C8CS00259B.

7.	Ribelli, T.G., Lorandi, F., Fantin, M., and Matyjaszewski, K., *Atom Transfer Radical Polymerization: Billion Times More Active Catalysts and New Initiation Systems.* Macromol Rapid Commun, 2019. **40**(1): p. e1800616. DOI: 10.1002/marc.201800616.

8.	Matyjaszewski, K., *Atom Transfer Radical Polymerization (ATRP): Current Status and Future Perspectives.* Macromolecules, 2012. **45**(10): p. 4015-4039. DOI: 10.1021/ma3001719.

9.	Fantin, M., Isse, A.A., Venzo, A., Gennaro, A., and Matyjaszewski, K., *Atom Transfer Radical Polymerization of Methacrylic Acid: A Won Challenge.* J. Am. Chem. Soc., 2016. **138**(23): p. 7216-9. DOI: 10.1021/jacs.6b01935.

10.	Tang, W. and Matyjaszewski, K., *Effects of Initiator Structure on Activation Rate Constants in ATRP.* Macromolecules, 2007. **40**(6): p. 1858-1863. DOI: 10.1021/ma062897b.

11.	Konkolewicz, D., Wang, Y., Zhong, M., Krys, P., Isse, A.A., Gennaro, A., and Matyjaszewski, K., *Reversible-Deactivation Radical Polymerization in the Presence of Metallic Copper. A Critical Assessment of the SARA ATRP and SET-LRP Mechanisms.* Macromolecules, 2013. **46**(22): p. 8749-8772. DOI: 10.1021/ma401243k.

12.	Zhang, Q., Wilson, P., Li, Z., McHale, R., Godfrey, J., Anastasaki, A., Waldron, C., and Haddleton, D.M., *Aqueous copper-mediated living polymerization: exploiting rapid disproportionation of CuBr with Me6TREN.* J. Am. Chem. Soc., 2013. **135**(19): p. 7355-63. DOI: 10.1021/ja4026402.

13.	Fantin, M., Isse, A.A., Gennaro, A., and Matyjaszewski, K., *Understanding the Fundamentals of Aqueous ATRP and Defining Conditions for Better Control.* Macromolecules, 2015. **48**(19): p. 6862-6875. DOI: 10.1021/acs.macromol.5b01454.

14.	Cordeiro, R.A., Rocha, N., Mendes, J.P., Matyjaszewski, K., Guliashvili, T., Serra, A.C., and Coelho, J.F.J., *Synthesis of well-defined poly(2-(dimethylamino)ethyl methacrylate) under mild conditions and its co-polymers with cholesterol and PEG using Fe(0)/Cu(ii) based SARA ATRP.* Polym. Chem., 2013. **4**(10). DOI: 10.1039/c3py00190c.

15.	Huang, T., Liu, H., Liu, P., Liu, P., Li, L., and Shen, J., *Zwitterionic copolymers bearing phosphonate or phosphonic motifs as novel metal-anchorable anti-fouling coatings.* J. Mater. Chem. B, 2017. **5**(27): p. 5380-5389. DOI: 10.1039/c7tb01017f.

16.	Augustine, K.F., Ribelli, T.G., Fantin, M., Krys, P., Cong, Y., and Matyjaszewski, K., *Activation of alkyl halides at the Cu0 surface in SARA ATRP: An assessment of reaction*

order and surface mechanisms. J. Polym. Sci., Part A: Polym. Chem., 2017. **55**(18): p. 3048-3057. DOI: 10.1002/pola.28585.

17.   Lligadas, G., Grama, S., and Percec, V., *Single-Electron Transfer Living Radical Polymerization Platform to Practice, Develop, and Invent.* Biomacromolecules, 2017. **18**(10): p. 2981-3008. DOI: 10.1021/acs.biomac.7b01131.

18.   Dong, H. and Matyjaszewski, K., *ARGET ATRP of 2-(Dimethylamino)ethyl Methacrylate as an Intrinsic Reducing Agent.* Macromolecules, 2008. **41**(19): p. 6868-6870. DOI: 10.1021/ma8017553.

19.   Jiang, X., van der Horst, A., van Steenbergen, M.J., Akeroyd, N., van Nostrum, C.F., Schoenmakers, P.J., and Hennink, W.E., *Molar-mass characterization of cationic polymers for gene delivery by aqueous size-exclusion chromatography.* Pharm. Res., 2006. **23**(3): p. 595-603. DOI: 10.1007/s11095-006-9574-4.

20.   Pei, Y. and Lowe, A., *Polymerization-induced self-assembly: Ethanolic RAFT dispersion polymerization of 2-phenylethyl methacrylate.* Polymer Chemistry, 2014. **5**: p. 2342-2351. DOI: 10.1039/c3py01719b.

21.   Zeng, F., Shen, Y., Zhu, S., and Pelton, R., *Atom transfer radical polymerization of 2-(dimethylamino)ethyl methacrylate in aqueous media.* J. Polym. Sci., Part A: Polym. Chem., 2000. **38**(20): p. 3821-3827. DOI: 10.1002/1099-0518(20001015)38:20<3821::Aid-pola130>3.0.Co;2-g.

22.   Jones, G.R., Whitfield, R., Anastasaki, A., Risangud, N., Simula, A., Keddie, D.J., and Haddleton, D.M., *Cu(0)-RDRP of methacrylates in DMSO: importance of the initiator.* Polym. Chem., 2018. **9**(18): p. 2382-2388. DOI: 10.1039/c7py01196b.

23.   Matyjaszewski, K., Shipp, D.A., Wang, J.-L., Grimaud, T., and Patten, T.E., *Utilizing Halide Exchange To Improve Control of Atom Transfer Radical Polymerization.* Macromolecules, 1998. **31**(20): p. 6836-6840. DOI: 10.1021/ma980476r.

24.   Peng, C.-H., Kong, J., Seeliger, F., and Matyjaszewski, K., *Mechanism of Halogen Exchange in ATRP.* Macromolecules, 2011. **44**(19): p. 7546-7557. DOI: 10.1021/ma201035u.

25.   Lide, D.R., *Dissociation Constants of Organic Acids and Bases*, in *CRC Handbook of Chemistry*. 2005, CRC Press: Boca Raton, FL. p. 8-52.

26.   Jones, G.R., Li, Z., Anastasaki, A., Lloyd, D.J., Wilson, P., Zhang, Q., and Haddleton, D.M., *Rapid Synthesis of Well-Defined Polyacrylamide by Aqueous Cu(0)-Mediated Reversible-Deactivation Radical Polymerization.* Macromolecules, 2016. **49**(2): p. 483-489. DOI: 10.1021/acs.macromol.5b01994.

27.   Tom, J., Hornby, B., West, A., Harrisson, S., and Perrier, S., *Copper(0)-mediated living radical polymerization of styrene.* Polym. Chem., 2010. **1**(4): p. 420-422. DOI: 10.1039/b9py00382g.

28.   Fan, Y., Migliore, N., Raffa, P., Bose, R.K., and Picchioni, F., *Synthesis of Zwitterionic Copolymers via Copper-Mediated Aqueous Living Radical Grafting Polymerization on Starch.* Polymers (Basel), 2019. **11**(2): p. 192. DOI: 10.3390/polym11020192.

29.   van de Wetering, P., Zuidam, N.J., van Steenbergen, M.J., van der Houwen, O.A.G.J., Underberg, W.J.M., and Hennink, W.E., *A Mechanistic Study of the Hydrolytic Stability*

of Poly(2-(dimethylamino)ethyl methacrylate). Macromolecules, 1998. **31**(23): p. 8063-8068. DOI: 10.1021/ma980689g.

30. Harrisson, S., Couvreur, P., and Nicolas, J., *Comproportionation versus Disproportionation in the Initiation Step of Cu(0)-Mediated Living Radical Polymerization.* Macromolecules, 2012. **45**(18): p. 7388-7396. DOI: 10.1021/ma301034t.

31. Ribelli, T.G., Augustine, K.F., Fantin, M., Krys, P., Poli, R., and Matyjaszewski, K., *Disproportionation or Combination? The Termination of Acrylate Radicals in ATRP.* Macromolecules, 2017. **50**(20): p. 7920-7929. DOI: 10.1021/acs.macromol.7b01552.

32. Matyjaszewski, K., Dong, H., Jakubowski, W., Pietrasik, J., and Kusumo, A., *Grafting from surfaces for "everyone": ARGET ATRP in the presence of air.* Langmuir, 2007. **23**(8): p. 4528-31. DOI: 10.1021/la063402e.

CHAPTER III: Improved End Group Retention for Cu^0-Mediated ATRP of PDMAEMA Under

Mildly Acidic Conditions

3.1 Abstract

Cu^0-mediated ATRP has been demonstrated to yield well-defined polymers for an ever-growing list of monomers, with narrow and reproducible molecular weight distributions. However, many aqueous systems have noted a low retention of active end groups upon chain extension, with inactive end groups accumulating over the course of polymerization even for primary polymerizations with $Đ < 1.2$. By modulating solution to mildly acidic conditions (*pH* 4), this study demonstrates high end group fidelity for poly(2-[dimethylamino]ethyl methacrylate) (PDMAEMA), a polymer that has traditionally shown low end group retention at high conversion in aqueous systems. Homopolymer chain extensions show excellent agreement with expected molecular weight shifts, with little to no broadening of the molecular weight distribution observed. NMR and FTIR results demonstrate integration of sulfonate-pendant methacrylates as a model block copolymer, yielding fully zwitterionic AB type copolymers with a facile one-pot approach.

3.2 Introduction

One of the most powerful aspects of reversible deactivation radical polymerization (RDRP) techniques is the retention of active end groups, allowing for subsequent chain extension for the synthesis of block copolymers or other complex polymer architectures. RDRP techniques have been used to synthesize novel polymer architectures with a far-reaching span of physical and chemical properties, with applications in targeted drug delivery, water purification, and among others.[1-6] However, the desire to push RDRP reactions into more economically and

environmentally friendly conditions often favor the use of aqueous conditions where possible, in accordance with the 12 principles of green chemistry. This introduces mechanisms for end group loss through hydrolysis, leading to poor end group retention and poor chain extensions upon addition of secondary monomers, even for systems with well-defined primary polymerizations.[5,7,8] This is especially true for atom transfer radical polymerization (ATRP), where active chain ends are in the form of alkyl halides which act as good leaving groups for hydrolysis.

Though many routes have been explored in effort to combat this effect, one that is still relatively unexplored is the modulation of *pH*. In recent years, solution *pH* has been explored in the context of ATRP to extend this system to acidic monomers such as methacrylic acid, which have traditionally been inaccessible due to cyclization side reactions.[9] However, the efforts to develop successful synthesis methods for these monomers have revealed ligands that are resilient to polymerization even under highly acidic conditions (*pH* < 1), though this is often associated with a slow broadening of MWDs, with *Đ* > 1.4 often observed.[9-11] These systems thus present a promising opportunity for the exploration of intermediate *pH*, which would be expected to minimize the effects of hydroxide-catalyzed hydrolysis without the broadening of MWDs observed at low *pH*. This also offers greater flexibility in the design of polymerization schemes, as the associated design considerations of operation under highly acidic conditions can be avoided if they are not strictly necessary.

In this study, aqueous ATRP polymerizations are presented to explore the effect of *pH* modulation on overall control of MWDs. Optimizations target polymerization which maintains i) narrow MWDs (*Đ* < 1.2); ii) high conversion (>90% of initial monomer); and iii) high retention

of active chains after primary polymerization. Sequential polymer chain extensions are used to assess the retention of active terminal halides at varied *pH*. PDMAEMA is used as a model polymer that has been previously shown to exhibit poor end group retention under aqueous conditions.[7] Polymerizations near neutral *pH* yield poorly defined polymerizations, with lowered conversion and poor end group retention as compared to prior polymerizations at the native *pH* of 9.6. However, polymerizations at mildly acidic conditions (ca. *pH* 4) demonstrate well-defined MWDs, with excellent chain extension demonstrated at near quantitative conversion. Use of a bromide to chloride halide exchange affords rapid initiation, with the exchange to chloride end groups providing further resilience to hydrolysis. To the author's knowledge, these results represent the greatest retention of active end groups for this polymer under aqueous conditions. Acidic conditions also extend this system to more hydrophobic amine-pendant monomers in 2-(diethylamino)ethyl methacrylate and 2-(diisopropyl)ethyl methacrylate, as well as anionic 3-sulfopropyl methacrylate. Block copolymerization of PDMAEMA-b-SPMA is further demonstrated, demonstrating the accessibility of zwitterionic and other complex polymer architectures readily accessible.

3.3   Materials and Methods

3.3.1   Materials

Toluene (CAS 108-88-3; 99.5%) and sodium phosphate, dibasic (CAS 7558-79-4; 99%) were purchased from Fisher Scientific. *α*-bromophenylacetic acid (BPAA, CAS 4870-65-9; 98%), 2-(diethylamino)ethyl methacrylate (CAS 105-16-8; 98%), 2-(diisopropylamino)ethyl methacrylate (CAS 16715-83-6; 97%), 3-sulfopropyl methacrylate, potassium salt (CAS 31098-21-2; 98%),

52

copper(II) chloride (CAS 7447-39-4; 98%), glacial acetic acid (CAS 64-19-7; 99%), PDMAEMA (M_N = 10 kDa, Đ ≤ 1.4), sodium hydroxide (CAS 1310-73-2; 97%), and triethylamine (CAS 121-44-8; 99.7%) were purchased from Sigma-Aldrich. Poly(ethylene glycol) (PEG, CAS 25322-68-3) and poly(methacrylic acid) (PMAA, CAS 25086-15-1) standards for gel permeation chromatography were purchased from Scientific Polymer Products. 2-(dimethylamino)ethyl methacrylate (DMAEMA, CAS 2867-47-2; 98%) was purchased from TCI America. 2-bromoisobutyric acid (BiBA, CAS 2052-01-9; 98%), hydrochloric acid (CAS 7647-01-0; 36.5%), methanol (CAS 67-56-1; 99.8%), sodium chloride (CAS 7647-14-5; 98%), and tris(2-pyridylmethyl)amine (TPMA, CAS 16858-01-8; 98%) were purchased from VWR. Type I ultrapure water (18.2 MΩ) was generated using a Millipore Synergy UV Water Purification System. Copper wire (d = 0.4 mm) was provided by the University of Oklahoma. DMAEMA, DEAEMA, and DPAEMA were passed over activated poly(styrene-co-divinyl benzene) resin (CAS 9003-70-7) before use to remove MEHQ inhibitors. All other reagents were used as received.

3.3.2   pH-Modulated Synthesis of PDMAEMA

Syntheses of PDMAEMA were carried out at 2 °C in 10 mL test tubes. All polymerizations were conducted with [DMAEMA]:[Initiator]:[Ligand]:[CuCl$_2$] = 100:1:0.4:0.4, [NaCl] = 1 M, [DMAEMA]$_0$ = 2 M, and Cu^0 added at 0.5 cm^2 mL^{-1} of solution, in accordance with previously optimized conditions. A representative synthesis is summarized as follows: in a clean vial, a pre-determined aliquot of concentrated hydrochloric acid was added to Type I ultrapure water, with a total volume of 4 mL. HCl concentration was varied between 0.3 M and 1.9 M during preliminary

studies. 2.5 mL (14.8 mmol) of DMAEMA was then added to the water-HCl mixture which was capped and gently agitated to mix the components. *pH* was measured and adjusted as necessary using 1 M HCl and 1 M NaOH. Additional Type I ultrapure water was then added to the monomer mixture to bring the final volume to 7.5 mL. 8.0 mg (59 μmol) of $CuCl_2$, 17.2 mg (59 μmol) of TPMA, and 438.3 mg (7.5 mmol) of NaCl were then added to a clean, dry test tube. This monomer mixture was then transferred to the test tube with the solid reagents, which was capped with a rubber septum and vortexed to homogenize. The reaction mixture was then placed in a 2 °C water bath to pre-cool the solution. In a separate test tube, a 33.5 cm length of copper wire ($d = 0.4$ mm; surface area/volume $= 0.5$ cm^2 mL^{-1}) was immersed in a 1:1 mixture of 35% HCl and methanol to fully reduce the copper surface. After 10-15 minutes, the HCl-methanol mixture was decanted, and then the copper was rinsed repeatedly with methanol and dried under N_2. The reaction mixture was uncapped and 31.9 mg of BPAA (148 μmol) was added, followed by vortexing to homogenize. The copper wire was then added to the test tube, and the rubber septa replaced. Reaction vessels were immersed in the 2 °C water bath for the duration of the polymerization. The reaction mixture was continuously sparged with N_2 during the reaction to maintain the inert atmosphere and mix the reaction mixture. Aliquots of 100 μL were withdrawn at regular time points to track conversion and MWD over the course of the reaction. Aliquots were diluted to a total volume of 1.5 mL using Type I ultrapure water. To quench the reactions, reaction vessels were uncapped and decanted from the copper wire into clean and dry vials and stored in a refrigerator overnight before further processing. Polymer products were purified by precipitation with heating above the lower critical solution temperature (LCST). After purification, polymers were dried in vacuo and stored until further characterization.

3.3.3   PDMAEMA Chain Extensions

Polymer chain extensions were conducted as a one-pot, sequential polymerization. After the primary polymerization, reaction vessels were uncapped, and a new aliquot of monomer added. Monomer aliquots were prepared with TPMA, Cu^{II}, and NaCl to maintain the concentrations present in the primary polymerization. A new length of Cu^0 was added with monomer aliquots to maintain a constant SA_{Cu}/V. The monomer solutions were not degassed prior to addition to the reaction vessel, in accordance with the high tolerance to oxygen previously demonstrated.

3.3.4   Characterization

3.3.4.1   Gel Permeation Chromatography

Gel permeation chromatography (GPC) was conducted on a Shimadzu Prominence HPLC with an Agilent Aquagel-OH Mixed H and Aquagel-OH 30 column bank. Analyses for PDMAEMA, PDEAEMA, and PDPAEMA use a 0.3 M sodium acetate, 0.15M triethylamine buffer ($pH = 4.0$) as the mobile phase, as previously established. Analyses for PSPMA use a 0.07 M sodium phosphate (dibasic), 0.2 M sodium chloride buffer ($pH = 9.0$). Chromatograms were collected with a Waters R410 differential refractometer and a Wyatt DAWN F light scattering detector. The light scattering detector was calibrated to the Rayleigh ratio of toluene. Refractometer response was calibrated using low polydispersity PEG standards. The incremental refractive index (dn/dc) for PDMAEMA was taken to be 0.20 mL/g as previously described in literature.[12] All chromatograms were collected using an eluent flow rate of 1 mL/min. Additional details for molecular weight calibration are discussed in Appendix A.3. Peak fitting was conducted using

Fityk curve fitting software (v. 1.3.1), assuming an exponentially modified Gaussian distribution for all peaks to capture any tailing towards low molecular weight.

3.3.4.2   Nuclear Magnetic Resonance

Nuclear magnetic resonance (NMR) spectra were collected using a Varian VNMRS 500 MHz spectrometer and analyzed using MestReNova software (v. 12.0.2). All NMR samples were dissolved in 10% D_2O-90% H_2O. Spectra were collected with H_2O solvent suppression using a total of 8 scans. A relaxation delay of 40 seconds was used to allow alkene peaks of unreacted monomer to relax between acquisitions. Chemical shifts were assigned according to values previously reported in literature.[13] Conversion is calculated based on the ratio of monomer C=C-H peak area (δ = 5.5-6 ppm) to the area of peaks corresponding to monomer -CH_3 and polymer -CH_2- (δ = 1.4-2 ppm). For DMAEMA, DEAEMA, and DPAEMA the overall conversion is calculated as follows, with additional details provided Appendix A.1.

$$Conv.(\%) = \frac{\delta_{1.4-2} - 3(\delta_6 + \delta_{5.5})}{\delta_{1.4-2} - \delta_6 - \delta_{5.5}}$$

For SPMA, conversion is instead calculated to account for the C-CH_2-C in the propyl pendant group, with the final calculation given by:

$$Conv.(\%) = \frac{\delta_{1.4-2} - 5\delta_6}{\delta_{1.4-2} - \delta_6}$$

3.4   Results and Discussion

3.4.1   Initial *pH* Modulation of Cu⁰-ATRP Syntheses

Reaction conditions for preliminary *pH*-modulated syntheses are summarized in Table III-1, with native *pH* included for comparison. These initial syntheses explore down to *pH* 6.5,

representing a ca. 10^3-fold reduction in [OH⁻]. Solution *pH* was modified by the addition of hydrochloric acid, with initial reactions prepared with predetermined [HCl] and *pH* measured after polymerization. However, DMAEMA-water mixtures for *pH* 6.5 syntheses were prepared by dropwise addition of HCl to *pH* 7 before the addition of the remaining reagents, as these conditions sit close to the end of the buffering region for DMAEMA (pK_a = 8.5) and will be more susceptible to steep changes in *pH* with even small experimental error. Though the addition of the acidic initiator does slightly shift the overall *pH* to 6.5*,* this approach was chosen to limit the impact of any hydrolysis or halide exchange for the bromide-functional initiator prior to polymerization. NaCl was added to supplement the total [Cl-] to 1 M, matching the optimized halide concentration at native *pH.* Interestingly, while these results demonstrate an initially well-maintained MWD for primary polymerizations, these polymerizations demonstrate a steady decrease in overall conversion and initiator efficiency, with I_{eff} < 30% at *pH* 8.1. Polymerization at *pH* 6.5 initially yields nearly no polymerization, with only 10% conversion observed in 4 hours (Table III-1, Entry 4). However, given the high concentration of HCl needed to adjust the *pH* for these conditions, the initial conditions were included with no added NaCl. Repetition of this polymerization with the inclusion of 1M NaCl (Table III-1, Entry 5) does improve conversion, with 47% conversion attained in 4 hours, suggesting the high concentration of protonated DMAEMA leads to electrostatic competition for the chloride ions in solution. However, even with this adjustment these conditions still yield mild broadening of the observed MWD to *Đ* = 1.31 and slowed conversion relative to native *pH*.

Table III-1: Synthesis conditions and molecular weight distributions for pH modulated ATRP of PDMAEMA.[a]

Entry	[HCl] (M)	pH	[NaCl] (M)	Conv.[b] (%)	$M_{N,theo}$ (kDa)	M_N[c] (kDa)	Đ[c]	I_{eff}[d] (%)
1	0	9.6	1	95	12.9	22.9	1.25	56
2	0.3	8.6	0.7	74	11.6	24.9	1.29	47
3	0.6	8.1	0.4	43	6.8	23.2	1.23	29
4	1.9	6.5	0	10	1.6	6.2	1.39	26
5	1.9	6.5	1	47	7.4	16.6	1.31	44
6[e]	0.3	8.6	0.7	58	9.1	23.1	1.23	50

[a]: All polymerizations conducted with [DMAEMA]:[BPAA]:[TPMA]:[CuCl₂] = 100:1:0.4:0.4, [DMAEMA]$_0$ = 2 M, T = 2 °C, and SA_{Cu}/V = 0.5 cm^2 mL^{-1}. [b]: measured by NMR. [c]: measured by aqueous GPC. [d]: I_{eff} = $M_{N,theo}/M_N$. [e]: SA_{Cu}/V = 0.1 cm^2 mL^{-1}.

Intermediate time points were analyzed for the polymerization at *pH* 8.6 to assess the overall kinetics of this polymerization, as it yields the greatest overall conversion while retaining moderately well-defined MWDs. This data is presented in Figure III-1. Though the first order rate plot displays a linear trend, overlaying this plot with that for the optimized conditions at native shows a sharp decrease in k_{app}, with 0.22 hr-1 observed at *pH* 8.6 as compared to 0.83 hr-1 at native *pH*. Interestingly however, the conversion is identical at the first time point of one hour, suggesting initially similar kinetic until ca. 40% conversion. Polymerization was then repeated at *pH* 8.6 with the lower Cu^0 loading of 0.1 cm^2 mL^{-1}, to assess an additional time point at lower conversion (Table III-1, Entry 6). These results demonstrate a similar behavior, with identical conversion at t = 1 hr, and the rates diverging after 2 hours. Importantly, these points of deviation between the different Cu^0 loadings occur at similar conversion, corresponding to a deviation above ca. 40%

conversion. This apparent two-step equilibrium is not fully understood and may signal a sharp

decrease in the number of active chain ends to maintain propagation of the reaction.
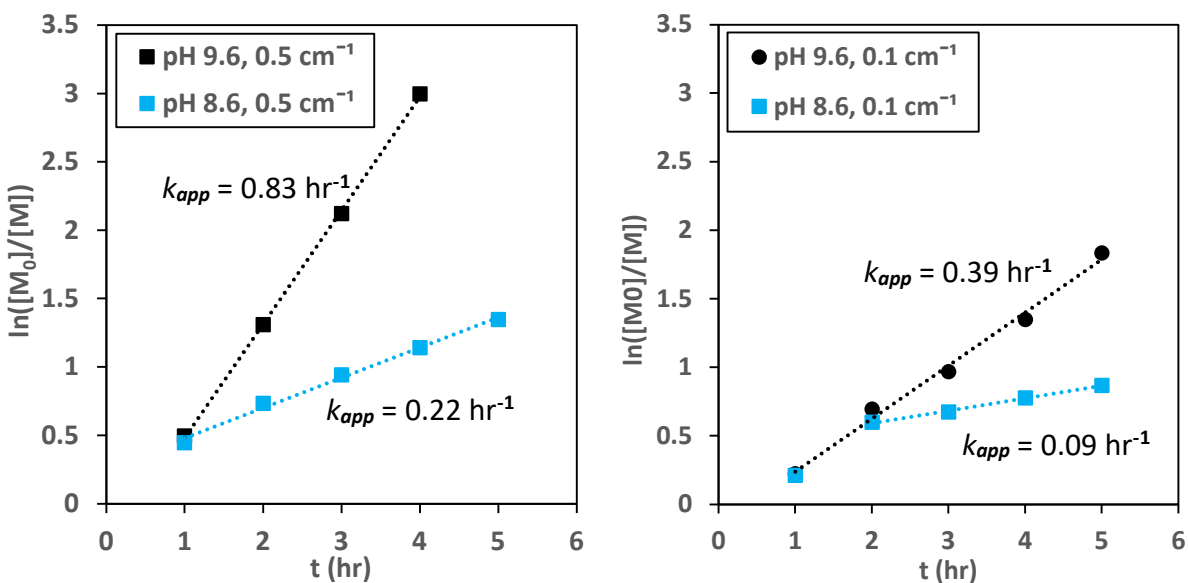
Figure III-1: 1st order rate plots for polymerization at pH 8.6. Left: polymerization with SA_{Cu}/V = 0.5 cm^2 mL^{-1}. Right: polymerization with SA_{Cu}/V = 0.1 cm^2 mL^{-1}.

3.4.1.1   Chain Extensions

To test for the retention of active end groups, syntheses at *pH* 8.6 were repeated for chain

extension experiments. The GPC traces for the primary and chain extended polymerizations are

presented in Figure III-2. These results confirm the interpretation of accumulating inactive chains,

despite the decreasing [OH$^-$] from native *pH*. There is a nominal shift to higher molecular weight,

but most of the chromatogram shows minimal shift from the primary MWD.   When

chromatograms are deconvoluted with peak fitting (Figure III-2), comparison of integrated areas

indicates only 37% of the total polymer chains successfully extend. This low extension indicates

a large proportion of terminated chains, likely giving rise to the observed decrease in the rate of conversion above 40% conversion.
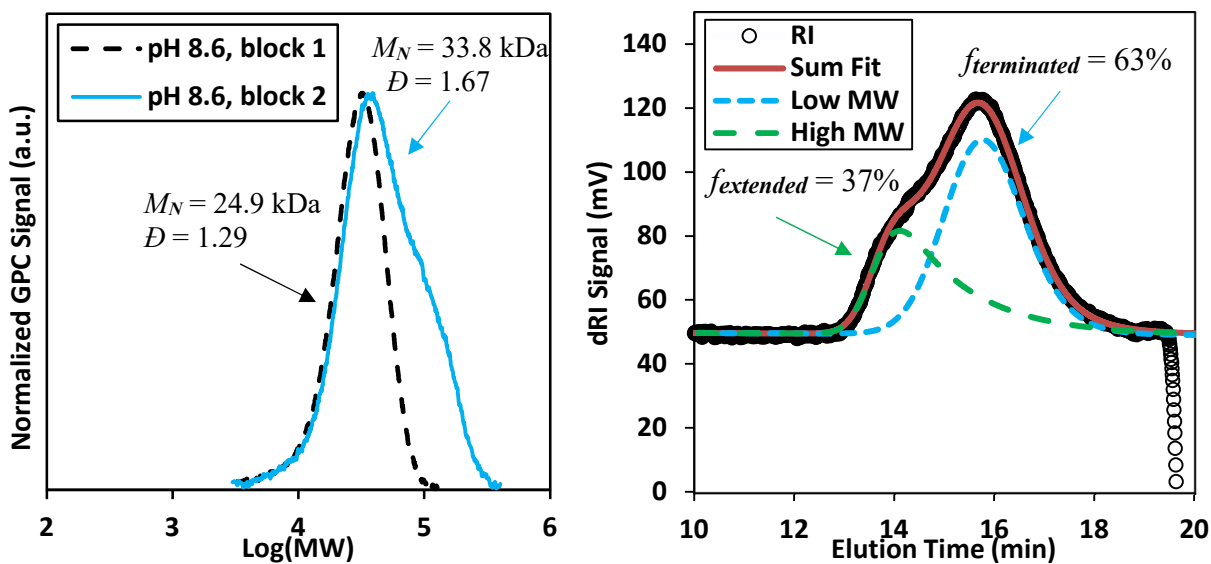
Figure III-2. GPC analysis for primary and chain extension polymerization at *pH* 8.6 (left), with peak deconvolution for end group quantitation (right).

These results are surprising, as they indicate a sharp drop in end group retention despite the ca. 10-fold reduction in [OH⁻]. This effect may be coupled to the increase in solubility accompanied by protonation of the tertiary amine pendant groups. At high *pH*, the high hydrophobicity of the polymer backbone may serve to shield the active end groups from hydrolytic attack. Indeed, this mechanism is known to shield the esters in PDMAEMA from hydrolysis, relative to monomeric DMAEMA.[14,15] As the hydrophilicity increases with protonation of the pendant amine groups, this shielding effect could be reduced to enable a faster rate of hydrolysis. This could be accelerated by a related phenomenon observed by van de Wetering, et al., where the rate of ester hydrolysis in monomeric DMAEMA shows a plateau near the *pK$_a$* of 8.4 due to a trade-off between

60

hydroxide concentration and monomer protonation, which increases local hydroxide concentration around the monomer.[14]

3.4.2   Polymerization Under Acidic Conditions

These data suggest the need to further reduce *pH* to retain proper control of the polymerization. A new polymerization was designed for *pH* 4 to explore the effect of further reducing the overall [OH⁻], with results summarized in Table III-2. This *pH* was chosen based on the results from van de Wetering et. al, where the rate of DMAEMA monomer hydrolysis shows a global minimum near *pH* 3-4, minimizing the impact of both acid- and base-catalyzed hydrolysis.[14] Furthermore, though successful ATRP has been demonstrated under highly acidic conditions using monomers such as methacrylic acid, these are often accompanied by a broadening of MWDs, with often with Đ > 1.4.[9,11] Mildly acidic *pH* may then represent an opportunity to limit hydrolysis, while still maintaining a higher degree of control over the final MWD. This reaction mixture was prepared with DMAEMA-water mixture adjusted to *pH* 4 prior to the addition of catalyst and initiator, as with the polymerization at *pH* 6.5. The final *pH* for the reaction mixture was measured as 3.5 after the addition of the remaining components (Table III-2, Entry 1). This polymerization still demonstrates a broader MWD than at native *pH* (M_N = 17.6, Đ = 1.31) but does improve conversion to 86% in four hours, recovering from the <50% conversion at *pH* 7.1 and 8.1. Interestingly, this overall data does still suggest a slight decrease in overall control of polymerization as compared to native *pH*, observed as a gradual tailing toward low molecular weight (Figure III-3). However, the return of high conversion within the same four-hour reaction

does suggest a higher retention of active end groups, with the possibility for further optimizations to regain the narrow final MWD.

Table III-2: Polymerization conditions and molecular weight distributions for polymerizations optimized for BiBA under acidic conditions.[a]

Entry	[HCl]	pH	Initiators	t (hr)	Conv.[b] (%)	$M_{N,theo}$ (kDa)	M_N[c] (kDa)	Đ[c]	I_{eff}[d] (%)
1	2.1	3.5	BPAA	4	86	13.5	17.6	1.31	77
2	2.1	3.5	BiBA	3	98	15.4	23.3	1.16	66
3[e]	2.1[e]	3.5	BiBA	3	75	11.8	26.8	1.29	44
4	1.9	6.5	BiBA	4	59	9.3	45.2	1.36	21
5	0	9.6	BiBA	4	63	9.9	41.2	1.38	24

[a]: All polymerizations conducted with [DMAEMA]:[Initiator]:[TPMA]:[CuCl$_2$] = 100:1:0.4:0.4, [DMAEMA]$_0$ = 2 M, [NaCl] = 1 M, and T = 2 °C. [b]: measured by NMR. [c]: measured by aqueous GPC. [d]: $I_{eff} = M_{N,theo}/M_N$. [e]: [NaCl] = 0.

During reagent preparation for this synthesis, it was noted that BPAA was more difficult to fully disperse than at *pH* 9.6 or 6.5, giving cause for concern of solubility limitations as the carboxylic acid is protonated at the lowered solution *pH*. The polymerization was repeated using 2-bromoisobutyric acid (BiBA), to ensure that the hydrophobicity of the phenyl group is not the limiting factor for initiation (Table III-2, Entry 2). This polymerization shows excellent control, with Đ of 1.16 and M_N of 23.3 kDa attained in 3 hours, with 98% conversion. Furthermore, this result demonstrates similar I_{eff} to that obtained under previously optimized conditions for native *pH*, with 66% I_{eff} compared to 63% observed at native *pH*. These results suggest that BPAA is a poor initiator for ATRP at this lowered *pH*.
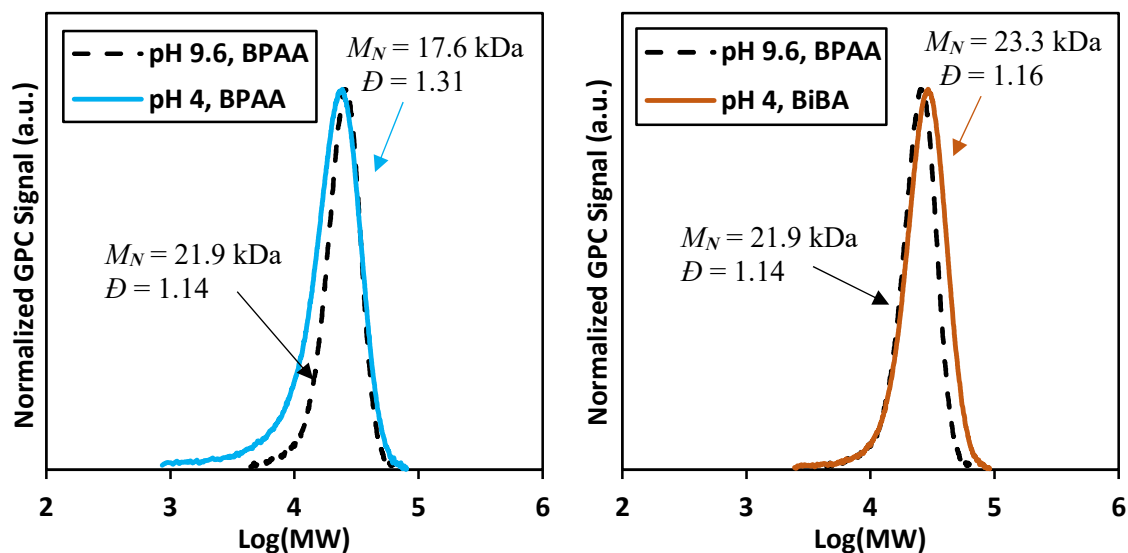
Figure III-3: Comparison of MWDs for PDMAEMA under optimized conditions at *pH* 9.6 and *pH* 4 with BPAA (left) and BiBA (right).

Interestingly, comparisons included to validate the performance of BiBA as an initiator at *pH* 7 and 9.6 yield poor control, with broader MWDs and $I_{eff} < 25\%$ in both cases (Table III-2, Entries 4 and 5; Figure III-4). These broadened MWDs are also a companied by a reduction in overall conversion, with only ca. 60% observed for both cases in a 4-hour polymerization. This is especially surprising for the *pH* 9.6 polymerization, as earlier polymerizations with less active initiators demonstrates little variation in the observed MWD between initiators with 10^3-fold difference in activity. Previously published results for methacrylic acid also demonstrate poor initiator efficiency for BiBA for *pH* < 2, suggesting a narrow window of accessibility for BiBA with methacrylic monomers.[9,11] Further investigation is required to validate the mechanism for the loss of initiator efficacy outside this window. Regardless, these overall results suggest the need

to bypass intermediate *pH* for these monomers, with neither BPAA nor BiBA yielding well-controlled polymerization near neutral *pH*.
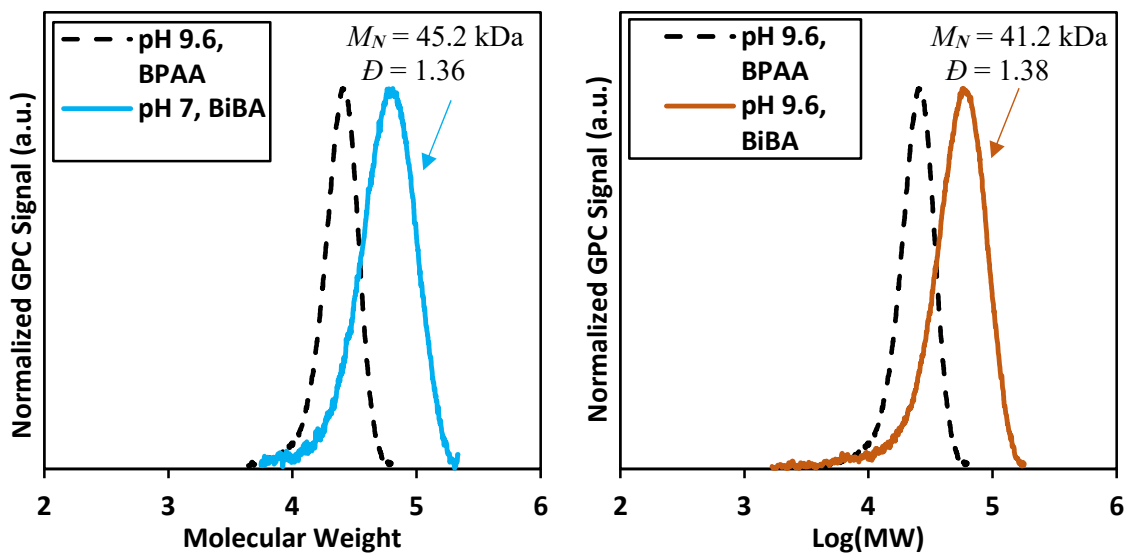
Figure III-4: Molecular weight distributions for PDMAEMA as synthesized with BiBA at pH 7 (left) and 9.6 (right).

3.4.2.1   Chain Extensions

Homopolymer chain extension was repeated for these newly optimized conditions. This synthesis demonstrates excellent chain extension, at near quantitative conversion (Table III-3, entry 2). The extension is accompanied by a slight broadening of MWD ($Đ = 1.20$), but there was no obvious sign of shouldering as observed at *pH* 9.6. Furthermore, with the addition of smaller blocks – adding an equivalent target D_P of 50 for each new block – $Đ$ were observed to continue to shrink even through the addition of a third aliquot of monomer, indicating high retention of active end groups (Table III-3, entries 3 and 4). This series of extensions also continues to demonstrate high conversion for each chain, with total measured conversion of 99% and 98%

64

measured for blocks two and three. This is accompanied by a gradual decrease in apparent I_{eff}, indicating a slow tailing towards low molecular weight due to accumulating inactive chains. However, the impact on the final MWD appears to be small, with most chains remaining in the active form.
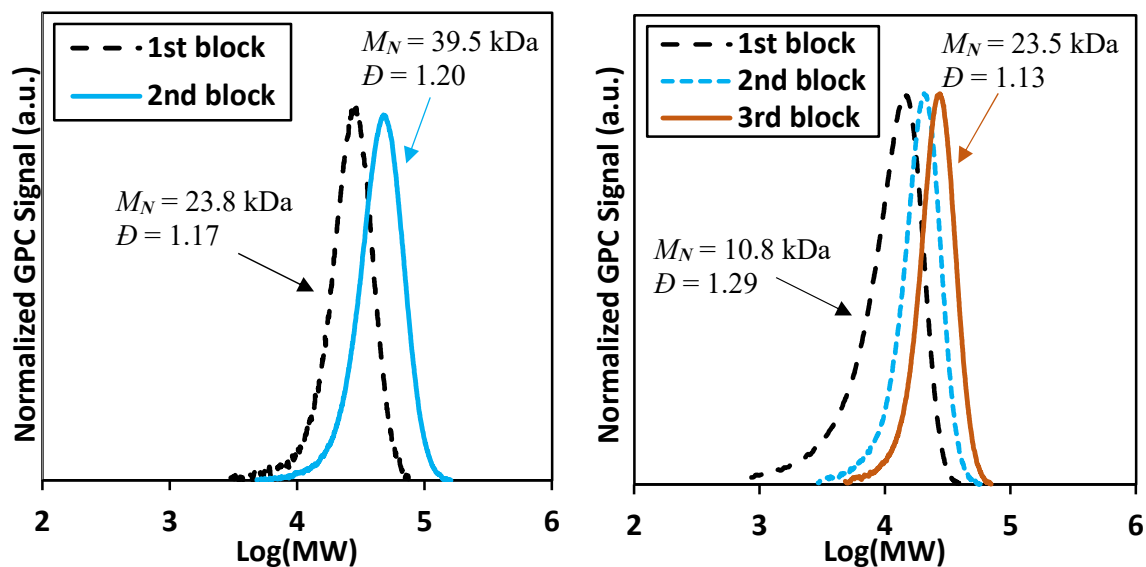
Figure III-5: GPC traces for chain extension experiments at *pH* 4. Left: targeting total D_P of 100 and 200. Right: targeting total D_P of 50, 100, and 150.

Further extensions were conducted to interrogate the importance of each component added with the secondary monomer spikes – that is, TPMA, Cu^{II}, and fresh Cu^0. Omission of the catalyst complex in monomer spikes yields successful chain extensions, with little qualitative difference observed. There is a slight broadening of the MWDs, with a *Đ* of 1.17 after the tertiary polymerization compared to 1.13 when additional Cu^{II}/TPMA is included. However, this effect appears to be minimal, with overall well-defined polymerizations still readily attainable through addition of Cu^0 alone. Omission of Cu^0 and catalyst both, however, yields poor control for the

chain extensions (Table III-3, Entry 8). The final MWD for this reaction is broadened to $Đ = 1.32$, with clear tailing observed towards low molecular weight that overlaps with the low molecular weight end of the primary polymerization chromatogram. Furthermore, this polymerization yields a decrease in the rate of conversion, with only 50% conversion observed in the same 3-hour reaction, suggesting the retention of the constant SA_{Cu}/V is the most important inclusion for maintaining well-defined chain extensions under these conditions.
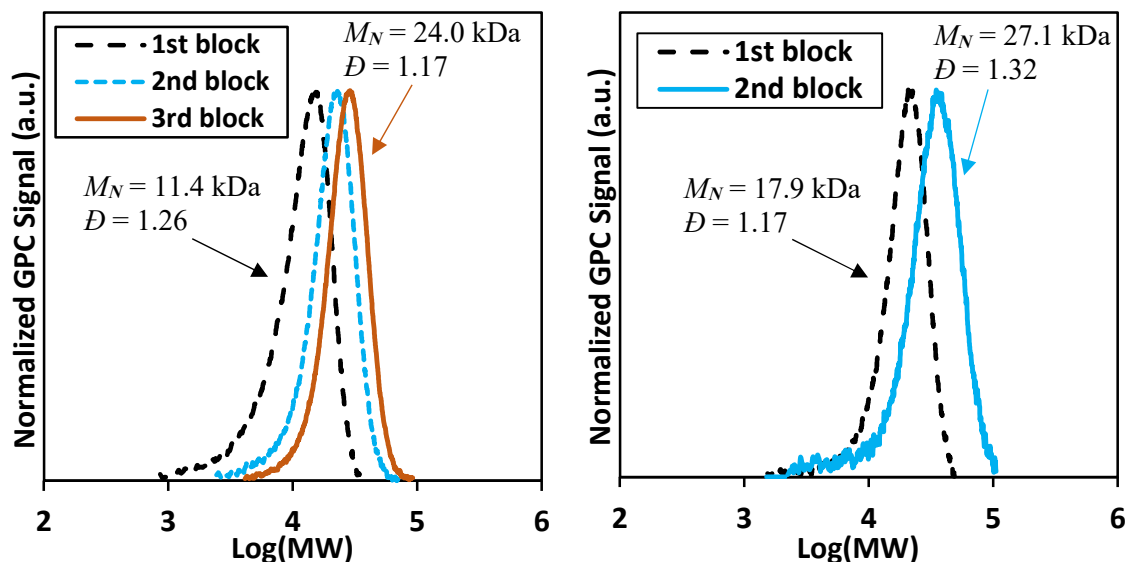
Figure III-6: GPC trace for chain extensions with omission of additional catalyst complex (left), and omission of additional catalyst complex and Cu^0 wire (right).

This is likely a result of saturation of the copper surface area by the additional monomer; with a surface atomic density of 10^{15} atoms cm^{-2}, the concentration of surface atoms can be calculated as:

$$S_{Cu} = 10^{15} \frac{atoms}{cm^2} * 0.5 \frac{cm^2}{mL} * \frac{10^3 mL}{L} * \frac{mol}{6.02 * 10^{23} atoms} = 8 * 10^{-7} \frac{mol}{L}$$

The concentration of reactants in solution is thus on the order of 10^6-fold greater than the available copper surface area, with [Monomer] = 2 M, [BPAA] = 0.02 M, and [TPMA] = 0.008 M. Effectively, the addition of an equivalent spike of monomer without the inclusion of additional copper wire serves to dilute the surface concentration of TPMA and dormant chains, slowing the rate of activation and thus the rate of polymerization overall. This mechanism then suggests competitive occupation of surface sites by DMAEMA units, either as the monomer or as individual pendant groups of the polymer localizing to the copper surface. The addition of copper wire with new monomer then maintains the equilibrium of adsorbed species at the Cu^0 interface, maintaining the same ATRP equilibrium.

To the authors' knowledge, these results represent the greatest retention of halide terminal groups under aqueous conditions for PDMAEMA, opening this system to the potential of well-defined block copolymers at high conversion, and likely represents a means of improving retention of active end groups across a wide range of monomers. In particular, the use of mildly acidic *pH* for Cu^0-mediated ATRP should provide a mechanism for minimizing the effects of end group hydrolysis without the associated broadening of MWDs often observed at *pH* < 2 (*Đ* > 1.4).[9,11]

Table III-3: Conditions and molecular weight distributions for PDMAEMA chain extensions.[a]

Entry	pH	Initiator	Starting M_N (kDa)	Added D_P	$M_{N,theo}$[c] (kDa)	Final M_N[d] (kDa)	Đ[e]
1	9.6	BPAA	19.7	100	35.4	31.9	1.39
2	8.6	BPAA	24.9	100	40.6	33.8	1.67
3	3.5	BiBA	23.8	100	39.5	39.4	1.20
4	3.5	BiBA	10.8	50	18.7	18.8	1.14
5	3.5	BiBA	18.8	50	26.6	23.5	1.13
6[f]	3.5	BiBA	11.4	50	19.2	18.8	1.19
7[f]	3.5	BiBA	18.8	50	26.6	24.0	1.17
8[g]	3.5	BiBA	17.9	100	33.6	27.1	1.32

[a]: All polymerizations were conducted with [Monomer]:[Initiator]:[TPMA]:[CuCl$_2$] = 100:1:0.4:0.4 and [Monomer]$_0$ = 2 M, with [NaCl] = 1 M. [b]: as measured by NMR. [c]: Assuming 100% conversion with 100% chain retention. [d]: as measured by GPC. [e]: I_{eff} = $M_{N,theo}$/M_N. [f]: [TPMA]$_{added}$ = [Cu^{II}]$_{added}$ = 0. [g]: [TPMA]$_{added}$ = [Cu^{II}]$_{added}$ = SA_{Cu}/V_{added} = 0.

3.4.3 Kinetics Analysis of Optimized Conditions

Polymerization was repeated with regular sampling to evaluate polymerization kinetics for the newly optimized conditions. These results demonstrate a sharp increase in the rate of polymerization, with 97% conversion attained in just 3 hours. This corresponds to an apparent rate constant of 1.5 hr^{-1}, nearly double that observed for optimized conditions at native *pH* (Figure III-7). There is a sharp drop in the rate of polymerization between 2 hours and 3 hours, corresponding to the region between 94 and 98% conversion. Polymerization solutions demonstrate high viscosity under these conditions, leading to a gradual increase in the size of the bubbles introduced into the reaction by the N$_2$ sparge. These larger bubbles likely decrease the

effective surface area of copper available at any given instant, leading to a drop in k_{app}. As such, this point is excluded for the calculation of k_{app}. This issue is expected to be less significant above the test tube scale, where better stirring and homogenizing options are available.

This accelerated rate of conversion indicates a shift in the ATRP equilibrium, with a higher steady state concentration of radicals available to propagate the polymerization. This phenomenon shows good agreement with previously demonstrated acceleration of kinetics in electrochemically mediated ATRP (eATRP) using TPMA, wherein k_{app} increases rapidly as *pH* decreases below ca. *pH* 5-6. In the context of eATRP, this acceleration is attributed to the shift in redox potential of the Cu-TPMA complex, which necessitates a change in applied voltage to maintain proper control over the polymerization. These results suggest a similar shift in the redox equilibrium for Cu^0-mediated ATRP, resulting in an increase in the equilibrium concentration of radicals.
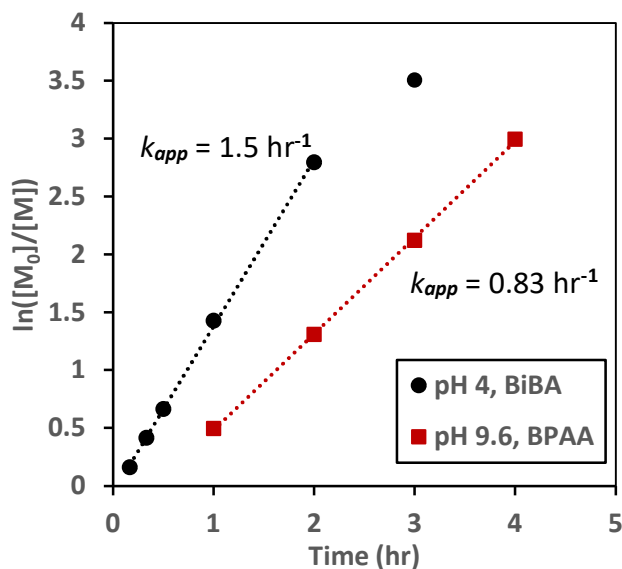
Figure III-7: Kinetic rate plot for polymerization of PDMAEMA at *pH* 4 vs *pH* 9.6.

These results also demonstrate a suppression of the inhibitory period often described for Cu^0-mediated ATRP,[8] with linear kinetics established by $t = 10$ minutes. Though extensive sampling at low conversion has not been conducted for the purposes of this study, extrapolation to the *x*-axis intercept yields an estimated inhibitory period of ca. 2 minutes, indicating a rapid initiation and establishment of the ATRP equilibrium. Similar treatment of kinetics plots for optimized conditions at native *pH* yields an estimated inhibitory period of 10-20 minutes, indicating slower initiation and equilibration.

3.4.4   Synthesis of PDEAEMA, PDPAEMA, and PSPMA

These conditions were also tested for syntheses of PDEAEMA and PDPAEMA, with results summarized in Table III-4 (Entries 2 and 3, respectively). PDEAEMA shows nearly identical results to PDMAEMA, with 98% conversion attained in 3 hours. This corresponds to an M_N of 20.7 kDa and *Đ* of 1.19, according to the calibration curve for PDMAEMA. PDPAEMA shows slightly lower conversion, at 82% in 3 hours. This is attributed to additional steric hinderance of the bulky isopropyl amino groups, which is likely to shield access to the alkene due to the cyclic resonance structure of the pendant group discussed previously. However, the observed MWD shows a significantly lower M_N at 7.8 kDa, with *Đ* of 1.45. It is important to note that this calibration underestimates the true molecular weight for PDEAEMA and PDPAEMA. The additional hydrophobicity of the amino pendant groups is likely to lessen the solvation of the polymer, shrinking the radius of gyration for the polymer chains. This results in a shift towards longer elution times and lower apparent molecular weights. In the case of PDPAEMA, the shift towards low molecular weight is sufficient to introduce a non-negligible overlap with the end of

resolution limit for the column bank used in this study, introducing a high degree of error This is

particularly evident in the observed I_{eff}, with 88% I_{eff} for PDEAEMA and 220% for PDPAEMA.

An initiator efficiency of >200% unlikely to represent a true characterization of the MWD, and

instead represents a significant deviation from the GPC calibration curve. Using the observed I_{eff}

for DMAEMA, an estimated M_N was calculated as:

$$M_{N,est} = \frac{M_{N,theo}}{0.66}$$

This calculation assumes identical initiator efficiency, which may not necessarily hold from one

monomer to another based on changes to radical stabilization for the varied pendant groups.

However, this should place a reasonable estimate on the true molecular weight for both

PDEAEMA and PDPAEMA.   Overall, the qualitative conclusions of these data can still be

interpreted to infer the overall control of the reaction, indicating a well-maintained polymerization

of all three monomers tested.

Table III-4: Conditions and molecular weight distributions for syntheses of PDMAEMA, PDEAEMA, PDPAEMA, and PSPMA at reduced *pH*.[a]

Entry	Monomer	Conversion[b] (%)	$M_{N,theo}$ (kDa)	M_N[c] (kDa)	$Ð$[c]	I_{eff}[d] (%)	$M_{N,est}$[e]
1	DMAEMA	98	15.4	23.3	1.16	66	-
2	DEAEMA	98	18.2	20.7	1.19	88	27.6
3	DPAEMA	82	17.5	7.8	1.45	220	26.5
4	SPMA	76	17.5	22.1	1.23	71	-

[a]: All polymerizations were conducted with [Monomer]:[BiBA]:[TPMA]:[CuCl2] = 100:1:0.4:0.4 and [Monomer]$_0$ = 2 M, with [NaCl] = 1 M, and t = 3 hr. [b]: as measured by NMR. [c]: as measured by GPC. [d]: I_{eff} = $M_{N,theo}/M_N$. [e]: $M_{N,est}$ = $M_{N,theo}$ / 0.66.

A final polymerization was conducted for 3-sulfopropyl methacrylate (SPMA), an anionic monomer which has been explored for use in heavy metal chelation and other metal binding fields.[16] These results demonstrate a well-defined molecular weight distribution, with $M_N = 22.1$ kDa (as sodium salt) and $Đ = 1.23$ observed in 3 hours (Table III-4, Entry 4). Interestingly, conversion does drop to 76% for this polymerization, suggesting a slower rate of propagation for the SPMA radical. This corresponds to an I_{eff} of 71%, indicating similar degree of control for this monomer as compared to the tertiary amines. The slight broadening of the MWD and slower conversion may indicate a slight loss of active chain ends over the course of this polymerization; further optimizations for this monomer may improve this result to better align with the conditions as optimized for the tertiary amine monomers. Regardless, this first-pass result demonstrates the versatility of this approach to synthesize stimuli responsive polymers and polyelectrolytes with a wide range of charge structures accessible.

3.4.4.1   Block Copolymerization – PDMAEMA-b-PSPMA

A final chain extension was prepared using 3-sulfopropyl methacrylate (SPMA), given the successful homopolymerization of PSPMA. The monomer aliquot was prepared identical to DMAEMA, with monomer diluted to 2 M concentration and adjusted to pH 4 and 1 M NaCl. The monomer solution was added to a PDMAEMA macroinitiator after a 3-hour primary polymerization, along with a fresh length of Cu^0 wire to maintain $SA_{Cu}/V = 0.5$ cm^2 mL^{-1}. The secondary polymerization was allowed to proceed for 3 hours, assuming a similar rate of polymerization for DMAEMA. After polymerization, a 100 μL aliquot was taken to dilute for GPC and NMR analyses, which showed instantaneous precipitation upon dilution. This is

attributed to formation of the inner salt upon dilution of the NaCl present in the reaction mixture. As such, GPC analyses were not conducted for this block copolymer to prevent damage to the instrumentation.

However, polymer solubility was regained upon addition of NaCl to disrupt the inner salt, allowing for NMR analysis, yielding a conversion for the SPMA block of 76%. The NMR spectrum for the purified block copolymer is shown in Figure III-8. The spectrum shows a small retention of monomeric SPMA through the precipitation process, observed as alkene peaks at δ = 6.1 ppm and 5.7 ppm. However, integration to the regions of polymer C-CH$_3$ (δ = 0.6-1.5 ppm) and N-CH$_2$- (δ = 3.5-3.9 ppm) yields no overlap with the signals of monomeric SPMA, and thus allows for calculation of relative block lengths. The shared C-CH$_3$ signals of the methacrylate backbone can be used as the basis of integration, as all repeat units will contain 3 protons in this region. Integration of the N-CH2- region then yields the fraction of DMAEMA groups in the block copolymer as:

$$f_{DMAEMA} = \frac{1.14}{2} = 57\%$$

Given the 76% conversion observed for the SPMA polymerization and the starting M_N of 23 kDa, the theoretical fraction of DMAEMA for these copolymers should be 66%. This indicates a greater length of the SPMA block, likely indicating a small fraction of the PDMAEMA macroinitiator that did not properly chain extend resulting in a longer overall average SPMA block length. However, the high fidelity of homopolymer chain extensions suggests this may be a function of the secondary monomer addition, rather than a true demonstration of end group loss for the primary polymerization. Indeed, this observation coupled with the slowed rate of

propagation for homopolymerization of PSPMA combined indicate a lowered end group retention, with lower overall concentration of radicals serving to slow the rate of the polymerization. However, the overall results presented still allow for the synthesis of well-defined block copolymers of block copolymers even for oppositely charge monomer species, allowing for the direct synthesis of zwitterionic and other complex polyelectrolyte structures, with a facile one-pot approach.
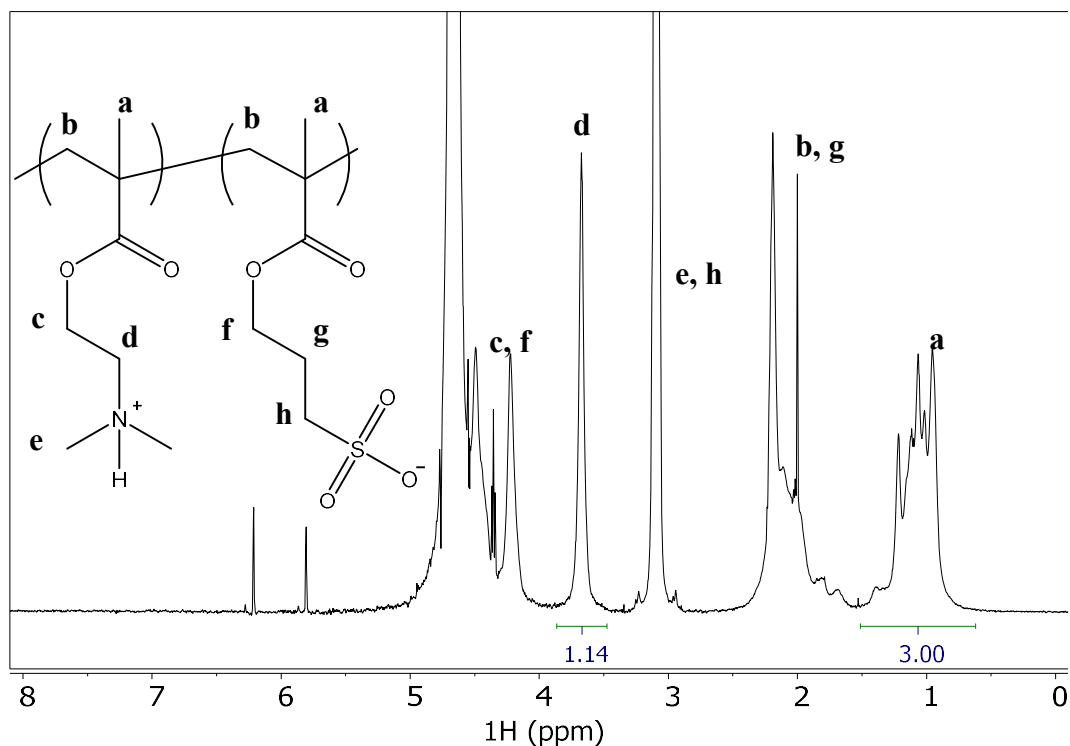
Figure III-8: NMR spectrum for PDMAEMA-b-SPMA in 90% H_2O-10% D_2O.

3.5   Conclusions

By modulating *pH* for the synthesis of PDMAEMA, a series of regimes is observed wherein control by Cu^0-mediated ATRP is well-defined for tertiary amine-pendant monomers. Notably,

syntheses near neutral *pH* yield poorer control than at native *pH*, despite a 10^2-fold decrease in [OH⁻] that would be expected to improve control over the ATRP equilibrium. However, reducing *pH* further to 4 results in a regain of control, with narrow MWDs obtained with near-quantitative conversion in 3 hours. Furthermore, chain extensions demonstrate excellent retention of active C-Cl end groups, with no visible shoulders observed in extended MWDs observed by GPC. Sequential polymerizations may be conducted at near-quantitative conversion for homopolymer extensions without the need for extensive degassing of solutions prior to addition. This represents a marked improvement over previously described aqueous syntheses for PDMAEMA, which have typically demonstrated a loss of functional end groups with increasing conversion. Furthermore, use of mildly acidic conditions allows for polymerizations using DEAEMA and DPAEMA, which are too hydrophobic to dissolve in water at native *pH*. Block copolymers are also attainable, with FTIR and NMR demonstrating the synthesis of PDMAEMA-b-PSPMA as a zwitterionic AB-type copolymer, without the formation of inner salts disrupting the course of the polymerization. These results demonstrate a promising system for the synthesis of stimuli-responsive polymers, both as homopolymers and as components of more complex polymer architectures.

This work has been submitted and accepted in part for publication in Macromolecules, DOI 10.1021/acs.macromol.1c01234.

3.6   References

1.   Ahmadkhani, L., Abbasian, M., and Akbarzadeh, A., *Synthesis of sharply thermo and PH responsive PMA-b-PNIPAM-b-PEG-b-PNIPAM-b-PMA by RAFT radical polymerization*

75

and its schizophrenic micellization in aqueous solutions. Des Monomers Polym., 2017. **20**(1): p. 406-418. DOI: 10.1080/15685551.2017.1314654.

2.   Anastasaki, A., Oschmann, B., Willenbacher, J., Melker, A., Van Son, M.H.C., Truong, N.P., Schulze, M.W., Discekici, E.H., McGrath, A.J., Davis, T.P., Bates, C.M., and Hawker, C.J., *One-Pot Synthesis of ABCDE Multiblock Copolymers with Hydrophobic, Hydrophilic, and Semi-Fluorinated Segments.* Angew Chem Int Ed Engl, 2017. **56**(46): p. 14483-14487. DOI: 10.1002/anie.201707646.

3.   de Souza, J.C.P., Naves, A.F., and Florenzano, F.H., *Specific thermoresponsiveness of PMMA-block-PDMAEMA to selected ions and other factors in aqueous solution.* Colloid and Polymer Science, 2012. **290**(13): p. 1285-1291. DOI: 10.1007/s00396-012-2651-9.

4.   Engelis, N.G., Anastasaki, A., Whitfield, R., Jones, G.R., Liarou, E., Nikolaou, V., Nurumbetov, G., and Haddleton, D.M., *Sequence-Controlled Methacrylic Multiblock Copolymers: Expanding the Scope of Sulfur-Free RAFT.* Macromolecules, 2018. **51**(2): p. 336-342. DOI: 10.1021/acs.macromol.7b01987.

5.   Herberg, A., Yu, X., and Kuckling, D., *End Group Stability of Atom Transfer Radical Polymerization (ATRP)-Synthesized Poly(N-isopropylacrylamide): Perspectives for Diblock Copolymer Synthesis.* Polymers (Basel), 2019. **11**(4): p. 678. DOI: 10.3390/polym11040678.

6.   Wang, G. and Zhang, L., *Synthesis, self-assembly and pH sensitivity of PDEAEMA–PEG–PDEAEMA triblock copolymer micelles for drug delivery.* Reactive and Functional Polymers, 2016. **107**: p. 1-10. DOI: 10.1016/j.reactfunctpolym.2016.08.001.

7.   Cordeiro, R.A., Rocha, N., Mendes, J.P., Matyjaszewski, K., Guliashvili, T., Serra, A.C., and Coelho, J.F.J., *Synthesis of well-defined poly(2-(dimethylamino)ethyl methacrylate) under mild conditions and its co-polymers with cholesterol and PEG using Fe(0)/Cu(ii) based SARA ATRP.* Polym. Chem., 2013. **4**(10). DOI: 10.1039/c3py00190c.

8.   Zhang, Q., Wilson, P., Li, Z., McHale, R., Godfrey, J., Anastasaki, A., Waldron, C., and Haddleton, D.M., *Aqueous copper-mediated living polymerization: exploiting rapid disproportionation of CuBr with Me6TREN.* J. Am. Chem. Soc., 2013. **135**(19): p. 7355-63. DOI: 10.1021/ja4026402.

9.   Fantin, M., Isse, A.A., Venzo, A., Gennaro, A., and Matyjaszewski, K., *Atom Transfer Radical Polymerization of Methacrylic Acid: A Won Challenge.* J. Am. Chem. Soc., 2016. **138**(23): p. 7216-9. DOI: 10.1021/jacs.6b01935.

10.   Fantin, M., Isse, A.A., Gennaro, A., and Matyjaszewski, K., *Understanding the Fundamentals of Aqueous ATRP and Defining Conditions for Better Control.* Macromolecules, 2015. **48**(19): p. 6862-6875. DOI: 10.1021/acs.macromol.5b01454.

11.   Fu, L., Simakova, A., Fantin, M., Wang, Y., and Matyjaszewski, K., *Direct ATRP of Methacrylic Acid with Iron-Porphyrin Based Catalysts.* ACS Macro Letters, 2018. **7**(1): p. 26-30. DOI: 10.1021/acsmacrolett.7b00909.

12.   Jiang, X., van der Horst, A., van Steenbergen, M.J., Akeroyd, N., van Nostrum, C.F., Schoenmakers, P.J., and Hennink, W.E., *Molar-mass characterization of cationic polymers for gene delivery by aqueous size-exclusion chromatography.* Pharm. Res., 2006. **23**(3): p. 595-603. DOI: 10.1007/s11095-006-9574-4.

13. Pei, Y. and Lowe, A., *Polymerization-induced self-assembly: Ethanolic RAFT dispersion polymerization of 2-phenylethyl methacrylate.* Polymer Chemistry, 2014. **5**: p. 2342-2351. DOI: 10.1039/c3py01719b.

14. van de Wetering, P., Zuidam, N.J., van Steenbergen, M.J., van der Houwen, O.A.G.J., Underberg, W.J.M., and Hennink, W.E., *A Mechanistic Study of the Hydrolytic Stability of Poly(2-(dimethylamino)ethyl methacrylate).* Macromolecules, 1998. **31**(23): p. 8063-8068. DOI: 10.1021/ma980689g.

15. Ros, S., Kleinberger, R.M., Burke, N.A.D., Rossi, N.A.A., and Stöver, H.D.H., *Charge-Shifting Polycations with Tunable Rates of Hydrolysis: Effect of Backbone Substituents on Poly[2-(dimethylamino)ethyl acrylates].* Macromolecules, 2018. **51**(15): p. 5752-5761. DOI: 10.1021/acs.macromol.8b00931.

16. Gu, J., Yuan, S., Shu, W., Jiang, W., Tang, S., Liang, B., and Pehkonen, S.O., *PVBC microspheres tethered with poly(3-sulfopropyl methacrylate) brushes for effective removal of Pb(II) ions from aqueous solution.* Colloids and Surfaces A: Physicochemical and Engineering Aspects, 2016. **498**: p. 218-230. DOI: https://doi.org/10.1016/j.colsurfa.2016.03.062.

CHAPTER IV: : Synthesis of PDMAEMA with Me$_6$TREN-Generated Cu^0 Powder

4.1 Abstract

Me$_6$TREN is known to favor disproportionation of Cu^I halides in solution to generate high surface area copper powder, which allows for rapid polymerization of monomers such as N-isopropylacrylamide while retaining well-defined molecular weight distributions. However, extension of this system to other stimuli-responsive monomers – especially those with basic or acidic moieties – has been limited. In this study, PDMAEMA is used to probe the behavior of this system with this class of weakly basic monomers. Syntheses near native *pH* modulation are demonstrated to proceed with poor control, yielding polymers with broad molecular weight distributions (*Đ* > 2). Syntheses at *pH* 8.6 demonstrate a modest improvement in MWD (*Đ* < 1.4), but further reduction in *pH* demonstrates detrimental results, with broad MWDs observed below *pH* 7 (*Đ* > 1.5). Polymerization halts altogether below *pH* 6, suggesting low potential for exploration of Me$_6$TREN for these monomers under even mildly acidic conditions. However, syntheses using TPMA with the in-situ generated Cu^0 powder demonstrate more promising results, with 80% conversion in 2 hours attainable using this source of copper, while maintaining a relatively narrow molecular weight distributions (*Đ* < 1.3).

4.2 Introduction

In recent years, the ATRP ligand tris[2-(dimethylamino)ethyl]amine (Me$_6$TREN) has been demonstrated to yield rapid disproportionation of Cu^I halides under aqueous conditions, spontaneously generating Cu^{II} species and Cu^0 powders with high surface area. This is induced by a rapid disproportionation reaction facilitated by Me$_6$TREN, continually generating "nascent"

Cu^0 nanoparticles over the course of the reaction. This mechanism is generally recognized as single electron transfer living radical polymerization (SET-LRP) and yields rapid polymerization for many acrylic monomers.[1-3] For monomers such as N-isopropylacrylamide (NiPAM), quantitative conversion is attainable in under 30 minutes while maintaining narrow molecular weight distributions ($Đ$ < 1.1).[3,4] Such a result represents astounding degree of control for such a rapid polymerization. This has become the gold standard for many controlled polymerization schemes to stand against.

However, extension of these results to other classes of monomers – especially those with acidic or basic moieties – has proven troublesome. Indeed, though the original studies demonstrated extension to other hydrophilic monomers, these were limited to nonionic monomers, with some later studies expanding this system to a handful of zwitterionic species, such as sulfobetaine analogues.[5] However, to date there has been no evidence of successful extension of this system to acidic or basic monomers, such as 2-(dimethylamino)ethyl methacrylate (DMAEMA), a *pH*- and temperature-responsive monomer with weakly basic amine pendant groups. Control of this system under aqueous conditions has generally only been shown with TPMA and other aryl ligands, with high quantities of organic modifiers required to maintain well-defined reactions for aliphatic ligands. However, the demonstration of independent regions of control for TPMA-mediated polymerization of PDMAEMA suggests there may be pockets of control attainable for this polymerization scheme as well.

In this study, previous results from the TPMA-mediated ATRP of PDMAEMA are utilized to explore the extension of this Me$_6$TREN system to PDMAEMA, extending its use to additional class of stimuli-responsive polymers. In particular, *pH* modulation is demonstrated to be integral

to the synthesis of well-defined polymers, with poor control observed for $pH > 9$. However, poor results are also demonstrated for polymerizations below pH 8, with polymerizations failing altogether below pH 6. This is the region where excellent control has been previously demonstrated for PDMAEMA using TPMA. Though this results in a limited availability for use in synthesis of block copolymers, relatively well-defined homopolymers may be synthesized at high conversion in under 2 hours through this route. Furthermore, preliminary polymerizations are presented that demonstrate the use of Me$_6$TREN/Cu^I-generated Cu^0 powder for TPMA-mediated polymerizations. This preparation yields moderately well-defined polymers, with $Đ <$ 1.3 observed for polymers at 80% conversion in 2 hours. Further implementation of this approach to optimized conditions for TPMA-mediated syntheses may yield a promising avenue for rapid synthesis of TPMA with well-defined MWDs.

4.3   Materials and Methods

4.3.1   Materials

Toluene (CAS 108-88-3; 99.5%) was purchased from Fisher Scientific. α-bromophenylacetic acid (BPAA, CAS 4870-65-9; 98%), copper(I) chloride (CAS 7758-89-6; 98%), copper(II) chloride (CAS 7447-39-4; 98%), glacial acetic acid (CAS 64-19-7; 99%), PDMAEMA ($M_N = 10$ kDa, $Đ \leq 1.4$), sodium hydroxide (CAS 1310-73-2; 97%), and triethylamine (CAS 121-44-8; 99.7%) were purchased from Sigma-Aldrich. Poly(ethylene glycol) (PEG, CAS 25322-68-3) standards for gel permeation chromatography were purchased from Scientific Polymer Products. 2-(dimethylamino)ethyl methacrylate (DMAEMA, CAS 2867-47-2; 98%) was purchased from TCI America. Hydrochloric acid (CAS 7647-01-0; 36.5%), sodium chloride (CAS 7647-14-5;

98%), tris[2-(dimethylamino)ethyl]amine (Me$_6$TREN, CAS 33527-91-2, 99%), and tris(2-pyridylmethyl)amine (TPMA, CAS 16858-01-8; 98%) were purchased from VWR. Type I ultrapure water (18.2 MΩ) was generated using a Millipore Synergy UV Water Purification System. DMAEMA was passed over activated poly(styrene-co-divinyl benzene) resin (CAS 9003-70-7) before use to remove MEHQ inhibitors. All other reagents were used as received.

4.3.2   Pre-disproportionation of Cu^I-Me$_6$TREN

1 mL of Type I ultrapure water and 16 μL (60 μmol) of Me$_6$TREN were added to a clean, dry test tube. The test tube was capped with a rubber septum and bubbled with N$_2$ for at least 15 minutes. 11.8 mg (120 μmol) of CuCl was added to a separate clean, dry test tube, which was capped with a rubber septa and sparged with N$_2$ for at least 15 minutes. After sparging both test tubes to displace oxygen in the head space and solution, the water-Me$_6$TREN mixture was transferred to the CuCl powder by cannula. This solution was continually sparged with N$_2$ to provide mixing, with at least 15 minutes of equilibration prior to polymerization, with the color of solution observed to shift to a deep blue with brown particulates accumulating at the bottom of the test tube, signaling the formation of Cu^0 and Cu^{II} species.
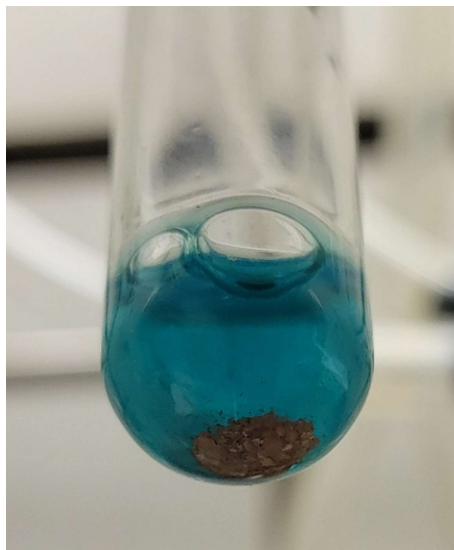
Figure IV-1: Example of Cu^0 powder generated by the disproportionation of CuCl and Me_6TREN.

4.3.3   Synthesis of PDMAEMA

Monomer solutions were prepared to the target *pH*, adjusting *pH* with 1M hydrochloric acid and sodium hydroxide as necessary. These mixtures were prepared at a concentration of 2.3 M, to yield a final monomer concentration of 2M after dilution by the CuCl-Me_6TREN mixture. A representative polymerization is described as follows: 31.9 mg (148 μmol) of BPAA and 306.8 mg (5.25 mmol) of NaCl were added to a clean, dry test tube. 6.5 mL of the DMAEMA-water mixture were added to the same test tube. The test tube was then capped with a rubber septum and subjected to three freeze-pump-thaw cycles to displace dissolved oxygen. After the final thaw, the monomer mixture was transferred to the CuCl-Me_6TREN mixture by cannula. Polymerization mixtures were sparged with N_2 throughout to maintain the inert atmosphere and provide mixing. 100 μL aliquots were sampled at regular time points to track molecular weight and conversion over the course of the polymerization. Polymer solutions were treated dropwise with 1M NaOH

after polymerization to precipitate the polymer by triggering of the lower critical solution temperature. The supernatant phase was then decanted, and polymer precipitates dried *in vacuo* prior to further analysis.

4.3.4 Characterization

4.3.4.1 Gel Permeation Chromatography

Gel permeation chromatography (GPC) was conducted on a Shimadzu Prominence HPLC with an Agilent Aquagel-OH Mixed H and Aquagel-OH 30 column bank. Analyses for PDMAEMA, PDEAEMA, and PDPAEMA use a 0.3 M sodium acetate, 0.15M triethylamine buffer ($pH = 4.0$) as the mobile phase, as previously established. Chromatograms were collected with a Waters R410 differential refractometer and a Wyatt DAWN F light scattering detector. The light scattering detector was calibrated to the Rayleigh ratio of toluene. Refractometer response was calibrated using low polydispersity PEG standards. The incremental refractive index (*dn/dc*) for PDMAEMA was taken to be 0.20 mL/g as previously described in literature.[6] All chromatograms were collected using an eluent flow rate of 1 mL/min. Additional details for molecular weight calibration are discussed in Appendix A.3. Peak fitting was conducted using Fityk curve fitting software (v. 1.3.1), assuming an exponentially modified Gaussian distribution for all peaks to capture any tailing towards low molecular weight.

4.3.4.2 Nuclear Magnetic Resonance

Nuclear magnetic resonance (NMR) spectra were collected using a Varian VNMRS 500 MHz spectrometer and analyzed using MestReNova software (v. 12.0.2). All NMR samples were dissolved in 10% D_2O-90% H_2O. Spectra were collected with H_2O solvent suppression using a

total of 8 scans. A relaxation delay of 40 seconds was used to allow alkene peaks of unreacted monomer to relax between acquisitions. Chemical shifts were assigned according to values previously reported in literature.[7] Conversion is calculated based on the ratio of monomer C=C-H peak area (δ = 5.5-6 ppm) to the area of peaks corresponding to monomer -CH$_3$ and polymer -CH$_2$- (δ = 1.4-2 ppm). The overall conversion is calculated as follows, with additional details provided Appendix A.1.

$$Conv.\,(\%) = \frac{\delta_{1.4-2} - 3(\delta_6 + \delta_{5.5})}{\delta_{1.4-2} - \delta_6 - \delta_{5.5}}$$

4.4 Results and Discussion

4.4.1 *pH* Adjusted Synthesis

Initial *pH* optimizations were conducted near the native *pH* of 9.6, to evaluate the initial performance of the Me$_6$TREN catalyst. Previous results suggest this ligand retains poor control under these reaction conditions, and initial results confirm this behavior, with polymerizations at *pH* 9.3 yielding a broad MWD ($Đ$ > 2.5) with poor initiator efficiency (I_{eff} = 18%), indicating little to no control maintained over the polymerization. As with polymerizations for TPMA, initial improvement is observed upon lowering *pH* to 8.6, aligning well with the *pK$_a$* of monomeric DMAEMA. Under these conditions, polymerization yields a final M_N of 35.2 kDa with $Đ$ = 1.36, representing a moderate degree of control. This is also accompanied by an increase to 99% conversion in only one hour, demonstrating a rapid polymerization. Though this does show a great deal of improvement from conditions at native *pH* for Me$_6$TREN, it does still show notable broadening toward low molecular weight and poorer initiator efficiency of 54% (Table IV-1, Entry 2). MWDs then begin to broaden, with $Đ$ > 1.4 at *pH* 8, though there is a modest improvement in

I_{eff} (Table IV-1, Entry 2). However, further reduction in *pH* to 7.8 yields continued broadening of MWD, with *Đ* = 1.59. This behavior mimics that observed for TPMA-mediated polymerizations; the loss of control as polymerization *pH* approaches the polymer *pK_a* of 7.5 further confirm the poor behavior of this ATRP system for controlling syntheses of these monomers near neutral *pH*.

Table IV-1: Polymerization conditions and molecular weight distributions for Me6TREN-Mediated Polymerizations of PDMAEMA.[a]

Entry	[HCl]	[NaCl] (M)	*pH*	*t* (hr)	Conv.[b] (%)	$M_{N,theo}$ (kDa)	M_N[c] (kDa)	*Đ*[c]	I_{eff}[d] (%)
1	0.1	0.9	9.3	1	65	13.3	77.7	2.51	18
2	0.3	0.7	8.6	1	99	15.5	35.2	1.36	44
3	0.3	0	8.6	1	70	6.3	59.3	1.73	11
4	0.3	0.3	8.6	1	99	15.5	90.3	1.46	17
5	2.0	1	6.5	2	81	12.6	48.5	1.53	26
6	2.1	1	5.5	2	0	0	n.d.	n.d.	-
7[e]	0.3	0.7	8.6	2	80	12.6	25.5	1.26	49

[a]: All polymerizations were conducted with [DMAEMA]:[BPAA]:[Me₆TREN]:[CuCl] = 100:1:0.4:0.8 and [DMAEMA]₀ = 2 M. [b]: as measured by NMR. [c]: as measured by GPC. [d]: *I_{eff}* = $M_{N,theo}/M_N$. [e]: Using TPMA as ligand.

4.4.2 Polymerization with Reduced Halide Loading

Syntheses were also conducted to evaluate the impact of halide concentration on overall control, as many Me₆TREN-CuCl polymerization schemes have been approached without the addition of any supporting halide. Polymerizations were repeated for *pH* 8.6, as these conditions yield the greatest control over final MWD. The furthest extreme of this, where NaCl is removed altogether, shows a steep drop in performance, with broad MWDs and a poor *I_{eff}* of only 11%.

Control is gradually regained as NaCl is added back in, with further improvements to a final MWD of $M_N = 35.2$ kDa, $Đ = 1.36$ when polymerizations are loaded with 1M NaCl, with high conversion still observed. Though these conditions do yield relatively broadened MWDs when compared to those for optimized conditions with TPMA, the ability to synthesize PDMAEMA to >90% conversion within an hour still presents a promising option for the synthesis of homopolymers.

4.4.3 Polymerization Under Acidic Conditions

Based on evidence for improved control over polymerizations of PDMAEMA using TPMA as the ATRP ligand, further reducing solution pH may yield a mechanism for improving control over the reaction. Despite excellent results demonstrated for TPMA at lower pH of 4, an intermediate pH of 5 was chosen for these polymerizations. Aliphatic ligands have not been demonstrated to retain the same degree of control for aqueous ATRP at low pH, with previous studies citing poor control when pH is decreased below 5 for PMDETA, though Me$_6$TREN was not studied below pH 6-7.[8] Polymerization at pH 6.5 demonstrates poor control ($Đ = 1.53$) and a further decrease in initiator efficiency to 26%. Further reduction to pH 5.5 results in cessation of polymerization altogether, with no polymer observable by GPC or NMR after 2 hours. Furthermore, these conditions are accompanied by a shift in color of the reaction mixture, with the typical light blue observed for Cu^{II}-Me$_6$TREN complexes disappearing (Figure IV-2). This is accompanied by a dark brown to purple precipitate gradually accumulating at the bottom of reaction mixtures over the course of the reaction, indicating aggregation and precipitation of the disproportionation generated Cu^0 particles. The disappearance of color from solution suggests displacement of the

copper center from the Me₆TREN complex, likely driven by protonation of the amine species to prevent proper coordination to the copper ions.
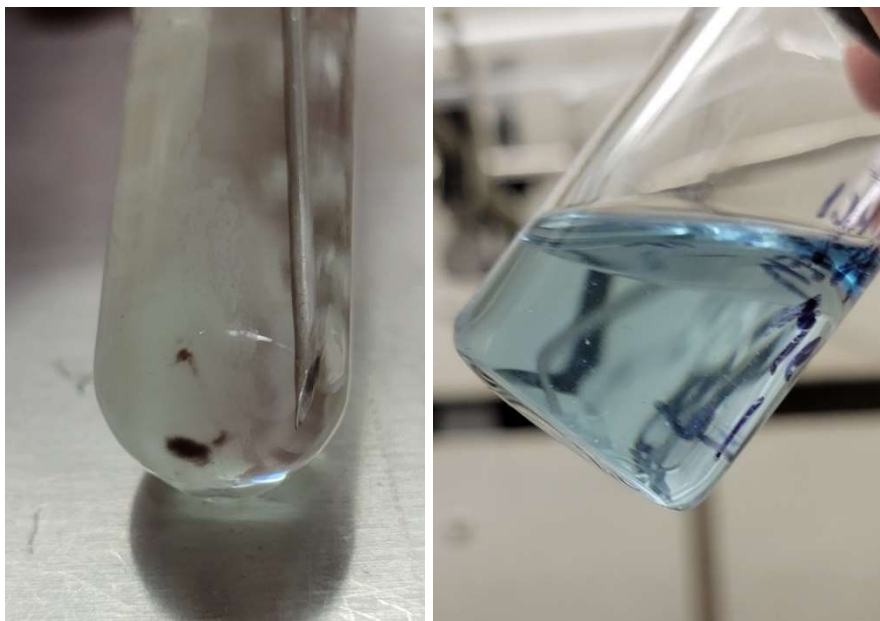
Figure IV-2: Left: Cu^0 precipitation and loss of color for polymerization at pH 5.5. Right: typical appearance for Me₆TREN-Cu^{II} complex.

These results suggest poor performance of Me₆TREN under even mildly acidic conditions. Previously published results indicated that aliphatic ligands do lose activity under acidic conditions, with PMDETA demonstrating no catalytic activity at *pH* 4. This is likely driven by protonation of the tertiary amines in the ligand species, with the protonated amines then unable to complex with Cu^I/Cu^{II} centers to mediate the ATRP reaction. These results highlight the limitations for Me₆TREN systems for maintaining control in the ATRP of stimuli-responsive polymers, especially those containing basic moieties. The deterioration in control as *pH* approaches the polymer *pK_a* of 7.5 does suggest that the polymer solvation at near-neutral

conditions is a limiting factor, as was the case for TPMA-mediated syntheses as well. These results also indicate poor prospects for extending this reaction system to acidic moieties.

4.4.4   TPMA with Pre-Disproportionated Cu^0 Powder

One interesting avenue for this system could be the use of Cu^I/Me$_6$TREN to generate the Cu^0 powder in-situ, which may be used to drive polymerization for a TPMA-mediated ATRP, which has been previously demonstrated to yield well-defined polymers for PDMAEMA. A polymerization was conducted to assess this effect, with the result summarized in Table IV-1, Entry 10 and the resulting MWD presented in Figure IV-3. The conditions chosen for this polymerization are intended as a point to directly compare with the exchange of ligand alone. These conditions do yield improvement in control compared to the Me$_6$TREN system, with a final Đ of 1.26. Furthermore, though this MWD does display broadening beyond that observed for optimized conditions for TPMA, the point of comparison for optimum Me$_6$TREN results at *pH* 8.6 represents a known set of conditions with lowered conversion and poor chain extension for TPMA. With the high activity Cu^0 powder approach here, polymerizations can attain >80% conversion in 2 hours, suggesting a promising route for faster polymerizations of PDMAEMA.

To assess any impact of this higher activity Cu^0 source on the retention of active chain ends, polymerization was repeated with the addition of a new aliquot of degassed monomer after two hours. This polymerization yields nearly identical results to those observed for Cu^0 wire, except for a more pronounced shoulder due to the accelerated conversion with the high Cu^0 surface area. The integration of the relative areas in the extended and terminated peaks yields a fraction of 46% of chains that undergo chain extension, a modest improvement from the 37% of chains extended

at similar *pH* for TPMA-mediated polymerizations. Overall, these results support the conclusion that neutral to weakly basic polymerization conditions for PDMAEMA yield meaningful results for homopolymerization but will ultimately limit the access to block copolymers and other architectures.
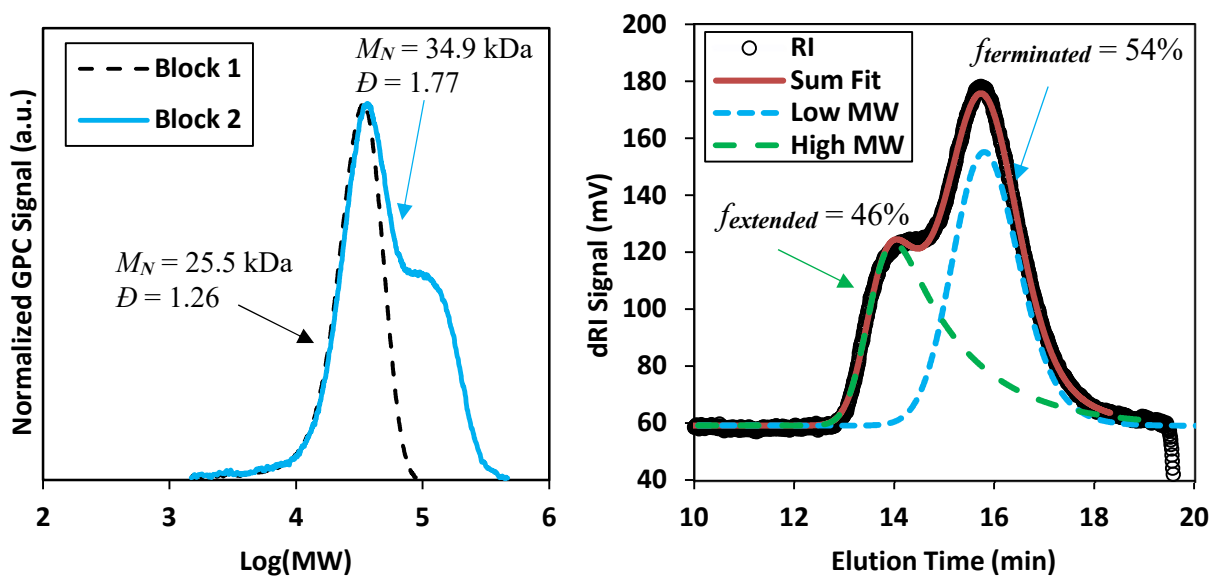
Figure IV-3: Left: chain extension results for PDMAEMA using TPMA and Cu^0 powder generated from Cu^I/Me$_6$TREN at pH 8.6. Right: peak deconvolution for the chain extension chromatogram.

However, the oxygen sensitivity of this approach should be considered in conjunction with the overall results presented; the generation of the high-surface area Cu^0 powder must be conducted in the absence of oxygen, to prevent the rapid oxidation of the surface to form copper oxides. At the test tube scale, extensive degassing is an inconvenience, but manageable; when scaling beyond the laboratory, however, this aspect may prove to be a considerable limitation to the accessibility of this synthetic approach. Though mechanism have been explored to introduce oxygen tolerance

to this system, they often rely on the addition of reducing agents such as hydrazine to fully reduce the generated copper powder.[9] This may be a feasible approach in moving toward an industrial scale but does introduce further safety and design considerations to handle hydrazine safely. The choice between these two catalyst systems thus comes down to a design decision: if the time needed for polymerization is the limiting design factor, this Me$_6$TREN-Cu^I catalyst presents the highest rate of polymerization. On the other hand, if the oxygen tolerance and removal of hydrazine or other aggressive reducing agents is the key consideration, the TPMA-Cu^0 wire catalyst system provides the most robust and facile approach.

4.5   Conclusions

By leveraging the rapid disproportionation of Cu^I and Me$_6$TREN for *in situ* generation of Cu^0 powder, the polymerization of PDMAEMA may be pushed to near quantitative conversion in as little as one hour. However, this approach comes with the limitation of broadening MWDs, with $Đ > 1.3$ observed even at the optimized *pH* of 8.6. Polymerizations near neutral *pH* demonstrate further broadening of final MWDs and slowed conversion, confirming the trends observed for TPMA-mediated ATRP under similar conditions. Combining these two polymerization schemes, with Cu^0 powder generated *in situ* by Me$_6$TREN/Cu^I but polymerization mediated by TPMA, yields an improved degree of control over the final MWD, with $Đ < 1.2$ attainable, with 80% conversion observed in 2 hours. However, this polymerization demonstrates a similar loss of active chain ends upon extensions, with only ca. 46% of PDMAEMA chains retaining the active C-Cl terminus, as evidenced by GPC deconvolution. Overall findings indicate the CuI/Me6TREN system has limited potential for extension to DMAEMA and in the context of block copolymers

and other complex architectures; however, this synthetic route does present the possibility for near-quantitative conversion with homopolymers of PDMAEA, with only moderate broadening of final MWDs observed at the optimized conditions of *pH* = 8.6.

4.6   References

1.   Konkolewicz, D., Wang, Y., Zhong, M., Krys, P., Isse, A.A., Gennaro, A., and Matyjaszewski, K., *Reversible-Deactivation Radical Polymerization in the Presence of Metallic Copper. A Critical Assessment of the SARA ATRP and SET-LRP Mechanisms.* Macromolecules, 2013. **46**(22): p. 8749-8772. DOI: 10.1021/ma401243k.
2.   Lligadas, G., Grama, S., and Percec, V., *Single-Electron Transfer Living Radical Polymerization Platform to Practice, Develop, and Invent.* Biomacromolecules, 2017. **18**(10): p. 2981-3008. DOI: 10.1021/acs.biomac.7b01131.
3.   Zhang, Q., Wilson, P., Li, Z., McHale, R., Godfrey, J., Anastasaki, A., Waldron, C., and Haddleton, D.M., *Aqueous copper-mediated living polymerization: exploiting rapid disproportionation of CuBr with Me6TREN.* J. Am. Chem. Soc., 2013. **135**(19): p. 7355-63. DOI: 10.1021/ja4026402.
4.   Herberg, A., Yu, X., and Kuckling, D., *End Group Stability of Atom Transfer Radical Polymerization (ATRP)-Synthesized Poly(N-isopropylacrylamide): Perspectives for Diblock Copolymer Synthesis.* Polymers (Basel), 2019. **11**(4): p. 678. DOI: 10.3390/polym11040678.
5.   Fan, Y., Migliore, N., Raffa, P., Bose, R.K., and Picchioni, F., *Synthesis of Zwitterionic Copolymers via Copper-Mediated Aqueous Living Radical Grafting Polymerization on Starch.* Polymers (Basel), 2019. **11**(2): p. 192. DOI: 10.3390/polym11020192.
6.   Jiang, X., van der Horst, A., van Steenbergen, M.J., Akeroyd, N., van Nostrum, C.F., Schoenmakers, P.J., and Hennink, W.E., *Molar-mass characterization of cationic polymers for gene delivery by aqueous size-exclusion chromatography.* Pharm. Res., 2006. **23**(3): p. 595-603. DOI: 10.1007/s11095-006-9574-4.
7.   Pei, Y. and Lowe, A., *Polymerization-induced self-assembly: Ethanolic RAFT dispersion polymerization of 2-phenylethyl methacrylate.* Polymer Chemistry, 2014. **5**: p. 2342-2351. DOI: 10.1039/c3py01719b.
8.   Fantin, M., Isse, A.A., Gennaro, A., and Matyjaszewski, K., *Understanding the Fundamentals of Aqueous ATRP and Defining Conditions for Better Control.* Macromolecules, 2015. **48**(19): p. 6862-6875. DOI: 10.1021/acs.macromol.5b01454.
9.   Fleischmann, S., Rosen, B.M., and Percec, V., *SET-LRP of acrylates in air.* Journal of Polymer Science Part A: Polymer Chemistry, 2010. **48**(5): p. 1190-1196. DOI: https://doi.org/10.1002/pola.23879.

CHAPTER V: Synthesis of Phosphate-Pendant Hydrogels by Aqueous ATRP

5.1 Abstract

Synthesis of hydrogels utilizing reversible deactivation radical polymerization techniques has been demonstrated to yield higher quality polymer networks than free radical techniques, due to the slower polymerization kinetics allowing assembly of polymer chains into less strained configurations, with better-defined pore sizes between crosslinks. However, to date these polymerization systems have generally been limited to simple hydrophilic monomers, with limited extension to stimuli-responsive moieties. In this study, the direct synthesis of 2-(methacryloyloxy)ethyl phosphate hydrogels is reported by TPMA-mediated ATRP under aqueous conditions, using the diene impurity in the commercial monomer as the crosslinking species. Cu^0 and ascorbic acid are compared as activating species, with ascorbic acid demonstrated to yield improved homogeneity in final hydrogels. Modulation of initiator content to target varying molecular weight of primary chains is explored to optimize conditions for hydrogels that retain shape through swelling without fracturing, despite the >15% content of BMOEP on a molar basis. This polymerization scheme may prove promising for extension to other acidic monomers, and the inclusion of comonomers for more complex hydrogel architectures.

5.2 Introduction

Hydrogels are a wide class of polymeric materials where a highly crosslinking hydrophilic network demonstrates remarkable swelling due to the inclusion of water as the polymer is hydrated by water. Due to the crosslinking between individual primary polymer chains, the network behaves effectively as one continuous polymer chain, and is unable to dissolve into water, with

hydration instead expanding the interstitial space between polymer chains. These materials have been extensively studied in the literature for use across a wide range of applications such as drug delivery, wound treatment, water remediation, and ion specific transport.[1-4] Most often these materials are synthesized by the inclusion of diene containing monomers during the polymerization process, introducing permanent covalent bonds to link individual chains together. The ratio of the diene to other comonomers in the overall formulation can then be tuned to modulate the physical characteristics of the resulting hydrogel, with increased diene content favoring an increase in the density of crosslinking which resists the swelling of the polymer network.

These materials are often synthesized through free radical polymerization (FRP) schemes, as these schemes are readily approachable and well-understood. However, it has been demonstrated that these approaches instill many of the same limitations as free radical polymerizations in linear polymers. Namely, the continuous generation of radical species to drive the polymerization to the point of gelation leads to a poor control over the primary chain structure, with a wide range of chain lengths giving rise to poor homogeneity of the final hydrogel.[5] Furthermore, the termination of high-molecular weight chains during polymerization can trap high-molecular weight chains in strained and unfavorable configurations, with no flexibility or freedom of movement to properly relax to a constrained form.[6]

Reversible deactivation radical polymerization (RDRP) schemes instead provide a mechanism for slowing the growth of propagating chains, yielding a primary polymer structure with greater homogeneity and repeatability. Indeed, hydrogels synthesized by RDRP methods have been demonstrated to have higher swelling than those synthesized with FRP methods.[5,7] However,

RDRP methods have traditionally been limited to a relatively narrow range of monomers, due either to poor reactivation in low activity monomers or the disruption of the catalysts needed to drive many RDRP polymerizations forward. However, in recent years atom transfer radical polymerization (ATRP) has been expanded to access a wide range of hydrophilic monomers, with direct synthesis in aqueous conditions readily attainable.[8-10]

In this study, the direct synthesis of hydrogels from 2-(methacryloyloxy)ethyl phosphate, a phosphate-pendant monomer, is reported using aqueous ATRP. This monomer and its diene, bis[2-(methacryloyloxy)ethyl] phosphate, have been explored as inclusions in hydrogel formulations for introducing *pH* and ionic strength responsiveness, with the phosphate moiety demonstrating tunable properties based on its protonation or deprotonation.[4,11,12] However, to date this has typically been done by significant dilution with comonomers, due to the inclusion of a diene impurity in commercial sources of the monomer (ca. 25% on a molar basis).[11,13] These hydrogels are generally restricted to no more than 5% MOEP or BMOEP on a molar basis, representing a limited contribution available for the stimuli-responsive moiety to the overall structure of the hydrogel. The use of ATRP in this study is explored to extend these hydrogels to 100% MOEP, as a proof of concept for exploring hydrogels with greater stimuli responsiveness. Cu^0 and ascorbic acid are compared as reducing agents for the activation of dormant chains, with ascorbic acid yielding superior results due to the heterogeneity introduced by Cu^0 for this synthetic route. Evaluation of the other reaction conditions available, including initiator concentration, allows for the direct synthesis of these hydrogels with high fidelity and good swelling characteristics, with optimized formulations yielding an equilibrium uptake of water of >2,500% relative to the dry mass in phosphate buffer solution (*pH* 7.4), and >6,000% in pure water.

5.3   Materials and Methods

5.3.1   Materials

α-bromophenylacetic acid (BPAA, CAS 4870-65-9; 98%), bis([2-methacryloyloxy]ethyl)phosphate (CAS 32435-46-4), copper(II) bromide (CAS 7758-89-6; 98%), copper(II) chloride (CAS 7447-39-4; 98%), hexane, mixture of isomers (CAS 107-83-5, 98.5%), phosphoric acid 2-hydroxyethyl methacrylate ester (CAS 52628-03-2; 90%), and potassium bromide (CAS 7758-02-3; 99%) were purchased from Sigma-Aldrich. Poly(methacrylic acid) (PMAA, CAS 25086-15-1) standards for gel permeation chromatography were purchased from Scientific Polymer Products and Sigma-Aldrich. Hydrochloric acid (CAS 7647-01-0; 36.5%), methanol (CAS 67-56-1; 99.8%), reagent alcohol (CAS 64-17-5; 95%), and sodium chloride (CAS 7647-14-5; 98%) were purchased from VWR. Type I ultrapure water (18.2 MΩ) was generated using a Millipore Synergy UV Water Purification System. Copper wire (d = 0.4 mm) and sheet was provided by the University of Oklahoma. MOEP was washed with hexanes before use to reduce the concentration of the bis-methacrylate impurity. All other reagents were used as received.

5.3.2   MOEP Purification

25 mL of MOEP, 25 mL of Type I ultrapure water, 100 mL of hexanes and a stir bar were added to a 500 mL round bottom flask. The flask was then capped, and the mixture was placed over a magnetic stir plate for 1 hour. The two-phase mixture was then poured into a separation funnel, and the aqueous phase recovered into a clean round bottom flask. The purified monomer was then stirred under reduced pressure to remove residual hexanes.

5.3.3 Cu^0-Mediated Synthesis of PMOEP

Syntheses were designed to target a range of degrees of polymerization between 100 and 2000. A representative synthesis for target D_P = 100 is as follows. 15.6 mg (53.7 µmol) of TPMA, 7.2 mg (54 µmol) of CuCl$_2$, 28.9 mg (134 µmol) of BPAA, and 131.5 mg (2.25 mmol) of NaCl were added to a dry test tube. 5 mL of the 1-1 purified MOEP solution and 2.5 mL of Type I ultrapure water were added to the same test tube, which was vortexed to homogenize. At the same time, a 33.5 cm length of Cu0 wire (d = 0.4 mm, SA_{Cu}/V = 0.5 cm^2 mL^{-1}) was immersed in a 1-1 mixture of HCl and methanol to fully reduce the surface. After 10-15 minutes, the wire was removed then rinsed thoroughly with methanol and dried under N$_2$. The wire was then added to the reaction mixture, which was capped with a rubber septum. An N$_2$ sparge needle was then added to the vessel and lowered into the solution to provide mixing to the reaction mixture along with an inert atmosphere for the ATRP reaction.

For polymerizations in preformed cylindrical molds, Cu^0 sheet was cut into 5 mm x 18 mm strips, which were immersed in a 1-1 mixture of HCl and methanol to fully reduce the surface. Cu^0 strips were then rinsed thoroughly with methanol and dried under N$_2$. Sheets were then curled into a cylindrical shape and pressed into the sides of pre-formed mold. The reaction mixture was then transferred to the Cu^0-loaded mold and sealed in an N$_2$-filled vessel at room temperature for 5 hours. Hydrogels were carefully extracted after polymerization, and Cu^0 sheets peeled away from the exterior before proceeding with swelling studies.

5.3.4   ARGET ATRP of PMOEP Using Ascorbic Acid

Syntheses were designed to target a range of degrees of polymerization between 100 and 500. A representative synthesis for target $D_P = 100$ is as follows. 1.9 mg (6.7 μmol) of TPMA, 1.9 mg (6.7 μmol) of CuBr$_2$, 14.4 mg (67.1 μmol) of BPAA, and 59.5 mg (0.5 mmol) of KBr were added to a clean and dry 20 mL scintillation vial. 5 mL of the 1-1 purified MOEP solution was added to the same vial which was gently agitated to homogenize. 100 μL of 2 M sodium ascorbate where then added to the test tube, with further vortexing to homogenize. Aliquots were then transferred to a pre-formed mold, which was covered with a glass slide and placed into a sealed N2-filled vessel. The vessel was placed on a 40 °C hotplate for the duration of the polymerization. After polymerization, the glass slide was carefully removed from the mold, and hydrogels extracted from the mold before swelling.

5.3.5   Hydrogel Swelling and Equilibration

Formed hydrogels were placed in pre-weighed metal mesh weigh boats (20 mesh, 0.016 gauge), which were then re-weighed with the added hydrogel to record starting mass. Loaded weigh boats were then carefully immersed in a dish filled with Type I ultrapure water for 12 hours, with water changed at least 3 time (ca. every 4 hours). Sample weigh boats were then carefully moved to a new container containing phosphate buffer solution, prepared by hand to the specifications for Dulbecco's phosphate buffer solution (*pH* 7.4), to neutralize the phosphate groups. After 12 hours polymer samples were removed and blotted dry with paper towels then weighed to record the swollen hydrogel weight. Hydrogels were then dried *in vacuo* for 24 hours. Dried hydrogels were weighed to determine the degree of swelling, according to the calculation:

$$S = \frac{W_W - W_D}{W_D}$$

Where:

$$S \equiv Swelling\ ratio$$

$$W_W \equiv Swollen\ weight, g$$

$$W_D \equiv Dry\ weight, g$$

5.4 Results and Discussion

5.4.1 MOEP Purification

Commercially-available MOEP is known to contain a high concentration of the bis-methacrylate component (BMOEP) as a residual impurity from the synthesis process, generally cited as ca. 25% on a molar basis.[13] This ratio is extraordinarily high for the molar ratios typically explored for hydrogels, which are generally 5% crosslinker or less on a molar basis, and indicates a need to extract reduce this . Hexane washing has been previously described to remove this diene impurity, though no quantitative description was provided.[14] Given the reported monomer density of 1.233 g mL^{-1}, and a ca. 10 wt% impurity from H_3PO_4, the starting mass for the 25 mL of MOEP used in hexane washes yields a starting mass:

$$25\ mL \times \frac{1.233g}{mL} \times 90\% = 28\ g\ \text{MOEP} - \text{BMOEP}$$

With the molar masses of MOEP and BMOEP (210.1 g mol^{-1} and 322.3 g mol^{-1}, respectively), and the 3:1 molar ratio of MOEP to BMOEP, this may be arranged as:

$$210.1\frac{g}{mol} \times n_{MOEP} + 322.3\frac{g}{mol} \times n_{BMOEP} = 28\ g$$

$$n_{MOEP} = 3n_{BMOEP}$$

98

Substitution then yields starting molar content of 0.088 mol MOEP and 0.029 mol BMOEP.

After removing dissolved hexanes under reduced pressure, the volume of the purified MOEP-H_2O mixture was remeasured. MOEP mixtures were found to lose 3 mL of volume through this purification process; assuming the density of commercially available bis-2-(methacryloyloxy)ethyl phosphate (BMOEP) of 1.28 g mL^{-1}, this corresponds to a loss of 3.8 g, or 0.012 mol. The final concentration of MOEP to BMOEP should then be:

$$x_{MOEP} = \frac{0.088 \; mol}{0.088 + 0.029 - 0.012 \; mol} = 84\%$$

Yielding a final ratio of MOEP:BMOEP of 84:16. It should be noted that this calculation does depend on the assumption that close to 100% of the extracted monomer is BMOEP. After concentration *in vacuo,* the extract did show full phase separation upon efforts to redissolve in water, similar to the behavior of pure BMOEP, but this does not guarantee that no MOEP was extracted by the hexane wash, either due to limited solubility in hexane or cosolvency provided by the extracted BMOEP. As such, this calculation should be thought of as a lower bound for the final concentration of BMOEP, while the true concentration may be marginally higher.

In addition, no further extraction was observed upon repetition of the monomer washing with a new batch of hexanes. This also suggests a limited approach to the removal of BMOEP from MOEP by hexanes. However, this purification is sufficient to solubilize the monomer in water at a 1:2 vol/vol% ratio, which is not possible with untreated MOEP. Still, this high diene content is likely to limit the accessibility of many FRP schemes without dilution by a secondary monomer, as the high degree of crosslinking will yield high internal stress as the network expands, resisting the expansion of the polymer network.[11,13] The use of ATRP may then provide an avenue to

decelerate the polymerization kinetics and target synthesis conditions that allow for the direct polymerization of this monomer without the need for heavy dilution to achieve a workable crosslinker content for FRP.

5.4.2   Cu^0-Mediated Synthesis of PMOEP

Initial polymerizations were performed in test tubes with Cu^0 wire added as the supplemental activator/reducing agent, in order to establish whether the TPMA catalyst is capable of maintaining polymerization for this monomer system. Reactions were initially performed at room temperature, in accordance with results demonstrated for methacrylic acid. Polymerizations demonstrate limited success, with only 8% conversion observed in 2 hours. These reactions are accompanied by the accumulation of a white precipitate on the surface of the Cu^0 wire, appearing to limit the effective surface area available to promote polymerization. FTIR analysis was conducted for the white precipitate, shown in Figure V-2. This spectrum demonstrates clear carbonyl signals at 1726 cm^{-1}, along with a sharp peak at 1639 cm^{-1} that is indicative of alkene C=C.[15] This may indicate limited solubility of the growing polymer chains, leading to aggregation along the Cu^0 wire with incorporation of residual alkene content due to the presence of BMOEP, and even coprecipitation of monomeric MOEP. Indeed, the native *pH* for MOEP reaction mixtures is ca. 0.4, due to the high percentage of phosphoric acid in commercially available MOEP (ca. 10% as reported in the SDS). Under these conditions then, both free oxygens in the phosphate structure would be expected to be nearly fully protonated, decreasing the overall solubility of the growing polymer chains. The accumulation of this hydrophobic content in the polymer backbone likely shifts the growing polymer chains to favor adsorption to the surface of the Cu^0 wire. Furthermore, given the

high content of BMOEP remaining in solution, this polymer is likely to crosslink and induce

gelation across the surface of the wire, further limiting the ability to desorb back into solution.
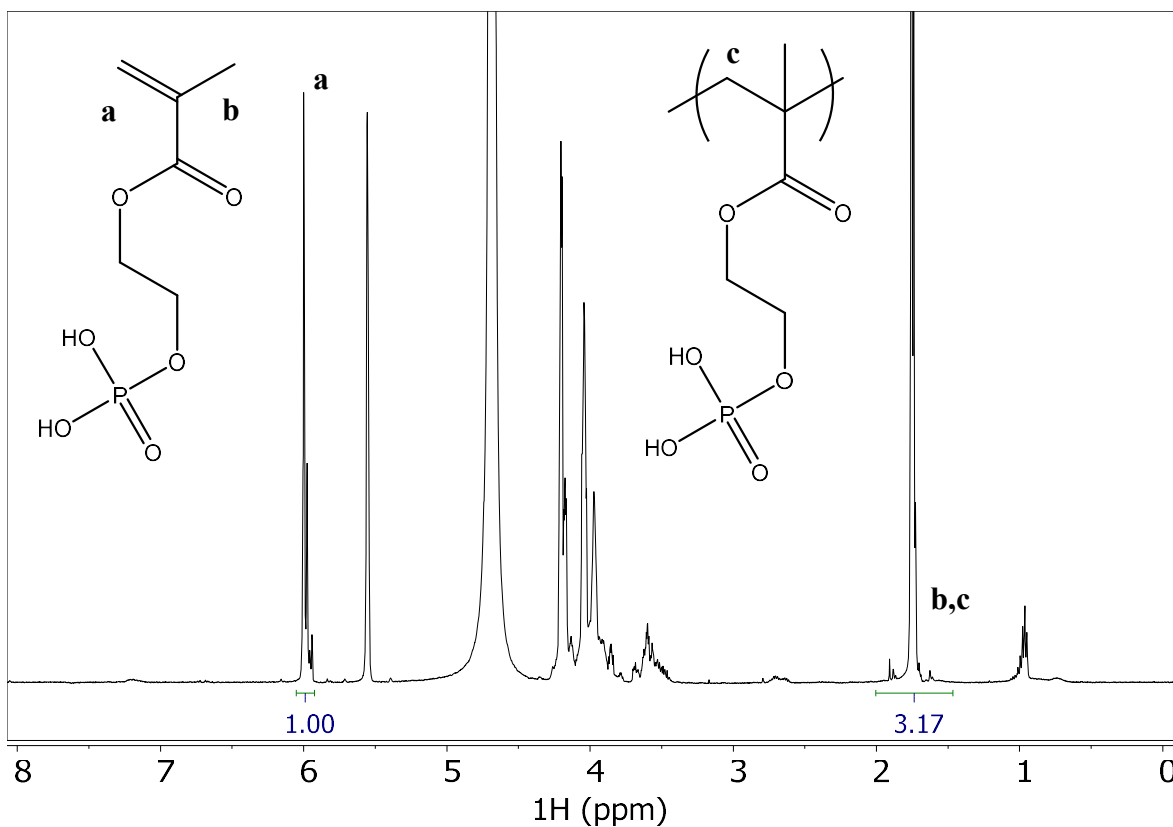
Figure V-1: NMR spectra for initial polymerization of PMOEP, showing limited polymerization (ca. 8% conversion).
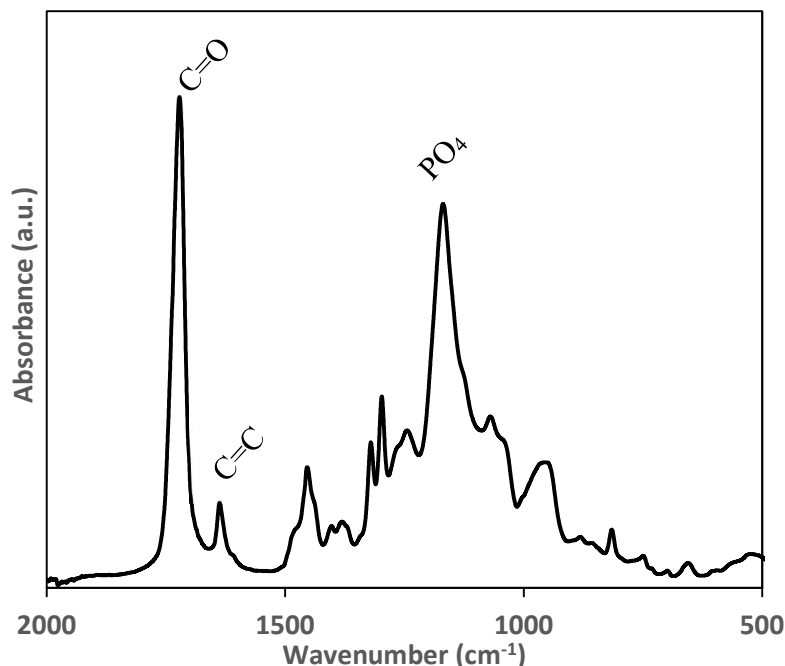
Figure V-2: FTIR spectrum for the precipitate observed on the surface of Cu^0 wire under fully aqueous conditions.

5.4.2.1 Fully Aqueous ATRP by External Sonication

Polymerizations were repeated in a sonication bath, to probe the effect of agitating the copper surface to induce continued turnover of the catalyst surface. These polymerizations demonstrate a marked improvement in conversion, with polymerization achieving 27% in 2 hours of polymerization, increasing further to 57% in 3.5 hours (). By $t = 4$ hr, the polymer solution had crosslinked to the point of full gelation, marking a critical gelation point of ca. 60% conversion for this formulation. This formulation should thus represent a promising starting point for the synthesis of pre-shaped hydrogels.

102
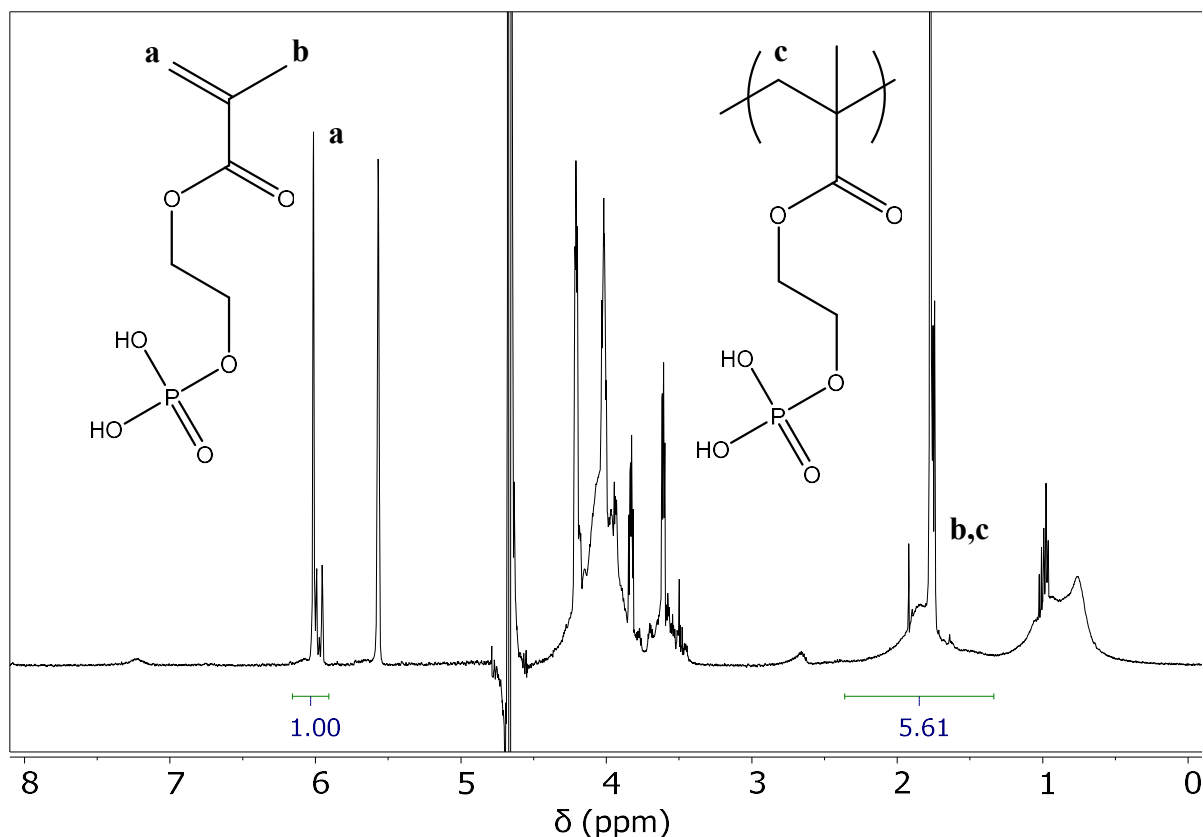
Figure V-3: NMR spectra for PMOEP mixture with sonication at t = 3.5 hr, demonstrating 57% conversion prior to gelation.

5.4.2.2   Polymerizations in Pre-formed Molds

With this data, new polymerizations were explored to synthesize hydrogels in pre-formed cylindrical molds. Molds were lined with pretreated strips of Cu^0, then loaded with the polymerization mixture and sealed in an N_2-filled vessel for 6 hours to polymerize, with continuous sonication. The loaded mold was placed in a glass petri dish, which was carefully lowered into the sonication bath, with sonication provided throughout. These initial polymerizations yielded poor results, with only some wells of the 16-well mold demonstrating any signs of polymerization, observed as a film of hydrogel lining the copper insert of the mold. This is likely a limitation of

the sonication route; the sonication bath is likely to produce standing waves and local areas of relatively high and low intensity in sonication, preventing proper polymerization across the entirety of the mold.

In effort to combat this, a polymerization was repeated with 20 vol% ethanol in water as the solvent for the polymerization. This inclusion should provide additional solubility to the monomer and growing chains, helping to prevent precipitation across the surface of the copper. Polymerizations were conducted with and without sonication, to assess whether the ethanol is sufficient to solubilize the polymer. Indeed, the polymerizations both yield similar results, with hydrogels observed for all 16 wells in both cases, suggesting the inclusion of ethanol is sufficient to replace the sonication route.

However, for both polymerizations with and without sonication, the hydrogels show poor homogeneity, with good gelation observed towards the exterior of the gel, but poor gelation towards the center of each well. This effect led to the tearing of hydrogels during the removal of Cu^0 sheets in all cases. This suggests poor diffusion between the Cu^0 surface and the interior of the mold, leading to asymmetric gelation behavior that blocks the Cu^0 surface before the full hydrogel polymerizes. However, the contribution of the NaCl supporting salt may be exacerbating this effect; this contribution is known to yield improved control over ATRP under aqueous conditions, but also generally slows the rate of polymerization in most cases. This deceleration may limit the gelation of the PMOEP chains, as the slowed kinetics allow greater time for the organization of growing chains near the Cu^0 surface to inhibit further activation of dormant chains.

Polymerizations were thus repeated with the omission of the added NaCl salt and indeed, these new polymerizations did yield full gelation of the reaction mixtures. Hydrogels were carefully

extracted from the mold, and Cu^0 sheets removed from the hydrogel surface before weighing and transfer to Type I ultrapure water baths to equilibrate under fully swollen conditions. Gels were synthesized with varied initiator content to target varied molecular weight of the primary polymer chains and probe their effect on the overall structure of the polymer network.

5.4.2.3   Shape Retention and Fracture During Swelling

During swelling, samples were monitored to examine their retention of shape and structure. Though gels did show good retention of gel structure initially, gels were observed to crack and eventually fracture as they continued to swell with water uptake. Gels with higher target D_P demonstrated less fracturing in general but were still not able to retain full shape throughout swelling. This was often observed as the shedding of smaller fragments around fracture points (Figure V-4). Interestingly, many fracture failures also demonstrated fracture along the top and bottom surfaces of the cylinder, appearing to expand outward and propagate fractures outward through the remainder of the hydrogel. This is likely a result of remaining heterogeneity in the gel network; as the polymerization proceeds, the radial distance from the Cu^0 sheet introduces a gradient in polymerization rate, and thus a gradient in gelation time. The gel network would then be expected to demonstrate a gradient in swelling and overall mechanical strength, leading to the asymmetric mode of failure observed during equilibration. Effectively, the hydrogels will have the highest degree of crosslinking – and thus resistance to swelling – at the exterior of the cylinder. As the interior continues to swell, the additional stress along the exterior of the cylinder eventually induces mechanical failure throughout the gel. These results suggest poor translation of Cu^0-mediated synthesis to synthesis of hydrogels in a pre-formed shape.

105
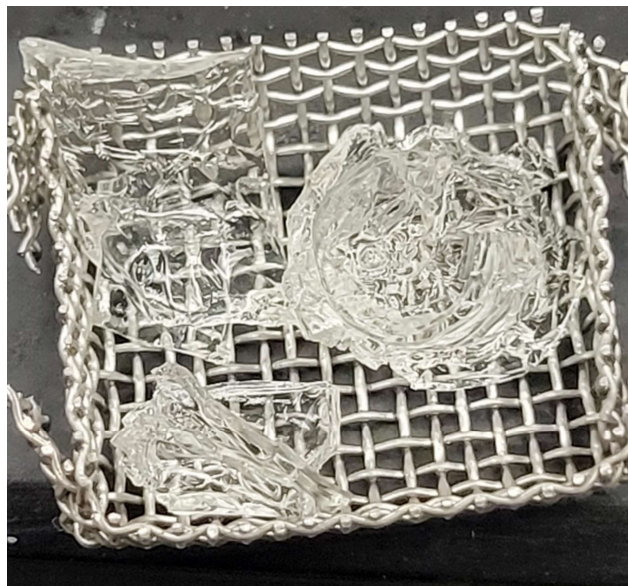
Figure V-4: Swelling behavior of PMOEP hydrogel as synthesized with Cu^0-mediated ATRP.

5.4.3   ARGET ATRP of PMOEP Using Ascorbic Acid

In effort to better homogenize the polymerization system, ascorbic acid-mediated ARGET ATRP was evaluated as an alternative to the Cu^0 reducing species. This mechanism has been explored previously for the synthesis of PDMAEMA-co-PEGDMA hydrogels and has recently been demonstrated for the polymerization of methacrylic acid under acidic conditions, so should be expected to yield meaningful control for this monomer system.[3,9]   Initial polymerization conditions were chosen based on successful results from the synthesis of MAA, with a target D_P of 100. A preliminary attempt for this method demonstrated poor results at the previous conditions established thus far through the study – that is, 1:2 vol% monomer to water at room temperature, utilizing NaCl and $CuCl_2$ to induce a halide exchange for retaining greater control over the ATRP equilibrium. This polymerization was limited to <20% conversion after 12 hours. Polymerization was thus repeated with a higher initial loading of monomer (1:1 vol%) using KBr and $CuBr_2$, with

the sealed reaction vessel place on a 40 °C hotplate for the duration of the reaction. These conditions are closer in line to the optimized conditions reported for PMAA using ascorbic acid-mediated ARGET ATRP. This polymerization demonstrated successful gelation after 6 hours and gels were successfully extracted from molds by gently wetting the glass cover slide and lifting from the mold. Polymerizations were then repeated for target D_P of 200, 300, and 400, to probe the effects of varied degrees of polymerization on overall network structure.

5.4.3.1   Shape Retention and Fracture During Swelling

ARGET-synthesized hydrogels demonstrated a greater uniformity in shape even before swelling, as the gels were not subject to surface roughness or asymmetry introduced by the Cu^0 sheet in previous formulations. Though $D_P = 100$ hydrogels demonstrated good retention of shape initially, they crumbled into many small fragments upon full equilibration, suggesting poor overall network strength and high internal stress during equilibration (Figure V-5). However, as the initiator concentration decreased, the retention of shape throughout swelling showed marked improvement. At $D_P = 200$, 6 out of 8 hydrogels fractured during equilibration; however, hydrogels show fracturing cleanly along the radial cross section, generally near to the center height of the cylinder (Figure V-6). This is attributed to the asymmetric initial swelling of the hydrogel; as the ends of the cylinder provide additional surface area, hydrogels will naturally swell faster from the ends inward, leading to asymmetric swelling during the transient equilibration process.

This asymmetry likely adds additional stress to the network, introducing small weakness and cracks that can propagate through the material as the center swells to equilibrium.

Figure V-5: Images for D_P =100 hydrogels demonstrating observed mode of failure during equilibration in water. Left: equilibrated in PBS. Right: after drying.
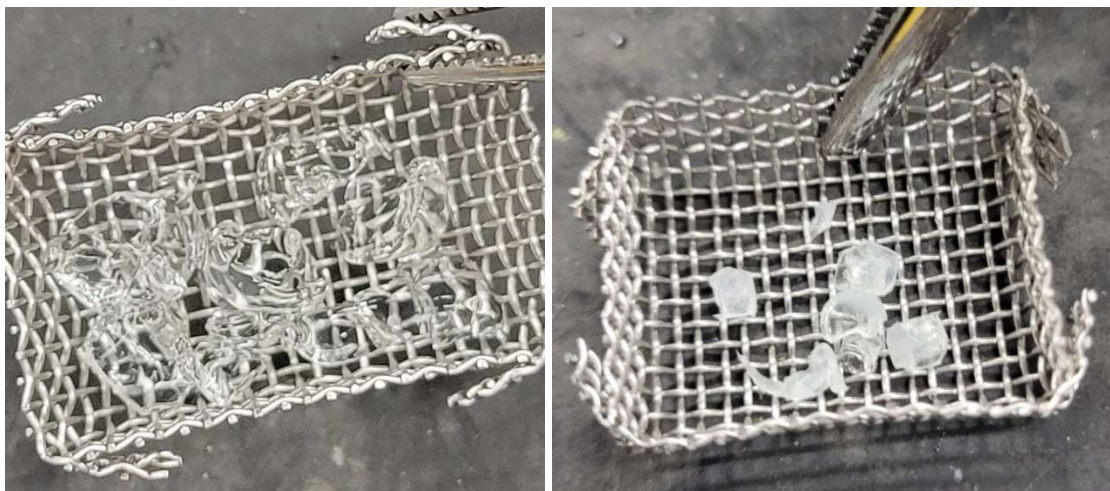

Figure V-6: Images for D_P = 200 hydrogels demonstrating observed mode of failure during equilibration in water. Left: equilibrated in PBS. Right: after drying.
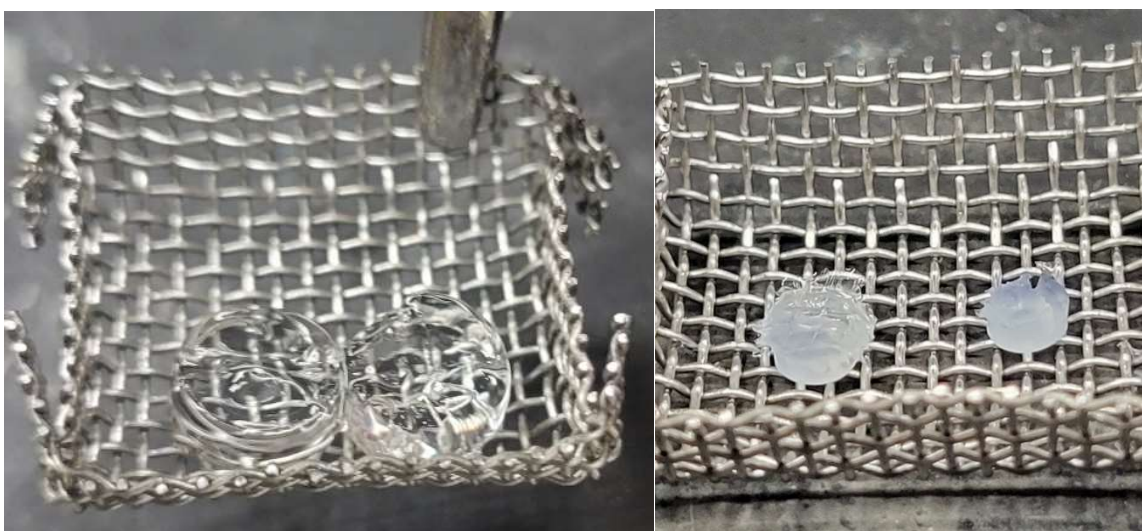
Further increasing the target D_P to 300 and 400 yields a decrease in the rate of polymerization, with small hydrogel cylinders observed after 6 hours, but most of the mold still filled with liquid. This is likely a reflection of the decreased loading of both the Cu^{II}/TPMA catalyst complex and the number propagating chains, yielding a lower number of active radicals and decreasing the overall rate of polymerization. However, upon repetition of the experiment with polymerizations allowed to run for 12 hours, fully formed hydrogels are observed, with a slightly yellow discoloration. This is assumed to be the oxidation of ascorbic acid to dehydroascorbic acid, marking full consumption of the added reducing agent. The gels synthesized under these conditions exhibit improved resilience to swelling, with $D_P = 300$ hydrogels retaining full structure in 7 out of 8 hydrogels synthesized. The one gel that did fracture showed a similar mechanism of failure to those failures observed at $D_P = 200$, with a clean fracture along the radial axis. Interestingly, the $D_P = 400$ hydrogels show poorer retention of shape, with 5 out of the 8 hydrogels synthesized fracturing along the radial axis during the initial equilibration period. This suggests a detrimental effect upon further increasing the target degree of polymerization above 300.

A polymerization was repeated for $D_P = 300$ and 400 utilizing a higher Cu^{II}/TPMA catalyst loading, increased from 1 mM Cu^{II} to 4 mM Cu^{II}. This comparison was designed to assess the impact of the lowered Cu^{II} concentration on the overall control and speed of the polymerization, as the hydrogels at D_P 300 did require longer reaction times to properly polymerize. These reactions did show full gelation within the expected 6-hour reaction window, suggesting the low catalyst loading at higher target D_P is responsible for the slowed conversion. However, these hydrogels showed poorer resilience to fracturing during swelling, with similar rates of failure observed as with the D_P 400 gels (ca. 50% of gels fracturing before fully equilibrated).

5.4.3.2 Swelling Ratio and Equilibrium Uptake

Swelling ratios were calculated for the equilibrated hydrogels, with results presented in Table V-1, presented with 95% confidence intervals. The equilibrium swelling ratio displays a nearly linear relationship with the target degree of polymerization, indicating a steady increase in the equilibrium uptake of water as the primary chain length increases. However, at $D_P = 300$ there is a sharp increase in swelling, with an average swelling ratio of 25.7. Swelling ratio then decreases to 13.6 upon increasing target D_P further to 400. This suggests a subsequent increase in crosslinking density past this point, in good agreement with the observation of increased fracturing for hydrogels at $D_P = 400$.

Table V-1: Polymerization conditions and swelling characteristics for PMOEP hydrogels as synthesized by ARGET ATRP.[a]

Entry	Target D_P	[BPAA]:[TPMA]:[CuBr$_2$]	Swelling Ratio[b]	Conversion[c] (%)
1	100	1:0.1:0.1	6.3 ± 0.2	74 ± 1.6
2	200	1:0.1:0.1	9.4 ± 0.5	59 ± 1.7
3	300	1:0.1:0.1	25.7 ± 1.3	33 ± 1.8
4	400	1:0.1:0.1	13.6 ± 2.8	55 ± 4.1
5	300	1:0.4:0.4	12.3 ± 1.1	-
6	400	1:0.4:0.4	13.9 ± 3.2	-

[a]: All polymerizations were conducted at 50 vol% MOEP with TPMA as ligand and BPAA as initiator, and [KBr] = 0.1 M. [b]: As determined in phosphate buffer solution, pH 7.4. [c]: Calculated gravimetrically.

Swelling ratios were also measured for the optimized $D_P = 300$ hydrogels in Type I ultrapure water, to assess the impact of the salts in PBS on swelling structure. This data is presented in Figure V-7. As expected for the high density of phosphate moieties, the exclusion of the sodium

and potassium cations relaxes the electrostatic interaction between the pendant phosphates and solution, leading to further expansion of the hydrogel to an average final swelling ratio of 61. A visual demonstration of the change in size between the dry hydrogel and the various states of swelling is presented in Figure V-8, demonstrating the clear change in volume across the various stages of swelling.
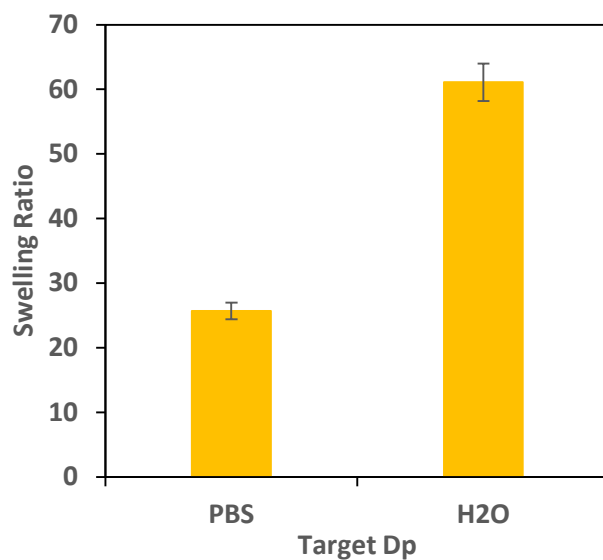
Figure V-7: Swelling ratio for PMOEP Hydrogels with Target Dp = 300, as equilibrated in PBS and Type I ultrapure water (pH 7).
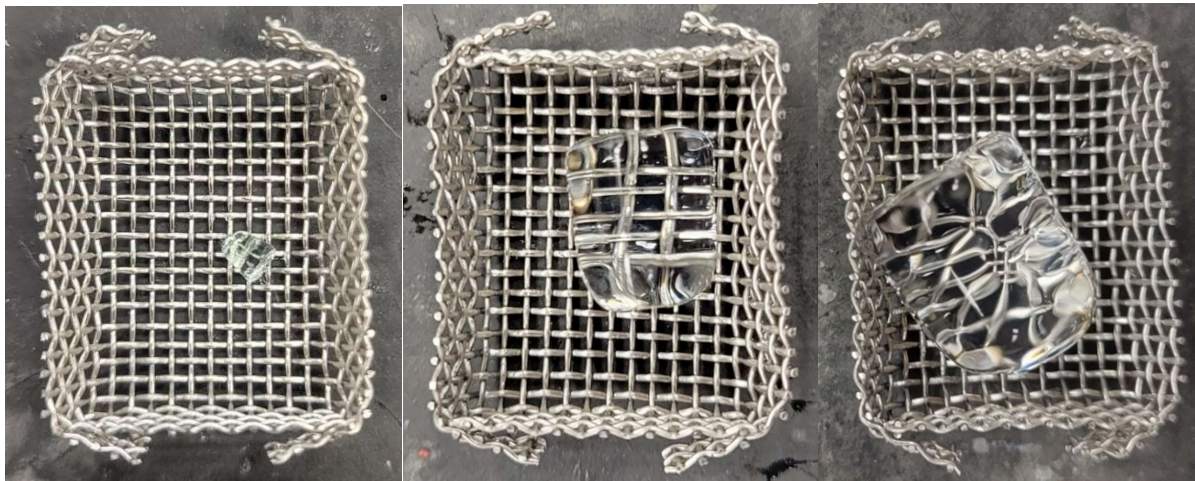
Figure V-8: Images of various states of swelling for PMOEP hydrogel (target D_P = 300). Left: dry gel. Middle: equilibration in PBS, pH 7.4. Right: equilibration in Type I ultrapure water.

These results suggest a reduction of overall degree of crosslinking with decreased initiator concentration, at least up until D_P > 300. This is counter to the conventional wisdom for FRP hydrogels which dictates that increased initiator concentration – that is, lower target D_P – yields an increase in the overall swelling ratio, due to the reduction in primary chain length.[16] Conversely, the results presented here demonstrate that increasing the length of individual chains improves the overall structure of the gel, enabling greater swelling. This is rather counterintuitive on first consideration, as one would expect longer primary chains to contain a greater number of crosslinking points, favoring the increase in crosslinking density. This result is likely owed to the controlled initiation step of ATRP; in FRP, radicals are continuously generated to initiate new chains, to balance for the loss of chains to termination. This high concentration of active chains then favors crosslinking, with longer chains naturally accumulating a higher overall quantity of crosslinks. However, under the conditions of ATRP initiation starts with a constant concentration

of chains, dictating the maximum number of radicals available for propagation. That is, a decrease in the concentration of initiator decreases the number of chains available to crosslink into, allowing chains to grow at a more uniform rate before the point of gelation.

However, it is also important to consider the ability for chains to "self-crosslink," with the radical at the end of one chain propagating into a pendant alkene on the same chain. This does not terminate the propagating chain, but instead introduces small loops into the polymer network that reduce the overall homogeneity of the hydrogel. Indeed, this effect has been noted to be dominant at high crosslinker loading for model gelation experiments in the ATRP of methyl acrylate with ethylene glycol diacrylate crosslinkers.[17] This effect is likely the cause for the observed decrease in swelling ratio at $D_P = 400$ – as the primary chain length increases, this rate of self-cyclization will become statistically favored as the random coil configuration of the growing polymer chain surrounds the active chain end with an ever-increasing number of pendant alkenes, with inter-chain crosslinking serving to further accelerate this localized . This mechanism would also explain the observed increase in variance for swelling at $D_P = 400$, as the accumulation of these pendant loops disrupt the regular order and organized structure of the hydrogel network. The accumulation of these defects would then provide weak points in the overall structure of the hydrogel to initiate the first crack in the hydrogel which may then propagate outward as the hydrogel continues to swell.[18]

Conversions were also calculated gravimetrically, based on the difference between the starting weight of the hydrogel and the weight of the hydrogel after swelling and subsequent drying. These measurements are effectively a measure of the conversion at the point of gelation, as the diffusion of monomer and catalyst to the terminal alkyl bromides will be so heavily hindered past the point of gelation. The trend in these gelation conversions appears to inversely mirror the trends in

swelling ratio, with conversion decreasing initially until $D_P = 300$, then increasing at $D_P = 400$. Gao et. al have previously demonstrated that the gelation conversion decreases in methyl acrylate gels with increasing crosslinker concentration relative to initiator, as the rate of crosslinking increases and leads to earlier gelation.[17] However, these experiments were conducted with a constant concentration of initiator and varied crosslinker concentration, rather than the series here that examines a constant concentration of crosslinker and decreasing concentration of initiator. The decrease in concentration of propagating chains would thus be expected to shift the point of gelation to high conversion, as the decreased concentration of chains limits the rate of crosslinking. Indeed, the same study demonstrates that decreasing the concentration of all components – that is, diluting with additional solvent – shifts the gelation point to higher conversion. The increase in gelation conversion at $D_P = 400$ then agrees with the interpretation of increased intra-chain crosslinking as the mechanism for the poor swelling behavior observed at $D_P = 400$.

The swelling characteristics for the hydrogels synthesized with increased catalyst loading show a decrease in equilibrium swelling, with an observed swelling ratio of 12.3. This degree of swelling shows good agreement with observation with increased rate of fracturing in the final hydrogels, with   This is a near two-fold decrease from the polymerization with lower catalyst loading, suggesting that slower kinetics are necessary to retain the well-defined hydrogel structure observed. This is likely related to both the increase in the rate of chain-to-chain and intra-chain crosslinking, with the increase in equilibrium radical concentration favoring an increase to both modes of crosslinking. Interestingly, the hydrogels as synthesized at $D_P = 400$ with increased Cu^{II} loading show nearly identical results to those synthesized with the lowered Cu^{II} loading, with swelling ratios of 13.9 and 13.2, respectively. This invariance to catalyst concentration at higher

D$_P$ suggests the onset of self-propagation cannot be offset at these higher primary chain lengths, with the accumulating defects in the hydrogel disrupting the expansion of the final polymer network. This system then relies on a delicate balance between these two factors, with a need to suppress the rapid crosslinking between chains that would lead to poor swellability, without reducing the initiator concentration to the point that the rate of intra-chain propagation begins to dominate the overall polymerization.
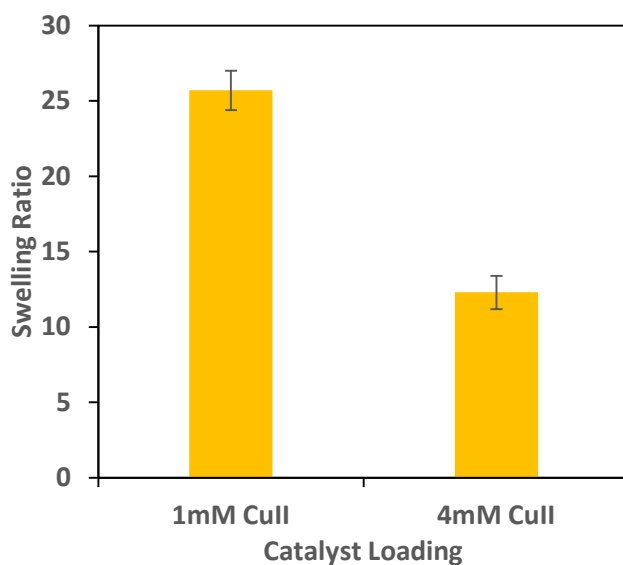
Figure V-9: Swelling ratios for PMOEP hydrogels at *D$_P$* = 300 with varied catalyst loading.

This mechanism for improved swellability with decreasing initiator concentration would also suggest there is likely an increase in latent diene in the higher *D$_P$* gels. Indeed, at a molar ratio of 84:16, this would suggest ca. 1 in 6 repeat units are BMOEP, with the pendant alkenes not consumed by crosslinking available for further modification after the synthesis of the polymer.

This may provide a promising avenue for introduction of surface modification of the hydrogels through click chemistries or other facile methods and should be further explored. Such routes would likely provide a facile approach for the fixation of proteins or other moieties to encourage cell adhesion, as well as the introduction of secondary or tertiary functional comonomers after gelation.

Overall, these conditions demonstrate excellent potential for the development of MOEP hydrogels in pre-shaped molds, with good retention of physical structure through the swelling process. These conditions are presented at 100% MOEP content but should extend to hydrogel formulations with the inclusion of comonomers for specific applications, with high content of MOEP still readily achievable. Furthermore, the low concentration of Cu^{II} used for the optimum gel formulation here (1 mM total Cu^{II}) represents a promising formulation for implementation in biomedical applications, where copper must be thoroughly removed prior to use.

5.5   Conclusions

Using aqueous ATRP, hydrogels have been synthesized for 2-(methacryloyloxy)ethyl phosphate using only the internal diene impurity as the crosslinker. This yields a hydrogel with high density of phosphate moieties, without the approach generally required for free radical polymerization techniques to heavily dilute the phosphate moiety with a tertiary monomer. Varying the initiator concentration for the polymerizations serves to tune the degree of crosslinking in final hydrogels by modulating both the total number of chains available for polymerization, as well as the concentration of active radicals through the reduction of Cu^{II}/TPMA concentration. The demonstrated optimum at a target D_P of 300 demonstrates excellent swelling characteristics

116

given the high crosslinker content present in the starting monomer, with an equilibrium swelling ratio of 6,100% in pure water. To our knowledge, these conditions represent the first instance of well-defined hydrogels for MOEP without addition of comonomers. These conditions may serve as a template for the introduction of comonomers to synthesize further functional hydrogels, with the phosphate content tunable to any desired ratio rather than the <5% often explored in literature for FRP approaches.

5.6   References

1.   Qi, X., Li, J., Wei, W., Su, T., Zuo, G., Pan, X., Zhang, J., and Dong, W., *Preparation of a Salecan/poly(2-acrylamido-2-methylpropanosulfonic acid-co-[2-(methacryloxy)ethyl]trimethylammonium chloride) Semi-IPN Hydrogel for Drug Delivery.* ChemMedChem, 2017. **12**(2): p. 120-129. DOI: 10.1002/cmdc.201600570.
2.   Qian, X., Villa-Diaz, L.G., Kumar, R., Lahann, J., and Krebsbach, P.H., *Enhancement of the propagation of human embryonic stem cells by modifications in the gel architecture of PMEDSAH polymer coatings.* Biomaterials, 2014. **35**(36): p. 9581-90. DOI: 10.1016/j.biomaterials.2014.08.015.
3.   Beziau, A., De Menezes, R.N.L., Biswas, S., Singh, A., Cuthbert, J., Balazs, A.C., Kowalewski, T., and Matyjaszewski, K., *Combining ATRP and FRP Gels: Soft Gluing of Polymeric Materials for the Fabrication of Stackable Gels.* Polymers, 2017. **9**(6): p. 186. DOI: 10.3390/polym9060186.
4.   Vilela, C., Martins, A.P.C., Sousa, N., Silvestre, A.J.D., Figueiredo, F.M.L., and Freire, C.S.R., *Poly(bis[2-(methacryloyloxy)ethyl] phosphate)/Bacterial Cellulose Nanocomposites: Preparation, Characterization and Application as Polymer Electrolyte Membranes.* Applied Sciences, 2018. **8**(7): p. 1145.
5.   Yoon, J.A., Gayathri, C., Gil, R.R., Kowalewski, T., and Matyjaszewski, K., *Comparison of the Thermoresponsive Deswelling Kinetics of Poly(2-(2-methoxyethoxy)ethyl methacrylate) Hydrogels Prepared by ATRP and FRP.* Macromolecules, 2010. **43**(10): p. 4791-4797. DOI: 10.1021/ma1004953.
6.   Sperling, L.H., *Crosslinked Polymers and Rubber Elasticity*, in *Introduction to Physical Polymer Science*. 2005. p. 427-505.
7.   Yu, Q., Xu, S., Zhang, H., Ding, Y., and Zhu, S., *Comparison of reaction kinetics and gelation behaviors in atom transfer, reversible addition–fragmentation chain transfer and conventional free radical copolymerization of oligo(ethylene glycol) methyl ether methacrylate and oligo(ethylene glycol) dimethacrylate.* Polymer, 2009. **50**(15): p. 3488-3494. DOI: https://doi.org/10.1016/j.polymer.2009.05.032.

8. Fantin, M., Isse, A.A., Venzo, A., Gennaro, A., and Matyjaszewski, K., *Atom Transfer Radical Polymerization of Methacrylic Acid: A Won Challenge.* J. Am. Chem. Soc., 2016. **138**(23): p. 7216-9. DOI: 10.1021/jacs.6b01935.

9. Fu, L., Simakova, A., Fantin, M., Wang, Y., and Matyjaszewski, K., *Direct ATRP of Methacrylic Acid with Iron-Porphyrin Based Catalysts.* ACS Macro Letters, 2018. **7**(1): p. 26-30. DOI: 10.1021/acsmacrolett.7b00909.

10. Fantin, M., Isse, A.A., Gennaro, A., and Matyjaszewski, K., *Understanding the Fundamentals of Aqueous ATRP and Defining Conditions for Better Control.* Macromolecules, 2015. **48**(19): p. 6862-6875. DOI: 10.1021/acs.macromol.5b01454.

11. Głowińska, A., Trochimczuk, A.W., and Jakubiak-Marcinkowska, A., *Novel acrylate/organophosphorus-based hydrogels for agricultural applications. New outlook and innovative concept for the use of 2-(methacryloyloxy)ethyl phosphate as a multi-purpose monomer.* European Polymer Journal, 2019. **110**: p. 202-210. DOI: https://doi.org/10.1016/j.eurpolymj.2018.11.020.

12. Stancu, I.C., Filmon, R., Cincu, C., Marculescu, B., Zaharia, C., Tourmen, Y., Basle, M.F., and Chappard, D., *Synthesis of methacryloyloxyethyl phosphate copolymers and in vitro calcification capacity.* Biomaterials, 2004. **25**(2): p. 205-13. DOI: 10.1016/s0142-9612(03)00485-x.

13. Grøndahl, L., Suzuki, S., and Wentrup-Byrne, E., *Influence of a diene impurity on the molecular structure of phosphate-containing polymers with medical applications.* Chemical Communications, 2008(28): p. 3314-3316. DOI: 10.1039/B803223H.

14. Toyomoto, Y., Matsuno, R., Konno, T., Takai, M., and Ishihara, K., *Preparation of poly(2-methacryloyloxyethyl phosphorylcholine)/hydroxyapatite hybrid matrix.* Transactions of the Materials Research Society of Japan, 2010. **35**(1): p. 123-126. DOI: 10.14723/tmrsj.35.123.

15. Kuptsov, A.H. and Zhizhin, G.N., *Handbook of fourier transform Raman and infrared spectra of polymers*. Physical sciences data. 1998, Amsterdam ; New York: Elsevier. 546.

16. Singhal, R., Tomar, R.S., and Nagpal, A.K., *Effect of cross-linker and initiator concentration on the swelling behaviour and network parameters of superabsorbent hydrogels based on acrylamide and acrylic acid.* International Journal of Plastics Technology, 2009. **13**(1): p. 22. DOI: 10.1007/s12588-009-0004-4.

17. Gao, H., Li, W., and Matyjaszewski, K., *Synthesis of Polyacrylate Networks by ATRP: Parameters Influencing Experimental Gel Points.* Macromolecules, 2008. **41**(7): p. 2335-2340. DOI: 10.1021/ma702823b.

18. Long, R. and Hui, C.-Y., *Fracture toughness of hydrogels: measurement and interpretation.* Soft Matter, 2016. **12**(39): p. 8069-8086. DOI: 10.1039/C6SM01694D.

CHAPTER VI: Temperature- and *pH*-Responsive Behavior of Poly(2-[dimethylamino]ethyl methacrylate)

6.1 Abstract

Poly(2-[dimethylamino]ethyl methacrylate) is a *pH*- and temperature-responsive polymer, with a known lower-critical solution (LCST) that is modulated by protonation of the tertiary amine pendant groups. Though multiple studies exist exploring the impact of ionic strength and other additives on this phenomenon, to date no comprehensive studies exist to isolate the impact of individual salts on this behavior. In this study, we report the LCST behaviors of PDMAEMA with varied *pH* in the presence of four varied anions: phosphate, sulfate, acetate, and chloride. Comparisons are drawn to understand the relative impact of their structure on the LCST behavior at varied degrees of protonation. Notably, phosphate presents the lowest LCST at intermediate protonation. This is associated with a higher *pH* as measured at the LCST, indicating the equilibrium *pH* must be considered as the solution is heated. Further consideration of the underlying thermodynamic equilibrium reveals that the full consideration of the LCST phenomenon must account for the impact of increasing temperature on the overall protonation to properly interpret the LCST, with preliminary results suggesting a convergence to a similar "critical protonation" to trigger the collapse of polymer chains. This approach may yield a deeper insight into the overall responsive behavior for PDMAEMA and similar polymers.

6.2 Introduction

Poly(2-[dimethylamino]ethyl methacrylate) has been explored in a wide range of applications in recent years, as the tertiary amine pendant group introduces a responsive behavior to both

temperature and *pH*.[1-8]   These responsive behaviors are coupled, as protonation of the tertiary amine shifts the overall hydrophilicity of the polymer and the resulting temperature responsive behavior. This effect has been well documented, with complex behaviors between varied *pH*, temperature, ionic strength, and polymer molecular weight established to yield varied impacts on the polymer responsiveness.[9]

Previous independent studies have verified that LCST is sensitive to ionic strength of the solution using sodium chloride, while others have demonstrated a varying dependence on counteranion structure with and without the presence of other additives such as urea, in effort to discern the contribution of the various electrostatic interactions to the overall LCST phenomenon.[5,9] However, these studies often are restricted to small subsets of the possible combinations of variables for the sake of brevity, or otherwise combine multiple variables that make uniquely teasing apart these variables difficult. Furthermore, the existing state of the literature generally approaches these characterizations by assigning an LCST based on the *pH* measured at room temperature, which is then heated to the point of the collapse from the freely solvated random coil configuration to the hyper-coiled state, marked by a rapid increase in solution turbidity. However, this approach neglects the underlying thermodynamics that may be driving the true LCST phenomenon.

In this study, we report the examination of the LCST for PDMAEMA from the perspective of a narrow set of *pH* and ionic strength, to assess the impact of these variables more closely at set conditions. Consideration of the underlying thermodynamic equilibrium at play during the heating of these polymer solutions reveals a strongly coupled dependency of *pH* and temperature to determine the ultimate LCST. Potentiometric titration at $T = 50$ °C reveal a sharp drop in pK_a

from the reported literature value to 6.3, indicating a high enthalpy of protonation of $\Delta H = -89$ kJ mol^{-1} as a preliminary calculation. Assessing the LCST phenomenon from the perspective of driving dissociation of the protonated DMAEMA pendant groups, preliminary results indicate a good correlation between the predicted degree of protonation at the point of polymer collapse, suggesting the trigger for LCST behavior in these polymers is the dissociation of the protonated DMAEMA species below a critical solubility limit. Continued investigation of this phenomenon is expected to help elucidate the underlying mechanism of the LCST phenomenon and allow for more predictive assessments in the approach to these polymers.

6.3   Materials and Methods

6.3.1   Materials

Sodium acetate trihydrate (CAS 6131-90-4; 99%) and sodium phosphate, dibasic (CAS 7558-79-4; 99%) were purchased from Fisher. Sodium hydroxide (CAS 1310-73-2; 97%), and sulfuric acid (CAS 7664-93-9; 95%) were purchased from Sigma-Aldrich. Glacial acetic acid (CAS 64-19-7; 99.7%), hydrochloric acid (CAS 7647-01-0; 36.5%), and sodium chloride (CAS 7647-14-5; 98%) were purchased from VWR. Type I ultrapure water (18.2 MΩ) was generated using a Millipore Synergy UV Water Purification System. Poly(2-[dimethylamino]ethyl methacrylate) was synthesized as described previously, with $M_N = 37.5$ kDa, $Đ = 1.13$. All reagents were used as received.

6.3.2   Sample Preparation – pH, Ionic Strength, and Anion Structure

PDMAEMA was synthesized as described previously, with a targeted degree of polymerization of 200. Samples were purified by precipitation on heating above the LCST through

two heating cycles, with the supernatant decanted from the precipitated polymer between cycles. Purified polymer was dried *in vacuo* prior to use. Stock solutions of NaOH, H_3PO_4, HCl, H_2SO_4, and CH_3COOH were prepared at 2 M and 0.1 M for *pH* adjustments. Polymer solutions were prepared at a starting concentration of 5 mg mL^{-1}. Solutions were then adjusted to the target *pH*, with added volumes of each reagent recorded during the *pH* adjustment. The corresponding sodium salt for the acid used to adjust *pH* was added to raise the total solution ionic strength to 0.1 M. Solution *pH* was remeasured and adjusted to the target *pH* as necessary. After the desired *pH* and ionic strength were obtained, PDMAEMA concentrations were recalculated. Additional polymer was added to bring the concentration back to 5 mg mL^{-1}, as needed. This process was repeated iteratively until all desired solution variables were obtained.

6.3.3   LCST Characterization

Prepared PDMAEMA solutions were added to polystyrene cuvettes, with ca. 3 mL total volume added. Cuvettes were inserted in a modified sample holder for a Shimadzu UV2101 UV-Vis spectrometer, with a liquid flow cell attached to an external circulating water bath for temperature control. Cuvette lids were modified to insert a Type K wire thermocouple into the upper portion of the polymer solution, above the beam path for the spectrometer. This thermocouple was attached to an external temperature controller (J-KEM Scientific, Model 210), which controlled power output to the water bath to apply the desired heating profile. Solutions were heated at a rate of 5 °C hr^{-1}, with transmittance at $\lambda = 633$ nm recorded every 60 seconds throughout the heating profile. LCST was determined by fitting an inverse S-curve to the raw data, such that:

$$Transmittance = 100 * \left(1 - \frac{1}{\exp(k * [LCST - T])}\right)$$

Curves were fit by varying k and $LCST$ to minimize the squared error between the model and experimental data.

6.4   Results and Discussion

6.4.1   LCST Calculation

The chosen fit for LCST dependency gives a means for improving objectivity in the assessment of LCST from raw data. Effectively, this curve models the decay of transmittance by fitting $LCST$ as the center point of the decay, using k as a shape factor to determine the width of the decay. This fit is readily achieved numerically and allows for rapid assessment of LCST without the need to manually sort through data and assign the data point closest to 50% transmittance as LCST. Furthermore, this fitting yields a shape factor k that may be used to assess the "sharpness" of LCST transitions between individual analyses in a more rigorous manner. An example fit is presented in Figure VI-1 to demonstrate the results of this fitting.
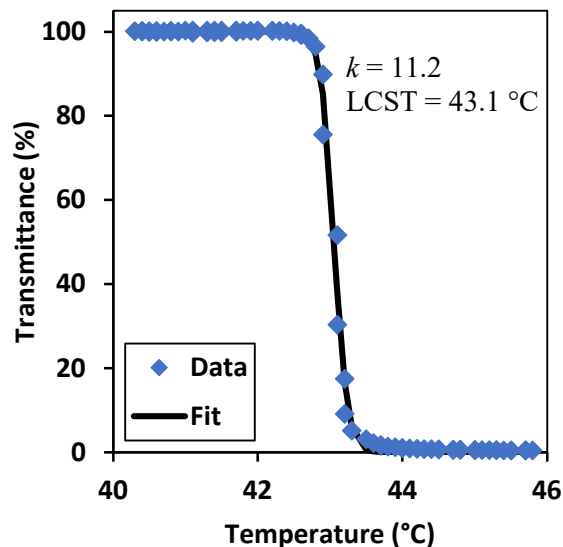
Figure VI-1: Example demonstration for fitting of LCST vs raw data.

6.4.2   Impact of Anion Structure

The role of salt structure in LCST for PDMAEMA has been loosely studied, with a handful of studies demonstrating a dependency on solution ionic strength as well as structure of the anion due to the impact of charge screening and coordination.[5] However, these studies have often narrowed focus to either one specific ion, or convoluted the impact of multiple salts simultaneously. Furthermore, these studies generally do not correct for ionic strength when comparing between individual salts of different valency, further convoluting the underlying interactions observed. In this study, salts are compared at constant ionic strength independent of one another to elucidate the individual role each may have in the LCST phenomenon. However, this approach does come with additional experimental difficulty; as LCST behavior is coupled to both *pH* and ionic strength, small experimental error in either variable will yield a shift in LCST. As such, the error observed in LCST makes distinguishing small shifts (< 1 °C) difficult.

However, the data collected still yield insight to the mechanism of the LCST phenomenon for PDMAEMA. Notably, the results at *pH* 10 follow a general Hoffmeister trend, with LCST increasing in the order of $SO_4 < PO_4 < CH_3COO < Cl$; however, this data is only presented with *n* = 1 as a point of comparison for near-zero protonation. Assuming a similar experimental error of ca. ± 1 °C observed for other experiments, the results for phosphate, acetate, and chloride are all within the expected error. However, the observed LCST of 32.2 °C for sulfate is sufficiently removed from those observed for the remaining salts, suggesting a greater impact. This result is in-line with the typical behavior expected for sulfate, which is known to be strongly salting out of proteins. When PDMAEMA is deprotonated and charge screening effects are negligible, this behavior induces a reduction in LCST, as the overall solvation of the polymer is weakened.

Table VI-1: LCST for PDMAEMA as a function of salt structure and pH at 0.1M total ionic strength.

Salt	pH	LCST (°C)	*k*
Phosphate	10	35	14.5
	9	37.9 ± 0.8	12.5 ± 3.4
	8.5	45.7 ± 0.2	16.3 ± 3.2
	8	58.6 ± 2.6	5.7 ± 4.7
Chloride	10	36.5	16.8
	9	41.7 ± 1.1	10.6 ± 0.6
	8.5	49.6 ± 1.0	7.4 ± 0.4
	8	>70	-
Sulfate	10	32.2	13.8
	9	40.8 ± 0.8	14.6 ± 1.4
	8.5	47.9 ± 0.9	7.1 ± 0.5
	8	>70	-
Acetate	10	35.8	6.8
	9	41.1 ± 0.8	14.4 ± 6.9
	8.5	47.9 ± 0.9	10.5 ± 0.9
	8	>70	-

Interestingly, as *pH* decreases, these data instead demonstrate a lower LCST for phosphate as compared to other salts, with an LCST of 37.9 °C at *pH* 9 and 45.7 °C at *pH* 8.5. LCST for solutions with sulfate, acetate, and chloride meanwhile show no statistical difference from one another at *pH* 8.5, with each showing a measured LCST between 48-49 °C. This shift indicates a suppression of the salting-out effect observed for sulfate at *pH* 10, with electrostatic attraction of the protonated pendant groups of the polymer likely serving to mitigate the impact on water-water stabilization that generally drives the salting-out effect. However, charge neutralization effects alone cannot fully describe the phenomenon for the reduction in LCST for phosphate compared to the other salts. At *pH* 9, phosphate ions should be present as ca. 98% HPO_4^{2-}, whereby electrostatic coordination with positively charged DMAEMA groups would be expected to be similar to that for SO_4^{2-}. This effect is even more pronounced at *pH* 8, where the LCST for all sulfate, chloride, and acetate samples all increase above the instrument limited set point of 70 °C, while phosphate samples yield an LCST of 59 °C. There is also a noticeable shift in *k*, the shape factor for the LCST, with the samples with chloride, sulfate, and acetate each displaying a decrease in *k* – corresponding to a broadening of the LCST transition.

Previous studies have drawn comparisons between phosphate and other salts, attributing the effect to specific ion binding and a corresponding shift in pK_a on the amine species of PDMAEMA;[5] however, the results presented here suggest a simpler explanation. We propose that this phenomenon is an indicator of the temperature dependency of solution *pH*, rather than an ion-specific binding. That is, as temperature increases, the added thermal energy naturally favors the increased dissociation of water into H^+ and OH^-; so long as the PDMAEMA chains are not fully protonated, this shift in equilibrium between the measured *pH* at room temperature and the

equilibrium *pH* at the LCST will shift towards increased protonation of the pendant groups. The overall effect of this is thus to increase LCST in the absence of buffering salts, as the increased protonation from heating shifts towards greater hydrophilicity. This effect is thus small at high *pH*, where the degree of protonation is already small. However, as *pH* approaches the *pKa* of PDMAEMA (ca. 7.5[10]), this effect becomes more pronounced as small shifts in *pH* greatly alter the protonation of the polymer.

6.4.3   Effect of *pH* and Degree of Protonation

To validate this effect, polymer solutions at *pH* 8.5 were heated to 46 °C – the average LCST for phosphate samples - and remeasured for *pH* using a *pH* probe equipped with an automatic temperature compensation probe. Indeed, these solutions demonstrate a measured *pH* of 8.14 for samples with phosphate and 8.07, 8.06, and 8.09 for samples with sulfate, acetate, and chloride respectively, suggesting this buffering effect contributes a slight shift in the available concentration of protons to protonate the PDMAEMA amine groups. Though this shift in *pH* is small calculating the degree of protonation for each solution given the *pKa* of 7.5 yields values α of 81% and 79%, respectively, providing a noticeable enough shift to separate the two in terms of their overall protonation. Indeed, reviewing the established literature for PDMAEMA, prior papers have demonstrated a dependency of LCST on *pH* of ca. 32 °C/*pH* unit, while within the range of 7.7 to 8.1.[5] For the measured *pH* at 46 °C, the difference between the phosphate solution and the remaining salts is on the order of 0.05 *pH* units – on this same scale, this would account for an LCST shift of ca. 2 degrees, which shows good agreement with the LCST shift observed. While this effect is small at lower temperatures, it amplifies as the LCST increases; when solutions are

heated further to 56 °C, the phosphate samples are measured to have pH = 7.93, while chloride, acetate, and sulfate samples have pH = 7.75, 7.76, and 7.78, respectively. Consideration of the buffering capacity for solution upon heating must thus be considered to understand the true final pH of the polymer solution during LCST measurements.

This mechanism is also consistent with observations of prior studies, which have demonstrated a change in LCST with increasing ionic strength for TRIS-HCl buffers but not phosphate buffers, and attribute this finding to the specific binding of DMAEMA to shift the pKa of the amine species. However, phosphate buffers are known to have a relatively stable relationship between pH and temperature, while TRIS buffers demonstrate a much more significant shift in pH with changing temperature, with a 0.05M pH 8 TRIS buffer showing a pH closer to 7.3 at 50 °C.[11] That is, the increased concentration of the TRIS-HCl buffer provides additional buffering capacity to overcome the shift in pH at the increased temperature of the LCST.

These results also highlight the importance of experimental design in considering the effects between differing solutions when comparing LCST across different pH, ionic strength, and salt structures. For the sake of experimental convenience, solutions are generally reported with an initial ionic strength and pH as measured at room temperature. However, this will not be the equilibrium pH at the temperature of the LCST and assigning the LCST dependency in this manner will lead to improper design for materials that are required to operate within in a narrow response window. This effect will naturally amplify in magnitude as the target LCST increases, as evidenced by the observation of LCST > 70 °C for sulfate, chloride, and acetate samples, despite an LCST of 56 °C for phosphate samples at identical ionic strength. Though this effect may be smaller at lower temperatures, it is not negligible.

Furthermore, this highlights a more complex limitation to the current state of the literature, whereby the specific thermodynamic equilibrium of the amine-proton association has generally not been considered for these polymers. By the same token that K_W should be expected to vary with temperature, the pK_a of PDMAEMA should be expected to vary, shifting the equilibrium and true quantity of protonated amine species as the solutions approach the LCST. To the best of our knowledge, the only approach to date for these polymers is to only quantify the LCST as a function of starting pH only, utilizing the observed LCST as a function of this initial pH to interpret the impact of protonation on the system. This approach loses the nuance of the underlying thermodynamic processes and may limit understanding of the overall LCST process for these materials, especially in the context of developing consistent systems for modeling these processes. If the pK_a of the polymer is instead consider rigorously, the protonation should be expected to behave according to the relationship:

$$\frac{dln(K_a[T])}{dT} = \frac{\Delta H}{RT^2}$$

Where:

$$K_a[T] \equiv Association\ constant, as\ f(T)$$

$$\Delta H \equiv Enthalpy\ of\ association/protonation$$

It is also convenient here to define the integrated equation for future use, assuming ΔH is constant within the range of temperature evaluated:

$$\ln(K_{a,2}) - \ln(K_{a,1}) = \frac{\Delta H}{R}\left(\frac{1}{T_1} - \frac{1}{T_2}\right)$$

Rearranging yields two useful forms, for calculating ΔH given known pK_a, as well as pK_a given a known pK_a and ΔH:

$$\log (K_{a,2}) = \log (K_{a,1}) + \log \quad)$$

$$\Delta H = \frac{R \ln \left(\frac{K_{a,2}}{K_{a,1}}\right)}{\left(\frac{1}{T_1} - \frac{1}{T_2}\right)}$$

Proper interpretation of this relationship relies on a well-defined understanding of the enthalpy of the dissociation for the DMAEMA-H+ pair, which has not been established in the literature. However, data for the dependency of pK_a vs temperature has been established for a wide range of similar tertiary amines in the context of CO_2 capture, which can help inform a general estimate.[12] The data presented in this study show a general trend towards increasing ΔH with decreasing pK_a, which may be re-plotted and fit to provide the estimate for PDMAEMA, as shown in Figure VI-2. Note that this is the plot of -ΔH, as the protonation is an exothermic process. Estimating from this fit, the pK_a of 7.5 for PDMAEMA would predict an enthalpy of protonation on the order of -20 kJ/mol.
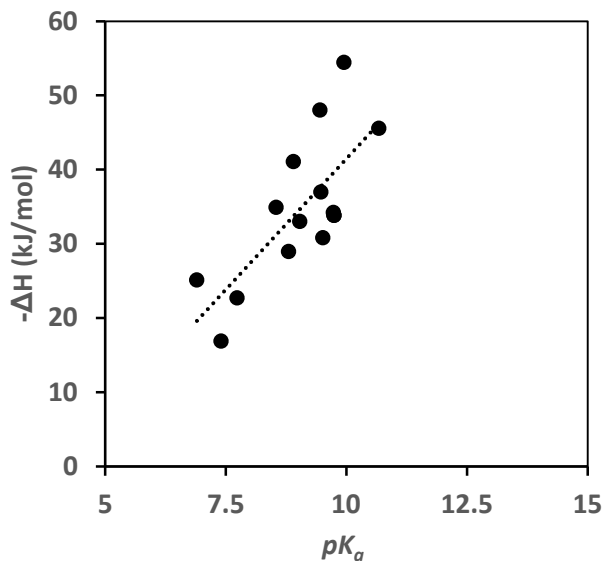
Figure VI-2: Enthalpy of protonation as a function of pKa for tertiary amines, as presented by Rayer et al.[12]

However, this approach still misses the nuance of the underlying thermodynamic equilibrium behavior; the estimation of ΔH from small molecules gives a useful first-pass understanding of the true protonation behavior, but the protonation of the polymer should not be expected to behave identically to a small molecule analog. This is evident in consideration in the shift from a pK_a of 8.5 for monomeric DMAEMA to 7.5 for PDMAEMA, as the electrostatic contribution of neighboring protonated groups and shifts the equilibrium to lower pH for the same degree of protonation.[10] Accounting for this affect is integral to understanding the true protonation behavior of PDMAEMA.

To assess the impact of temperature on pKa for PDMAEMA, a potentiometric titration was conducted at 50 °C for a polymer sample with no added salts, at a concentration of 5 mg mL^{-1}. These conditions were chosen to best match those explored throughout the rest of this study. This

data is presented in Figure VI-3. This titration illustrates a small transition near *pH* 8, corresponding to 4% protonation by molar balance of the added HCl. Notably, this first transition aligns exactly with the reverse LCST transition; above this pH, the polymer solution is fully opaque, but as the pH is reduced through this transition the solution slowly clarifies, with the inflection point marking the point of qualitative translucence where objects on the opposite side of the vial can be observed through the solution. This behavior then signifies the minimum protonation required to disrupt the initial hyper-coiled state of the polymer chains when above the LCST – above this pH, protonation is insufficient to solubilize the pendant amine groups, and the chain collapses to shield the hydrophobic polymer backbone. The exclusion of water from this hyper-coiled state then shifts the protonation equilibrium to a higher *pH*, which is quickly disrupted as the polymer is protonated and the polymer chain extends back into its extended chain configuration. This establishes the true degree of protonation for the LCST at 50 °C, in the absence of added salts. This is in stark contrast to the value that would be predicted assuming the *pK$_a$* and *pH* at room temperature, which would suggest α = 24% at *pH* = 8.
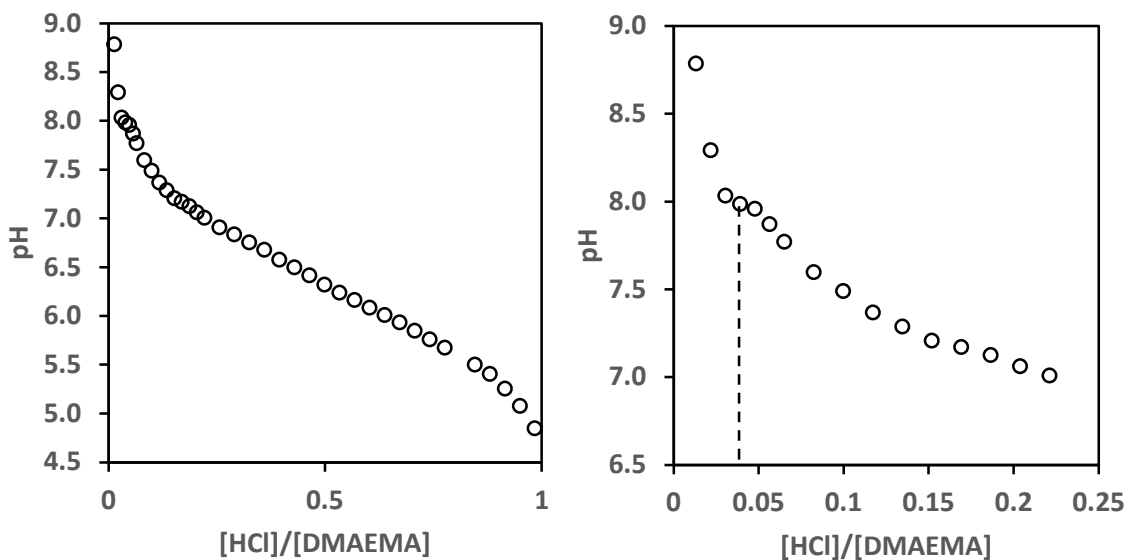
Figure VI-3: Left: Titration for PDMAEMA at T = 50 °C. Right: inset of titration to visualize LCST transition at α = 0.04.
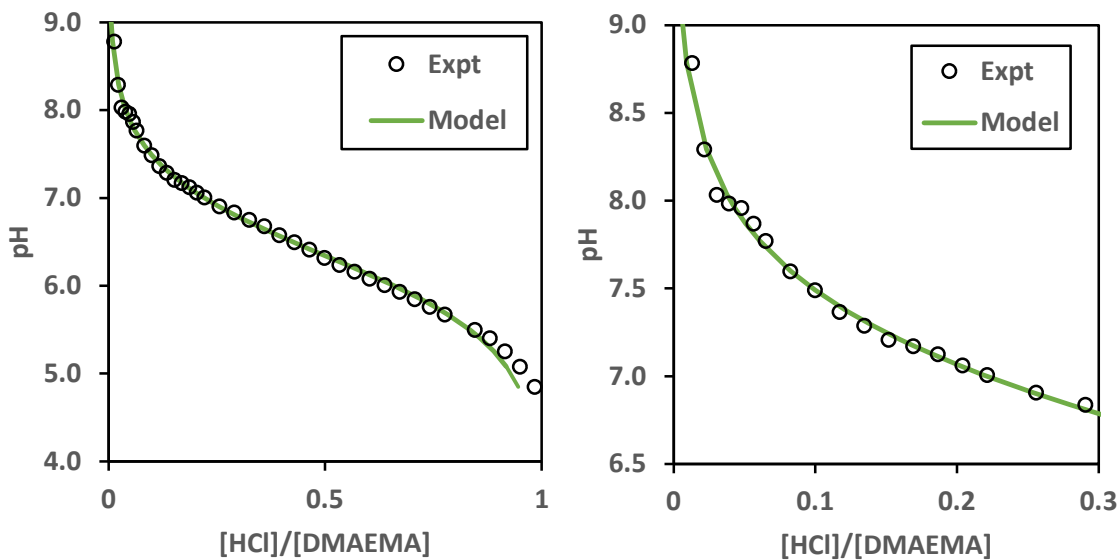

Figure VI-4: Titration curves with model fit, as described by the Hill equation.

It is important here to discuss the determination of pK_a for polyelectrolytes here. Due to the interaction between adjacent pendant groups, the protonation behavior is not perfectly described

133

by the typical Henderson-Hasselbalch equation. Instead, this behavior may be modeled by the modification using the Hill coefficient:[13,14]

$$\alpha = \frac{1}{1 + 10^{n(pKa - pH)}}$$

The value of n represents a correction factor for the impact of competitive or cooperative binding which shifts the protonation behavior relative to pH. This equation was fit to the experimental data, varying n and pK_a to minimize the square error (Figure VI-4), yielding $pK_a = 6.3$, $n = 0.83$. While this model clearly does not capture the full details of the protonation behavior, it does fit the overall trend of the titration well enough to use for establishing the pK_a of the polymer. This shift to $pK_a = 6.3$ is then a substantial decrease from the value of 7.5 at 25 °C; assuming a constant ΔH as outlined above, the corresponding enthalpy may be calculated as:

$$\Delta H = \frac{\ln\left(\frac{10^{-6.3}}{10^{-7.5}}\right) * .008314 \frac{kJ}{mol * K}}{(\frac{1}{298.15K} - \frac{1}{323.15K})} = 89 \; kJ/mol$$

This is a greater than four-fold increase above the loose prediction for a small molecule analog with similar pK_a. Furthermore, using this estimate for ΔH and the measured pH at 46 °C, the degree of protonation at the LCST may be calculated for the pH 8.5, phosphate samples as:

$$pK_a(46°C) = 7.5 - \log\left(\exp\left(\frac{\frac{89kJ}{mol}}{0.008314 \frac{kJ}{mol * K}}\left(\frac{1}{298.15K} - \frac{1}{319.15K}\right)\right)\right) = 6.5$$

$$\alpha = \frac{1}{1 + 10^{0.83(8.14 - 6.5)}} = 4.2\%$$

which is well below the 9% protonation calculated using pH and pK_a at room temperature. Interestingly, this value shows good agreement with the observed degree of protonation at the observed transition from the titration without added salts. When the degree of protonation is calculated for the remaining salts at pH 8.5 and phosphate at pH 8, all four samples converge to same value of 3-4%, suggesting a strong correlation between the different samples studied and this transition, even despite the deviation from the true protonation behavior near the LCST transition. It should be noted that these conditions do all fall close to the temperature of 50 °C used to measure pK_a for the higher temperature, which could impart some bias to this calculation; however, these transitions are measured across a wider range of pH, and the agreement with the sample as measured in the absence of added salts suggest this behavior is integral to the mechanism behind the LCST phenomenon for PDMAEMA.

Table VI-2: Calculated pKa and degree of protonation for measured LCST and pH conditions.

Salt	pH	LCST (°C)	pK_a	pH @ LCST	α (%)
Phosphate	8.5	45.7 ± 0.2	6.5	8.14	4.2
	8	58.6 ± 2.6	6.0	7.63	4.2
Chloride	8.5	49.6 ± 1.0	6.3	8.09	3.2
Sulfate	8.5	47.9 ± 0.9	6.4	8.07	3.9
Acetate	8.5	50.4 ± 0.9	6.4	8.06	4.0

This highlights the heavily connected nature of the pH- and temperature-responsiveness for these polymers; the responsiveness is not either pH or temperature, as both are inextricably linked. These data suggest that the LCST observed at lower pH is not despite the protonation to the polymer – rather, the protonation serves offset the effect of dissociation, requiring a higher

temperature to reach a critical degree of protonation to induce the collapse of the polymer. This "critical protonation," then, would be expected to be a function of overall hydrophobicity; as molecular weight increases and the hydrophobicity of the polymer backbone becomes more dominant, the required protonation to solvate the polymer would increase. This should also be consistent across the more hydrophobic polymers of poly(2-[diethylamino]ethyl methacrylate) and poly(2-[diisopropylamino]ethyl methacrylate), with the greater hydrophobicity of the pendant groups also requiring a higher degree of protonation to remain soluble. Indeed, on a theoretical level this mechanism is also consistent with the observed dependencies on salt content that have been previously described; as the screen effect for various salts alters the electrostatic repulsion between individual pendant groups, their enthalpy of protonation would change accordingly, shifting the resulting pK_a at a given temperature, and the overall protonation as a result. The same consideration extends this effect to molecular weight dependence, as the accumulation of hydrophobicity in longer polymer chains would be expected to increase the necessary protonation to retain the overall solubility of the polymer chain. This trend should be further explored, to establish the consistency across a wider range of pH, temperature, and ionic strength.

6.4.4   LCST Stability – Impact of Storage Conditions

Interestingly, some samples prepared show a separation in observed LCST; this is most notable at pH 8.5 for acetate samples. As shown in Figure VI-5, there is separation into two distinct groups of observed LCSTs, with one centered at 50 °C and the other at 61 °C. Through comparison between the two samples, the only apparent difference was the fit of the cap used to store vials under refrigeration between use, with the samples showing a higher LCST noticed to have worn

down caps that not properly seat to seal the vial during storage. Typical times between storage and use are between one and three days, so this effect arises relatively quickly.
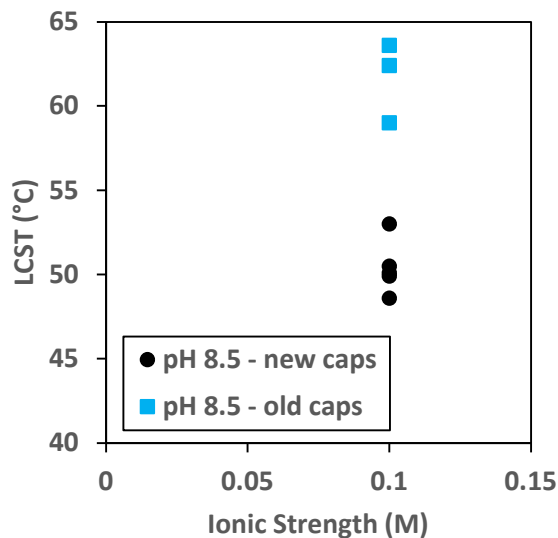

Figure VI-5: Different clustering of LCSTs for samples stored with well-sealing vs. poorly-sealing caps.

The first culprit considered is the hydrolysis of PDMAEMA pendant groups, reducing the content of tertiary amine groups along the polymer backbone. However, NMR validates the retention of pedant groups with high fidelity even after one months in storage, as demonstrated by no change in the apparent height for the peaks at δ = 3.0 and 3.7, which correspond to residual dimethylaminoethanol from monomer degradation prior to purification (Figure VI-6). Any degradation of the polymer pendant groups would then be expected to appear as a relative increase in the height of these peaks. Though generally restricted to conditions near or below *pH* 7, prior studies have demonstrated similar results for PDMAEMA, with little to no hydrolysis observed in solution on the timescale of months, with an estimated hydrolysis rate constant of 10^{-9} s^{-1}.[10,15]

137

These results support this observation at elevated *pH*, indicating hydrolysis is not the cause of this variation.
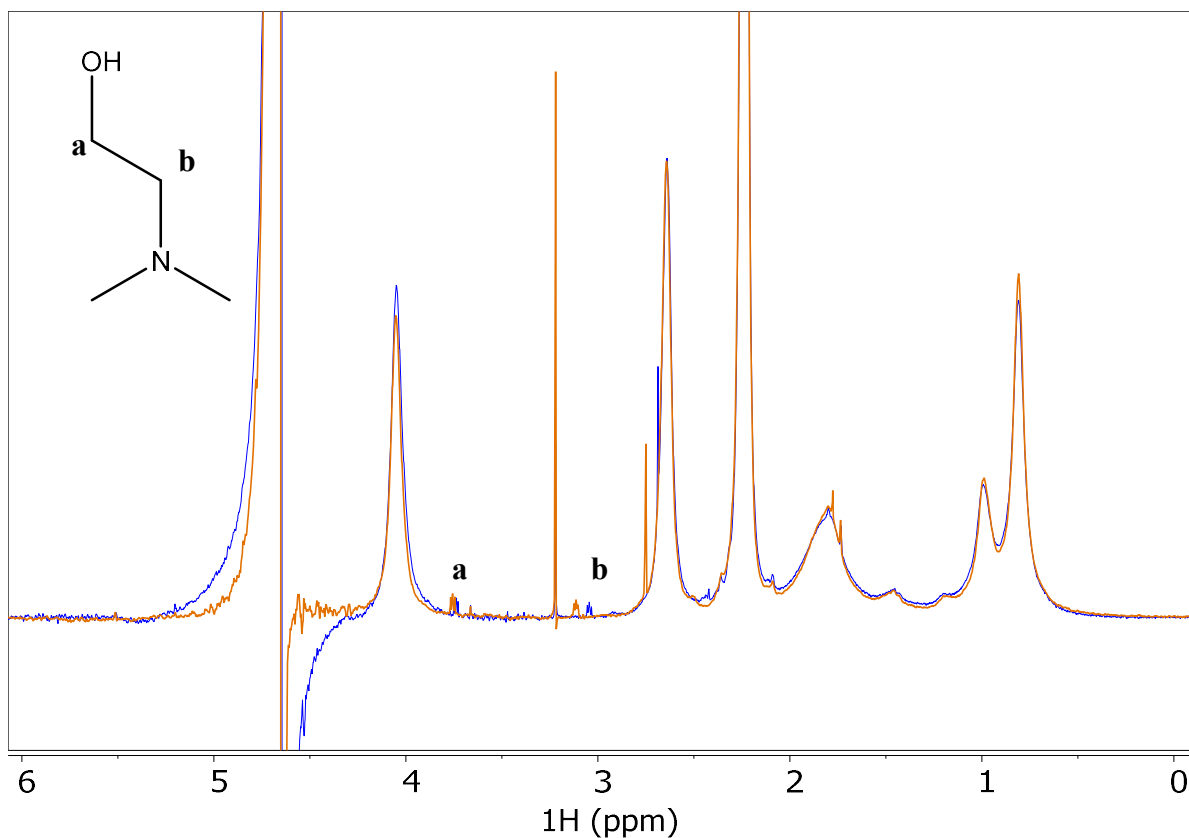

Figure VI-6: NMR spectra for PDMAEMA solution immediately after preparation (blue) and after one month storage under refrigeration (orange).

With further consideration, the most likely culprit is dissolved CO_2. The impact of CO_2 concentration would not be entirely surprising; indeed, PDMAEMA and its copolymers have been previously explored as potential systems for the synthesis of CO_2-responsive polymers, whereby polymer self-assembly or solubility may be modulated by bubbling with CO_2 or N_2 to reversibly shift the polymer behavior. However, this solution behavior is typically attributed to the shift in

solution *pH* upon bubbling with CO_2, with the acidity of the formed carbonate equilibrium leading to a sharp decrease in *pH*.[2] However, little experimentation has been done to decouple the two effects, whereby solution *pH* and CO_2 concentration may independently modulate the LCST behavior of PDMAEMA. Rather, solutions are bubbled with a large excess of CO_2, with *pH* measured before and after bubbling, and the corresponding LCST measured under both conditions. This may miss the nuance of smaller fluctuations in the concentration of CO_2, such as the effects of equilibrium CO2 concentration at varied temperature. This effect is relatively small, but non-negligible; for example, using the published values for the Van 't Hoff dependency of CO_2 solubility of $-\Delta_{sol} H/R = 2400$, the relative difference in CO_2 solubility between 25 °C and 2 °C – the approximate difference between storage at room temperature and storage under refrigeration – is:

$$\frac{H(T_1)}{H(T_2)} = \exp\left(-\frac{\Delta_{sol}H}{R}\left(\frac{1}{T_1} - \frac{1}{T_2}\right)\right) = \exp\left(2400\left(\frac{1}{275.15} - \frac{1}{298.15}\right)\right) = 2.0$$

That is, refrigeration alone leads to a ca. 100% increase in the equilibrium concentration of CO_2. If CO_2 can form more stable complexes with PDMAEMA by coordination of carbonate complexes with the tertiary amine, this may provide a mechanism for the drift observed in LCST during storage for poorly sealing vessels. This effect is not fully understood and should be investigated further.

6.5 Conclusions

The *pH*- and temperature responsiveness of PDMAEMA is assessed as a function of anion content at constant ionic strength, revealing a dependence on the buffering capacity of the salt when *pH* is reduced below 9. However, when the greater impacts of temperature and *pH* are

considered together, rather than separately, there is a clear need to assess the effect of heating on the overall protonation/deprotonation equilibrium for the system. Titration reveals a sharp decrease in pK_a between the previously reported value of 7.5 at 25 °C and a value of 6.3 at 50 °C, corresponding to an enthalpy of protonation of 89 kJ mol^{-1}. Preliminary comparison of the recorded LCST as a function of pH demonstrate that the systems studied provide a clear connection between the LCST and the degree of protonation at the point of transition. This effect should be studied further to expand beyond the narrow set of conditions established here and may represent a means to resolve the impact of a large range of variables to the fundamental thermodynamic processes the mediate the LCST phenomenon.

6.6   References

1.   Zou, H. and Yuan, W., *CO2- and thermo-responsive vesicles: from expansion–contraction transformation to vesicles-micelles transition.* Polymer Chemistry, 2015. **6**(13): p. 2457-2465. DOI: 10.1039/C5PY00024F.
2.   Shieh, Y.-T., Lin, Y.-T., and Cheng, C.-C., *CO2-switchable behavior of chitosan-g-poly[(2-dimethylamino)ethyl methacrylate] as an emulsifier.* Carbohydrate Polymers, 2017. **170**: p. 281-288. DOI: https://doi.org/10.1016/j.carbpol.2017.04.095.
3.   Lee, H., Son, S.H., Sharma, R., and Won, Y.Y., *A discussion of the pH-dependent protonation behaviors of poly(2-(dimethylamino)ethyl methacrylate) (PDMAEMA) and poly(ethylenimine-ran-2-ethyl-2-oxazoline) (P(EI-r-EOz)).* J. Phys. Chem. B, 2011. **115**(5): p. 844-60. DOI: 10.1021/jp109151s.
4.   Razavi, B., Abdollahi, A., Roghani-Mamaqani, H., and Salami-Kalajahi, M., *Light-, temperature-, and pH-responsive micellar assemblies of spiropyran-initiated amphiphilic block copolymers: Kinetics of photochromism, responsiveness, and smart drug delivery.* Mater. Sci. Eng. C Mater. Biol. Appl., 2020. **109**: p. 110524. DOI: 10.1016/j.msec.2019.110524.
5.   de Souza, J.C.P., Naves, A.F., and Florenzano, F.H., *Specific thermoresponsiveness of PMMA-block-PDMAEMA to selected ions and other factors in aqueous solution.* Colloid and Polymer Science, 2012. **290**(13): p. 1285-1291. DOI: 10.1007/s00396-012-2651-9.
6.   Venault, A., Hsu, K.J., Yeh, L.C., Chinnathambi, A., Ho, H.T., and Chang, Y., *Surface charge-bias impact of amine-contained pseudozwitterionic biointerfaces on the human blood compatibility.* Colloids Surf B Biointerfaces, 2017. **151**: p. 372-383. DOI: 10.1016/j.colsurfb.2016.12.040.

7.   Sahnoun, M., Charreyre, M.-T., Veron, L., Delair, T., and D'Agosto, F., *Synthetic and characterization aspects of dimethylaminoethyl methacrylate reversible addition fragmentation chain transfer (RAFT) polymerization.* J. Polym. Sci., Part A: Polym. Chem., 2005. **43**(16): p. 3551-3565. DOI: 10.1002/pola.20813.

8.   Zheng, J.Y., Tan, M.J., Thoniyot, P., and Loh, X.J., *Unusual thermogelling behaviour of poly[2-(dimethylamino)ethyl methacrylate] (PDMAEMA)-based polymers polymerized in bulk.* RSC Advances, 2015. **5**(76): p. 62314-62318. DOI: 10.1039/c5ra12816a.

9.   Mohammadi, M., Salami-Kalajahi, M., Roghani-Mamaqani, H., and Golshan, M., *Effect of molecular weight and polymer concentration on the triple temperature/pH/ionic strength-sensitive behavior of poly(2-(dimethylamino)ethyl methacrylate).* Int. J. Polym. Mater. Polym. Biomater., 2017. **66**(9): p. 455-461. DOI: 10.1080/00914037.2016.1236340.

10.   van de Wetering, P., Zuidam, N.J., van Steenbergen, M.J., van der Houwen, O.A.G.J., Underberg, W.J.M., and Hennink, W.E., *A Mechanistic Study of the Hydrolytic Stability of Poly(2-(dimethylamino)ethyl methacrylate).* Macromolecules, 1998. **31**(23): p. 8063-8068. DOI: 10.1021/ma980689g.

11.   Reineke, K., Mathys, A., and Knorr, D., *Shift of pH-Value During Thermal Treatments in Buffer Solutions and Selected Foods.* International Journal of Food Properties, 2011. **14**(4): p. 870-881. DOI: 10.1080/10942910903456978.

12.   Rayer, A.V., Sumon, K.Z., Jaffari, L., and Henni, A., *Dissociation Constants (pKa) of Tertiary and Cyclic Amines: Structural and Temperature Dependences.* Journal of Chemical & Engineering Data, 2014. **59**(11): p. 3805-3813. DOI: 10.1021/je500680q.

13.   Onufriev, A., Case, D.A., and Ullmann, G.M., *A Novel View of pH Titration in Biomolecules.* Biochemistry, 2001. **40**(12): p. 3413-3419. DOI: 10.1021/bi002740q.

14.   Bodnarchuk, M.S., Doncom, K.E.B., Wright, D.B., Heyes, D.M., Dini, D., and O'Reilly, R.K., *Polyelectrolyte pKa from experiment and molecular dynamics simulation.* RSC Advances, 2017. **7**(32): p. 20007-20014. DOI: 10.1039/C6RA27785C.

15.   Ros, S., Kleinberger, R.M., Burke, N.A.D., Rossi, N.A.A., and Stöver, H.D.H., *Charge-Shifting Polycations with Tunable Rates of Hydrolysis: Effect of Backbone Substituents on Poly[2-(dimethylamino)ethyl acrylates].* Macromolecules, 2018. **51**(15): p. 5752-5761. DOI: 10.1021/acs.macromol.8b00931.

CHAPTER VII: Conclusions and Recommendations

7.1   Aqueous ATRP for the Synthesis of Stimuli-Responsive Polymers

With the conditions explored herein, a versatile and facile method for the synthesis of hydrophilic, stimuli-responsive monomers has been established. Sequential optimization of the ATRP method have generated a method which retains a high degree of control over molecular weight distributions with rapid kinetics (t ≤ 4 hr), high tolerance to oxygen, and high retention of functional end groups for sequential synthesis of block copolymers.   The TPMA-Cu^0 polymerization system demonstrates excellent promise for the implementation across a wide range of polymer systems, including anionic and cationic polymers. The high tolerance to oxygen – eliminating the need for prior degassing altogether, even for the sequential addition of secondary monomers – marks a readily approachable synthetic route without the need for the time-intensive and difficult to scale degassing protocols traditionally called for in ATRP. The versatility of this polymerization scheme for stimuli responsive monomers also presents the potential for synthesis of complex polyelectrolytes, with the high concentration of chloride salt added for the purpose of maintaining a well-defined polymerization also serving to screen charge accumulation between oppositely charged pendant groups, as evidenced by the direct synthesis of AB-type zwitterionic block copolymers. Though this system will not be perfectly optimized for every monomer exchange, the conditions presented here should provide a blueprint that can be readily adapted to optimize the synthesis conditions for a new monomer system.

The exploration of an Me$_6$TREN-Cu^I catalyzed polymerization route shows promise for pushing these reactions towards even faster kinetics but does introduce limitations. Notably, the

accelerated kinetics come at the cost of broadening molecular weight distributions and a greatly decreased tolerance for oxygen. This route may still show promise dependent on the specific design criterion; if the sole driving criterion is the rate of polymerization, the Me6TREN-catalyzed polymerization will yield conversions greater than 90% in one hour, but with limited accessibility to block copolymers or other complex architectures. If high end group fidelity is the key design parameter, the Cu^0-TPMA catalyzed system should be used instead. The Me6TREN is also limited to $pH > 7$, with poor results demonstrated for even mildly acidic pH (ca. 6.5). In general, the TPMA-mediated system is both more robust and more facile across a wide range of monomer types and conditions and should be considered as the primary synthesis route moving forward.

Preliminary results not presented here have also demonstrated successful extension of this polymerization to surface-initiated ATRP, with successful polymerization from the surface of silica-encapsulated magnetic nanoparticles. This successful implementation will be integral to future studies and the design of novel materials to target water remediation and heavy metal removal.

7.2 Phosphate-Containing Hydrogels

To the author's knowledge, the work presented in this dissertation demonstrates the first instance of a successful polymerization for PMOEP into well-defined hydrogels without significant dilution by other monomers. These materials are thus expected to have a high responsiveness to pH, ionic strength, and metal valency. These conditions are present as a proof of concept for exploring these materials with a higher concentration of the responsive moiety than previously described in literature, with several sources citing the direct polymerization of such

hydrogels as untenable due to the high diene content of the monomer. The work presented here has demonstrated that even this worst-case scenario, with crosslinker connect as high as 16 mol%, is achievable in a well-defined hydrogel using ATRP. Though the physical characterization presented herein is limited, the preliminary results from swelling ratio suggest a high porosity even with the high crosslinker content. Using the conditions presented here, these hydrogel formulations may be easily adjusted to include smaller fractions of comonomers to tune the overall mechanical properties and swellability of the hydrogels, utilizing mechanical testing to interrogate the impact of various ionic strength and cation loading to assess the impact at varied ratios of total phosphate. These results then provide the preliminary basis for establishing the further development of these materials, with the next stages of this project currently under design within the group.

7.3 *pH*- and Temperature-Responsiveness of PDMAEMA

The data presented here represent a novel approach to the consideration of the LCST phenomenon in PDMAEMA, by considering the effects of temperature on both the hydrophobic forces balancing the solubility of the polymer backbone and the dissociation of the protonated DMAEMA pendant groups. By characterizing the temperature-dependance of the pK_a for PDMAEMA, the varied LCST at different temperature and *pH* can be resolved to correspond to nearly identical degrees of protonation at the onset of the LCST, suggesting the temperature and *pH* responsive behaviors of these polymers are deeply correlated. To date, this mechanism has only been explored over a narrow range of conditions, and still requires further validation before it can be accepted as the sole driver of the overall LCST process. However, careful consideration

of other underlying variables that have been previously shown to impact LCST suggest this mechanism could still account for these changes, with the "critical protonation" representing the true solubility limit coupled between both temperature and *pH*. Further investigation should be conducted for this system to expand the conditions explored for this system, as well as expanding the range of temperature used for calculating the ΔH component. Expansion to other polymers may also help to validate the impacts of this mechanism, as increasing hydrophobicity of the pendant groups is assessed to determine their critical protonation in relation to the system presented here. Expansion of this system to gain further insight to the underlying thermodynamic process driving this responsive behavior should also provide the necessary understanding to approach these systems with computational models in the future.

APPENDIX A: Equipment Standard Operating Procedures

A.1   Conversion Determination by NMR

Samples for NMR analysis were taken from the same aliquots as prepared for GPC analysis, to minimize the impact of volume reduction on the overall SA_{Cu}/V for the ongoing reactions. This results in a high concentration of non-deuterated water in the NMR samples, necessitating the use of water-suppression to reduce the impact of the H-O-H peaks at $\delta = 4.7$ ppm. The general process is summarized as follows:

1. 100 µL of the polymerization mixture is removed using a clean, gas-tight syringe after flushing with N_2.

2. The 100 µL aliquot is added to a clean, dry 1.5 mL glass vial.

3. 1.4 mL of Type I ultrapure water is added to the sample vial to dilute the total volume to 1.5 mL.

4. 400 µL of this sample is removed using an adjustable 100-1000 µL pipette, and added to a clean, dry NMR tube.

5. 50 µL of D_2O is added to the NMR tubes to bring the total volume to 450 µL (10% D_2O v/v%).

6. NMR tubes are vortexed to homogenize before analysis, and the exterior carefully cleaned with a Kimwipe or other lint-free tissue.

7. The sample for analysis is loaded into the NMR, and the signal lock and gradient shims adjusted according to normal protocols.

8. A standard ^1H spectrum is recorded, with a spectral window of $\delta = 10$ ppm to -2 ppm, 45° pulse, and gain set to zero.

a. Gain must be set to zero for this measurement to avoid detector overflow.

9. The collected spectrum is converted to a WET analysis, using Experiment > Convert Settings > Solvent Suppression > WET.

10. Peak reduction is set at the maximum of the H_2O peak in the ^{1}H spectrum, in general ca. 4.67 ppm.

11. WET pulse shape is set under Acquisition > WET > Make wetshape.

12. Spectra are collected with an acquisition delay of 40 μs, auto-gain enabled, and a minimum of 4 scans.

a. If detector is saturated during acquisition, an error will alert the user. Stop acquisition and reduce gain by 2 dB before restarting. Repeat as needed.

A representative NMR spectrum for PDMAEMA is included in Figure A.1, with integration values included. The alkene signal at $\delta = 6.0$ ppm is used as the basis of integration. Chemical shifts are assigned using previously published values.[1] Conversion is calculated from NMR spectra by comparing the area of the peaks for monomer C=C-H ($\delta = $ 5-6 ppm) to the combined area of the peaks for monomer C=C-CH_3 and polymer -CH_2- ($\delta = $ 1.4-2 ppm). The unreacted monomer shows a split between two coupled alkene peaks, with one pair at $\delta = 6.0$ and 5.6 ppm and one pair at $\delta = 5.5$ and 5.2 ppm. The peaks at $\delta = 6.0$ ppm and 5.5 ppm were chosen as the basis of integration for identifying residual monomer. The region from $\delta = $ 1.4-2 ppm shows two sharp peaks at $\delta = 1.81$ and 1.75 ppm, corresponding to C=C-CH_3 in the unreacted monomer. The remaining broad peaks in this region correspond to the -CH_2- backbone in PDMAEMA. Combining these assignments thus yields two equations:

$$X = \delta_6 + \delta_{5.5}$$

$$3X + 2Y = \delta_{1.4-2}$$

where:

$$X \equiv DMAEMA\ molar\ ratio, monomer\ form$$

$$Y \equiv DMAEMA\ molar\ ratio, polymer\ form$$

$$\delta_n \equiv Area\ of\ peak\ at\ chemical\ shift\ n.$$

Solving and substituting for Y then yields:

$$Y = \frac{\delta_{1.4-2} - 3(\delta_6 + \delta_{5.5})}{2}$$

which may then be used to calculate total conversion as:

$$Conversion = \frac{Y}{X + Y} = \frac{\delta_{1.4-2} - 3(\delta_6 + \delta_{5.5})}{\delta_{1.4-2} - \delta_6 - \delta_{5.5}}$$
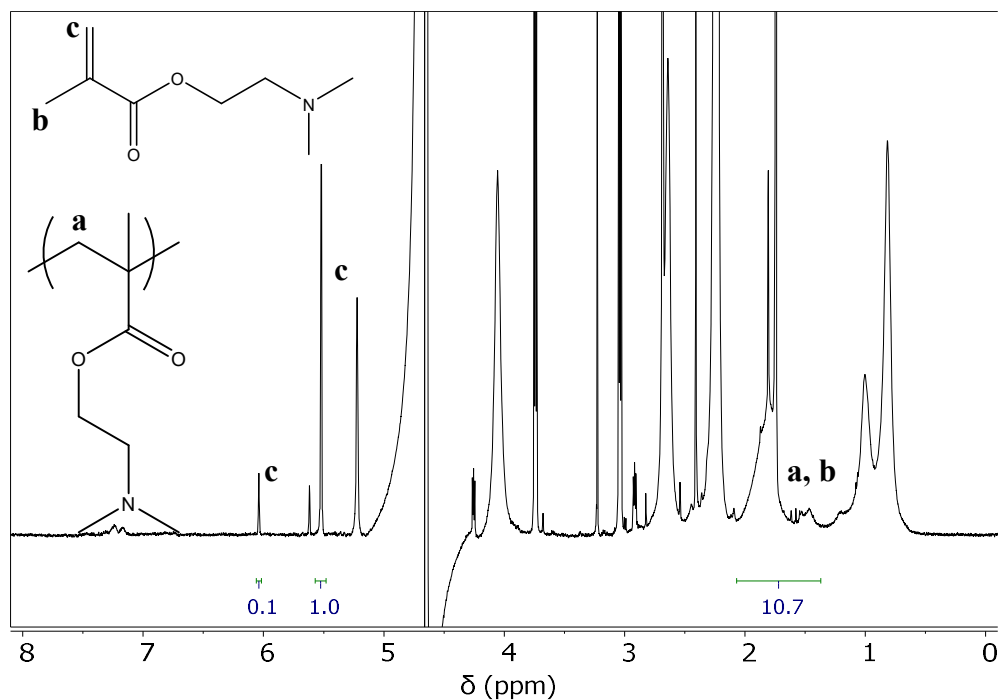
Figure A.1 Representative annotated NMR spectrum for PDMAEMA reaction mixture.

149

This same calculation holds true for both PDEAEMA and PDPAEMA as well, as both monomers
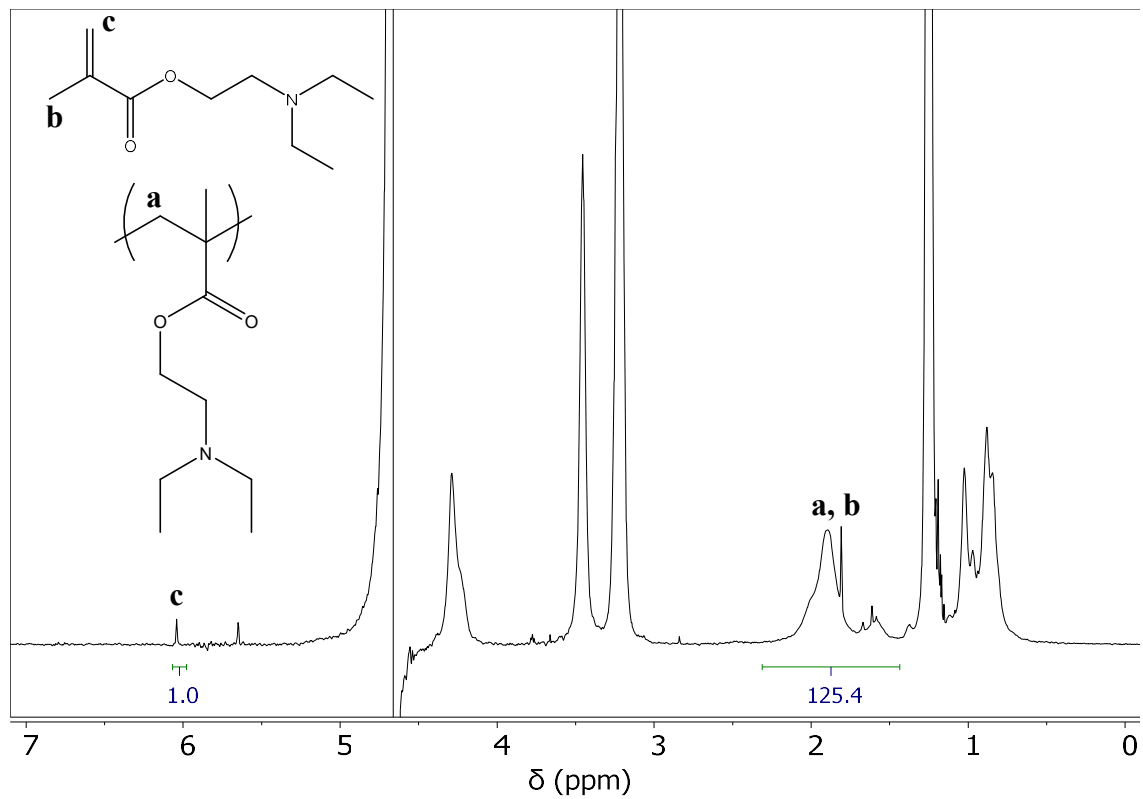
lack any other protons that will overlap with this region.

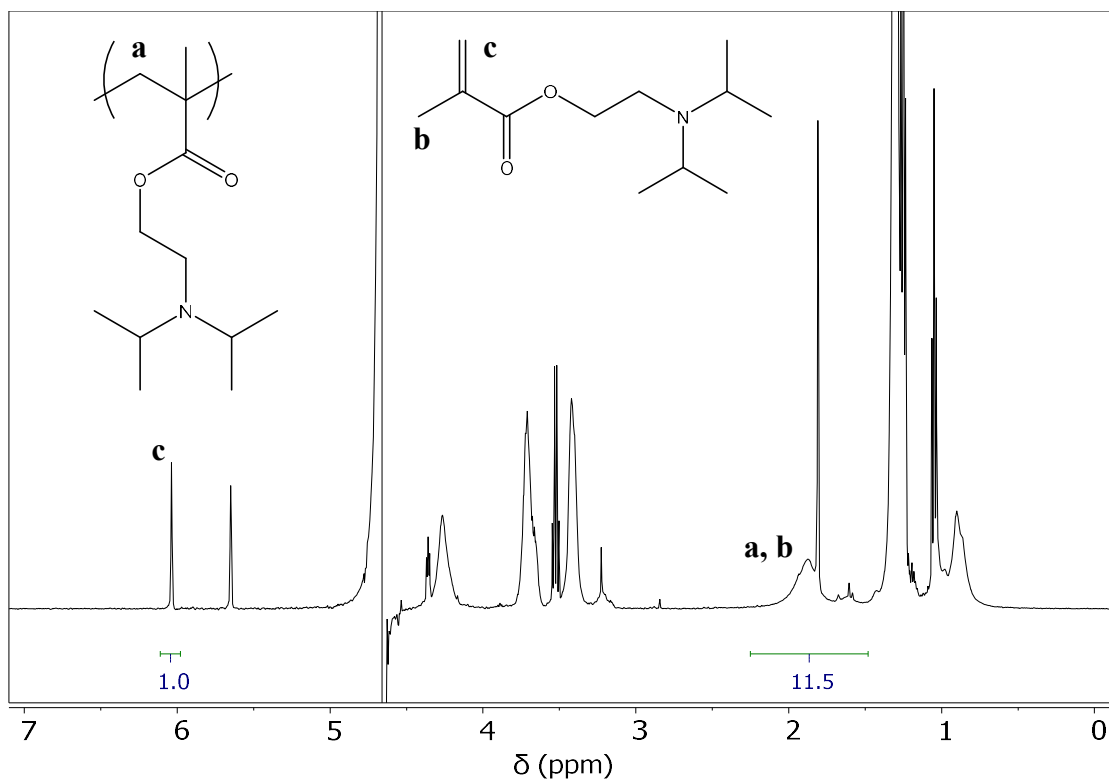**Figure A.2** Representative annotated NMR spectrum for PDEAEMA reaction mixture.

Figure A.3   Representative annotated NMR spectrum for PDPAEMA reaction mixture.

However, for PSPMA the C-CH₂-C of the propyl pendant group appears at $\delta = 2$ ppm, so this signal must be accounted for. This monomer exhibits no visible hydrolysis, as it was only polymerized under acidic conditions. The conversion calculation for PSPMA may then be set up as the series of equations:

$$X = \delta_6$$

$$5X + 4Y = \delta_{1.4-2}$$

where:

$$X \equiv SPMA \; molar \; ratio, monomer \; form$$

$$Y \equiv SPMA \; molar \; ratio, polymer \; form$$

151

Solving this series for Y and substituting as before then yields:

$$Conversion = \frac{Y}{X+Y} = \frac{\delta_{1.4-2} - 5\delta_6}{\delta_{1.4-2} - \delta_6}$$

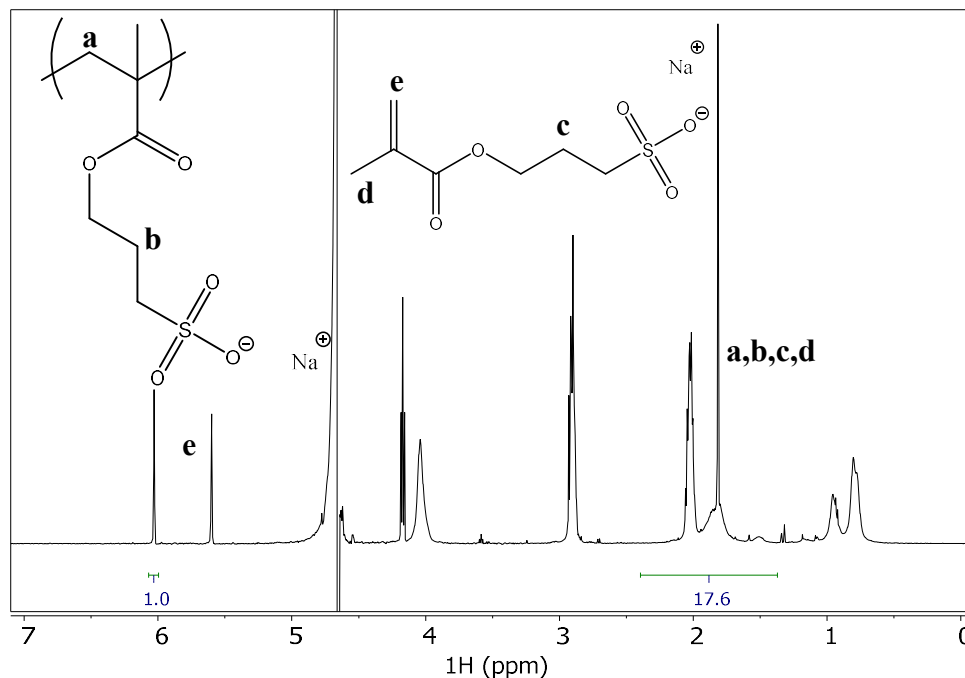**Figure A.4** Representative NMR spectrum for PSPMA reaction mixture.

A.1.2 Error for NMR Calculations

For all systems studied herein, conversion calculations utilize the furthest downfield protons for the alkene integration. This decision is made to account for any signal ablation caused by the water suppression for signals close to the chemical shift of water (ca. 4.7 ppm). A representative spectrum is presented in to demonstrate the potential loss of signal observed close to the suppressed signal. This spectrum corresponds to a polymer with measured conversion of 77% using the signals at $\delta = 6.0$ and 5.5 ppm as outlined above. For the signal at $\delta = 6.0$ ppm – corresponding to the unhydrolyzed monomer – the second proton integrates to 1.0 as expected, suggesting any

effects from signal ablation are negligible at the first decimal point, which is the precision used for all calculations presented in this work. Though the first signal for the hydrolyzed monomer is further upfield at $\delta = 5.5$ ppm, the shift of 0.1 ppm is small enough that reasonable confidence can be placed in this integration. However, comparison to the second signal at $\delta = 5.2$ ppm indicates a clearer loss of signal, with the difference between 9.5 and 8.3 representing a ca. 12% decrease in signal. This sample is presented as one of the worst-case samples observed from the data collected in these studies, as an example to probe potential error from assignment of basis of integration.
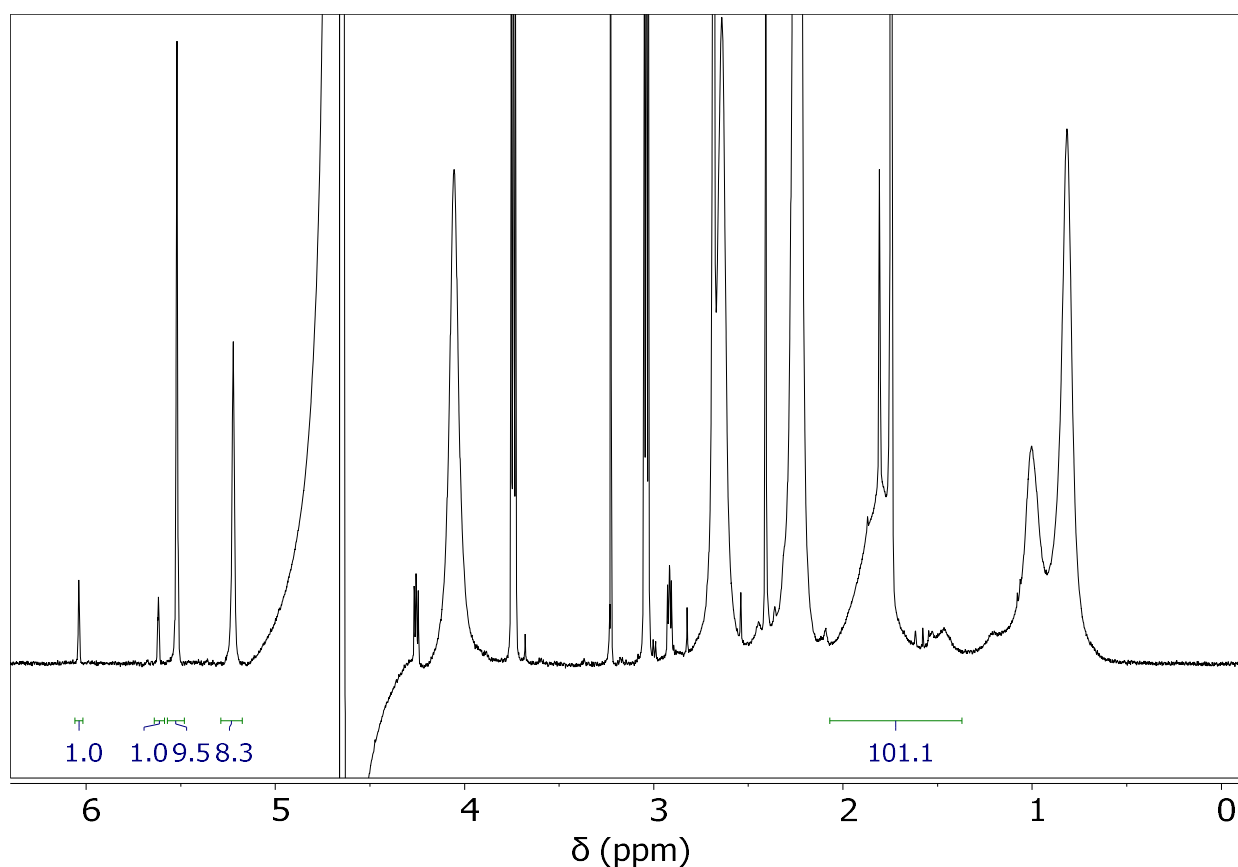

Figure A.5   Representative NMR spectrum for PDMAEMA reaction mixture, with all alkene signals integrated.

If conversion calculations are repeated using the upfield alkene signals (δ = 5.6 and 5.2 ppm, respectively), the resultant conversion is:

$$Conversion = \frac{Y}{X + Y} = \frac{101.1 - 3(1.0 + 8.3)}{106.1 - 1.0 - 8.3} = 80\%$$

as compared to 77% calculated using the method used throughout this work. Similar results if the signal at 5.6 ppm is used as the basis of integration (Figure A.6). This would slightly overpredict conversion, skewing results towards higher I_{eff}.
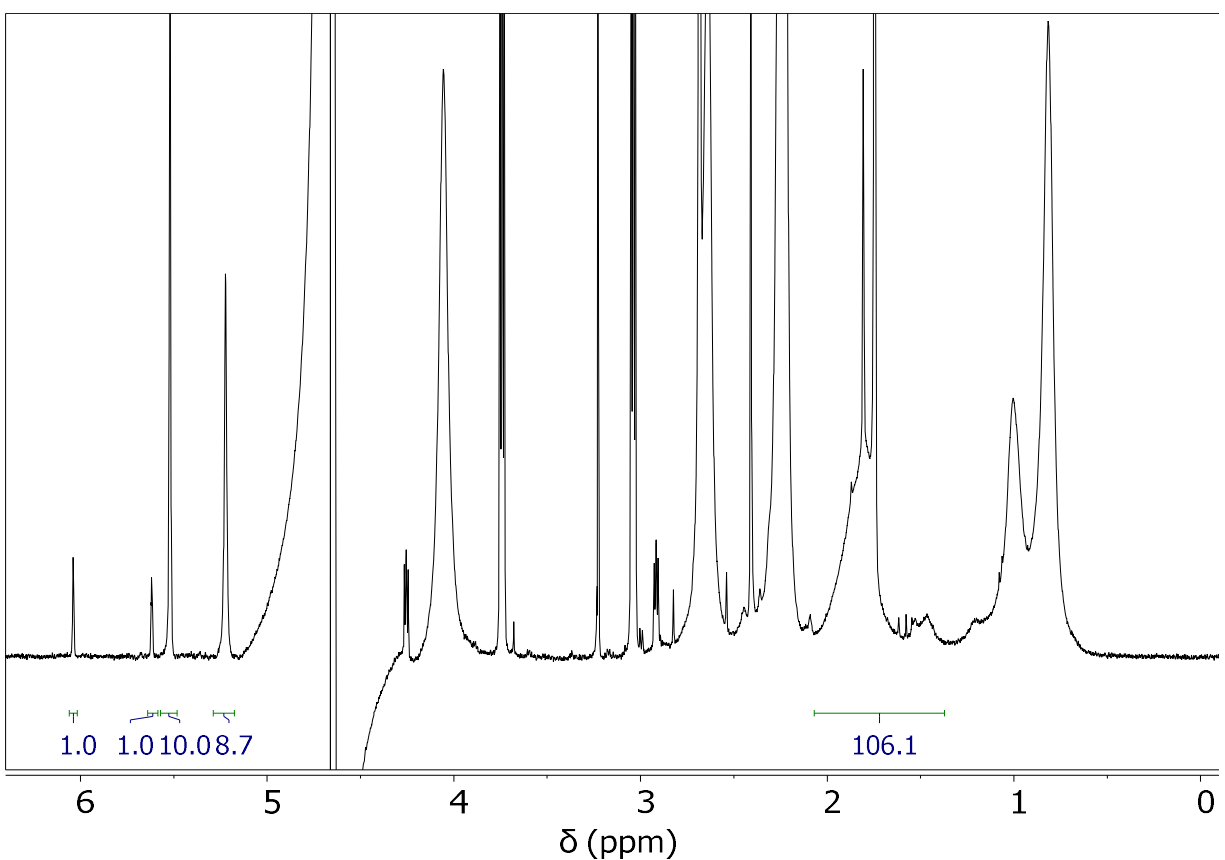

Figure A.6   Representative NMR spectrum for PDMAEMA reaction mixture with δ = 5.6 ppm as basis of integration.

However, it should also be noted that this effect is only important for syntheses at *pH* > 7, where monomer degradation proceeds quickly enough to accumulate considerable fractions of methacrylic acid and dimethylaminoethanol between sampling and NMR analysis. For syntheses under the final optimized conditions at *pH* 4, the hydrolysis is negligible over the time scales of this study, with prior work estimating the rate of monomer hydrolysis between 10^{-8} and 10^{-9} s^{-1} under these conditions.[2] These analyses then present only two distinct alkene peaks at δ = 6.1 and 5.7 ppm, negligible bias between the two alkene peaks. A representative spectrum presented in Figure A.7 and A.8.
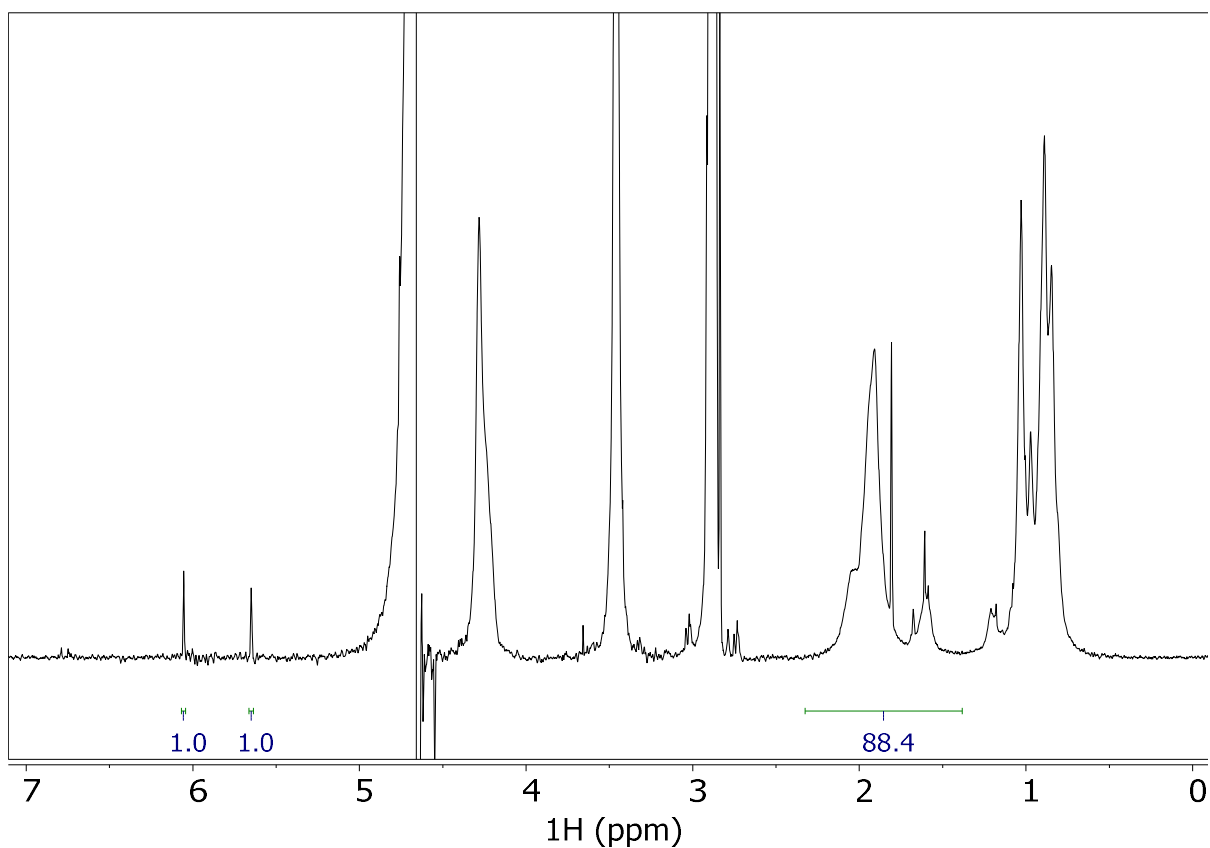

Figure A.7 Representative NMR spectrum for PDMAEMA reaction mixture (*pH* 4). Basis of integration is at δ = 6.1 ppm.
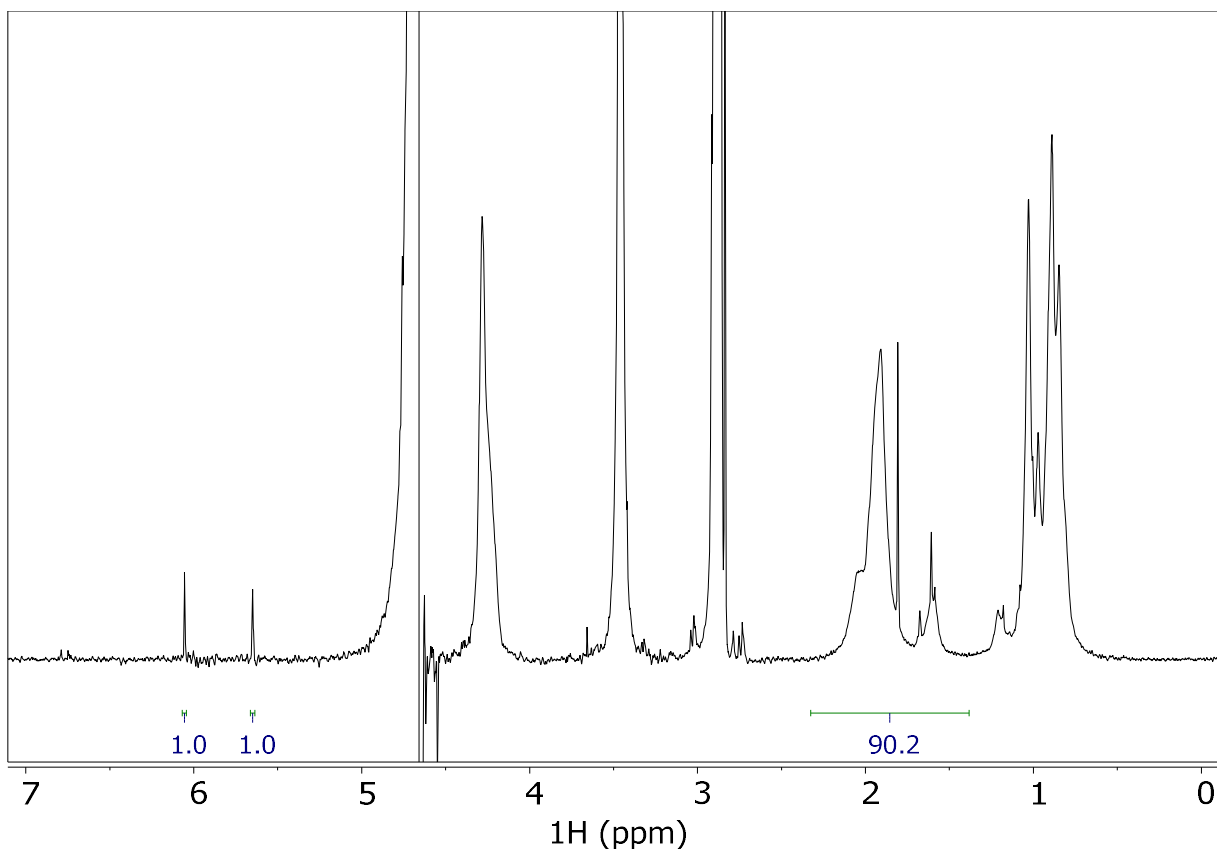
Figure A.8   Representative NMR spectrum for PDMAEMA reaction mixture (*pH* 4). Basis of integration is at δ = 5.7 ppm.

Conversions are then calculated as:

$$Conv_{6.1} = \frac{Y}{X+Y} = \frac{88.4 - 3(1.0)}{88.4 - 1.0} = 98\%$$

$$Conv_{5.7} = \frac{Y}{X+Y} = \frac{90.2 - 3(1.0)}{90.2 - 1.0} = 98\%$$

Indicating a negligible change in the calculated conversion for these systems.

References

1.   Pei, Y. and Lowe, A., *Polymerization-induced self-assembly: Ethanolic RAFT dispersion polymerization of 2-phenylethyl methacrylate.* Polymer Chemistry, 2014. **5**: p. 2342-2351. DOI: 10.1039/c3py01719b.

2.   van de Wetering, P., Zuidam, N.J., van Steenbergen, M.J., van der Houwen, O.A.G.J., Underberg, W.J.M., and Hennink, W.E., *A Mechanistic Study of the Hydrolytic Stability of Poly(2-(dimethylamino)ethyl methacrylate).* Macromolecules, 1998. **31**(23): p. 8063-8068. DOI: 10.1021/ma980689g.

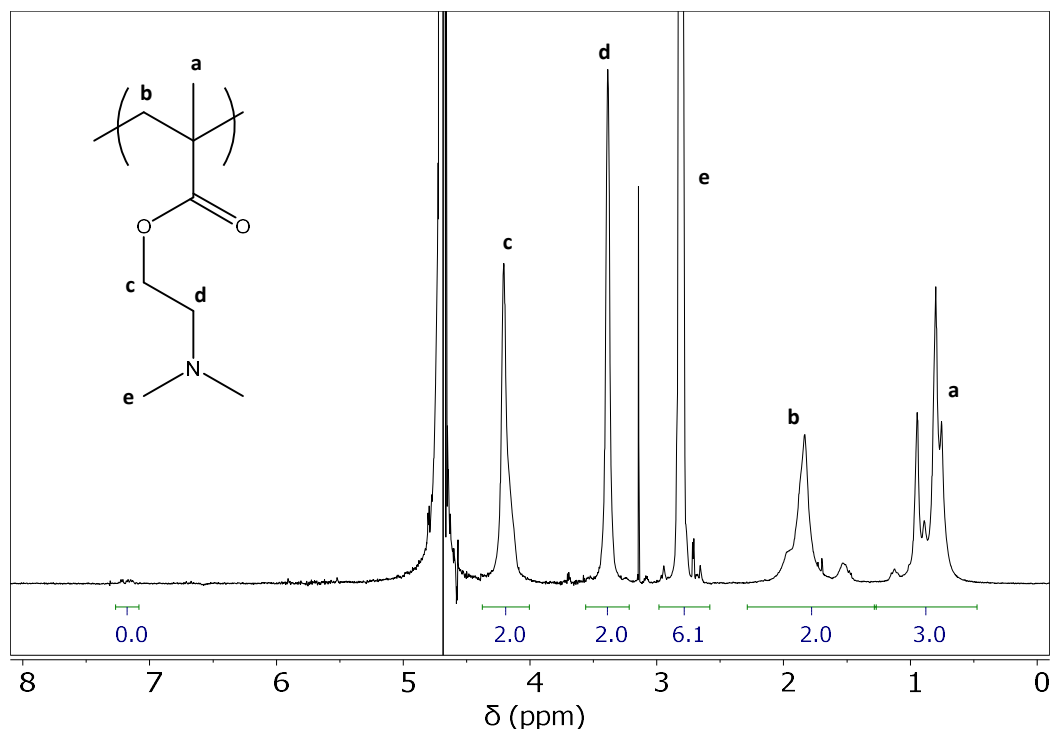## A.2   Pendant Group Retention for PDMAEMA by NMR

Figure A.9   Representative annotated NMR spectrum for PDMAEMA after purification.

Figure A.9 corresponds to a PDMAEMA sample after precipitation by heating the polymer solution above 40 °C. The polymer has been dissolved in 90% H2O-10% D₂O, with one drop of concentrated HCl added to the NMR tube to protonate the tertiary amine pendant groups. This protonation reduces the electron density of the nitrogen, shifting the nitrogen-adjacent species further downfield to improve resolution between groups. All spectra acquisition parameters are identical to those outlined in section A.1. The relative integration between the assigned peaks for C-CH₃:C-CH₂-C:O-CH₂:N-CH₂:N-CH₃ show excellent agreement with the theoretical values of 3:2:2:2:6. These results suggest high retention of the pendant groups, with no significant hydrolysis during polymerization.

158

A.3 Multi-angle Light Scattering and GPC Validation

As the MALS (multi-angle light scattering) detector used for this study is fairly dated, the data displays some noise and system variance especially at low concentrations—near the peak tails or lower molecular weights where scattering intensity is naturally low. To counteract any data artifacts due to low concentrations and improve confidence in the results, MALS data for all the samples in this study were plotted on a single graph, with the outer tails trimmed off to eliminate the low-signal regions of each peak. A polynomial regression was then applied to determine the average line of best fit. A 5$^{\text{th}}$ order polynomial was chosen to capture the tailing behavior observed as the molecular weight approaches the high- and low-resolution limits for this column bank. This true calibration curve is presented in Figure A.10. A PDMAEMA sample of known molecular weight was purchased from Sigma-Aldrich (average M_N 10,000 by NMR end group analysis; $Đ \leq$ 1.4 by GPC) and analyzed to validate the final calibration curve. The validation results using this method for the PDMAEMA 'standard' are presented in Figure A.11. An M_N of 10.7 kDa and $Đ$ of 1.30 were measured, which are in excellent agreement with the technical specifications provided by the vendor for this polymer.
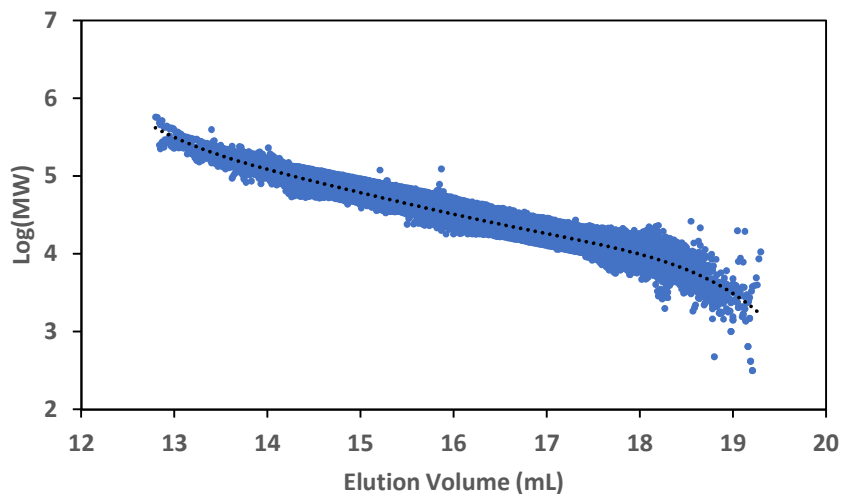
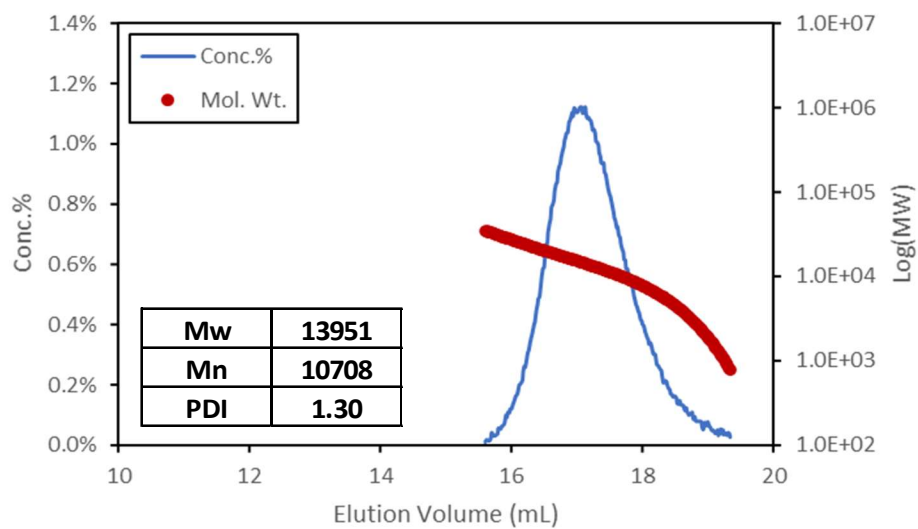**Figure A.10** True GPC calibration curve for PDMAEMA generated from averaged MALS data

Figure A.11 GPC analysis for PDMAEMA 'standard' with vendor-provided MN of 10 kDa and Đ < 1.4.
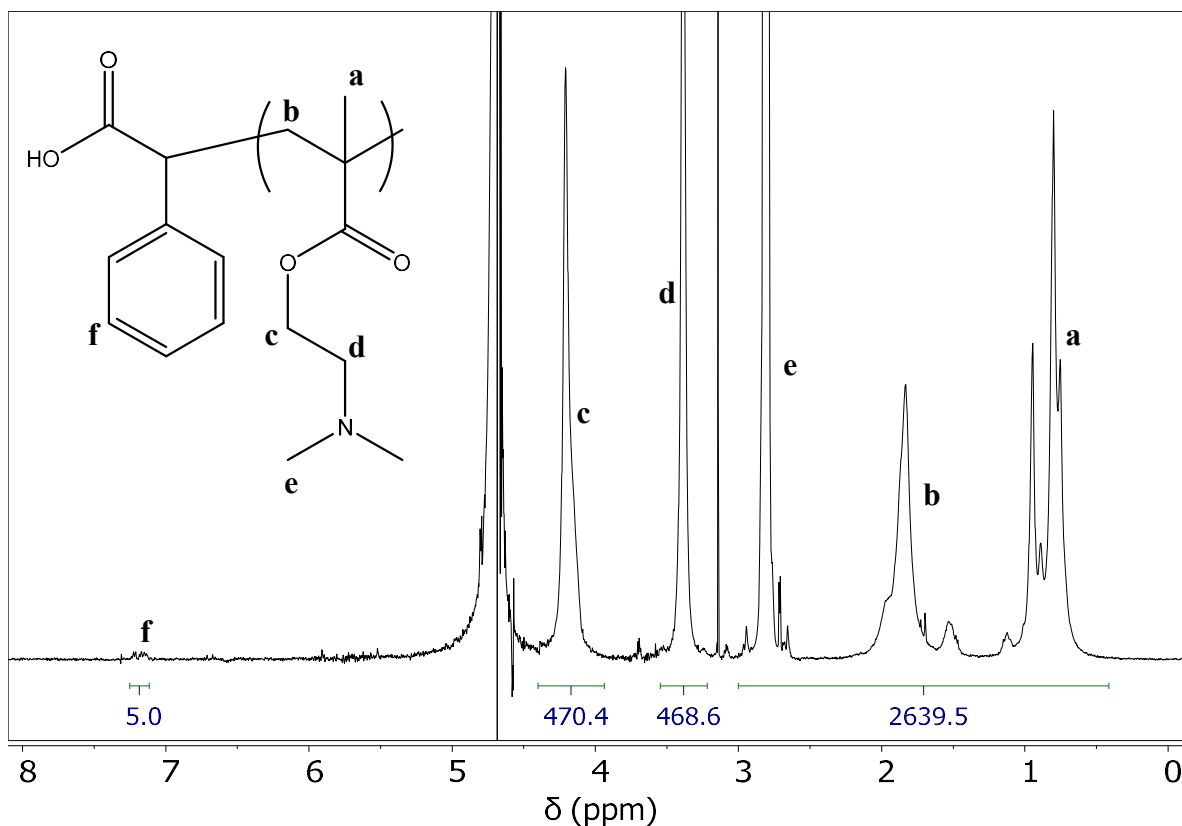
160

Figure A.12 NMR spectrum for PDMAEMA after purification (target D_P = 200).

Further validation was conducted for a polymer sample as synthesized utilizing the optimized

conditions at *pH* 9.6, with a target D_P of 200. This polymer sample was purified by heating above

the LCST for 15 minutes, with the polymer allowed to aggregate and precipitate, and the liquid

phase decanted. Fresh Type I ultrapure water was then added to the solid polymer to redissolve,

and the heating/decanting cycle repeated. The purified polymer was dried *in vacuo* prior to further

analysis. This dried polymer was dissolved at ca. 2 mg mL^{-1} for GPC and NMR analysis. End

group analysis may be conducted for the purified polymer, using the phenyl protons from the

BPAA initiator group as the basis of integration (Figure A.12). With this group set to integrate to

5 protons, the average molecular weight may be calculated as:

$$M_N = \frac{\sum A_{DMAEMA}}{n_{H,DMAEMA}} \times MW_{DMAEMA} = \frac{2639.5 + 468.6 + 470.4}{15} \times 157.21 Da = 37.5 \, kDa$$

GPC analysis was then conducted for this polymer sample, with MWD presented in Figure A.13.

The calculated M_N for this sample is 37.0 kDa, showing excellent agreement with the calculated

M_N from NMR. This data overall suggests excellent agreement between the GPC calibration
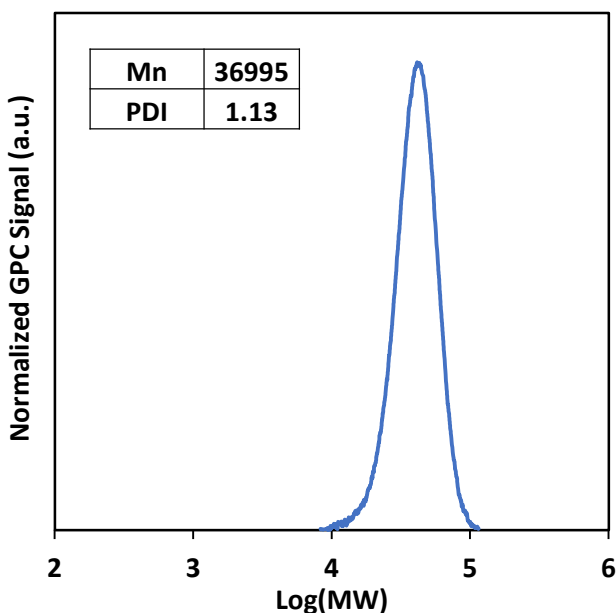
curve and the true molecular weight.

| Mn | 36995 |
| PDI | 1.13 |

Figure A.13 GPC analysis for purified PDMAEMA, MN = 37.5 kDa by NMR end group analysis.

APPENDIX B: Polymerization Protocols

B.1   Procedure for Optimized TPMA & Cu⁰-Mediated ATRP – Native *pH*

The procedure below is outlined as described in Chapter II and III, with stepwise instructions for greater detail. A representative polymerization is conducted as follows:

1. Place immersion cooling coil in water bath, equipped with magnetic stirrer and temperature probe. Ensure that stir bar and temperature probe are not directly underneath the cooling coil to prevent trapping them in ice.

2. Turn on immersion cooler, ensuring no equipment blocks the intake or outtake manifold.

3. Turn on magnetic stir plate, with stirring rate set to ca. 300 RPM.

   a. Bath will take ca. 30 minutes to cool to equilibrium.

4. Measure and cut a length of copper wire at 33 cm.

   a. Assumes wire with $d = 0.014$" – if using a different gauge wire, adjust length to maintain the surface area of copper as ca. 3.75 cm^2.

5. Coil the copper wire around a ballpoint pen, pencil, etc. and add the coiled wire to a clean, dry test tube (test tube A).

6. Add 3 mL of 36% hydrochloric acid and 3 mL of methanol to the test tube containing the copper wire and cap with a rubber septum. Gently swirl or vortex to homogenize.

7. Let the copper wire sit under the acid-methanol mixture for 15-20 minutes to reduce the oxidized surface and breakdown the protective waxy coating.

8. To a clean, dry test tube (test tube B) add:

   a. 31.9 mg α-bromophenylacetic acid (BPAA)

b. 17.2 mg tris(2-pyridylmethyl)amine (TPMA)

c. 405 mg sodium chloride

d. 8.0 mg copper(II) chloride

9. Carefully uncap test tube A and decant the liquid to waste. Be careful to not dump the copper wire into waste!

10. With gloved hands, carefully remove the copper wire and wipe dry with a Kimwipe or other low-contamination fabric.

a. Inspect the surface of the wire for residue of the waxy outer coating or any remaining oxidation. The surface should be reflective throughout; if there are visible portions that are matte or still covered by the waxy coating, repeat the acid-methanol wash.

11. Add 5 mL of Type I ultrapure water to test tube B and cap with a rubber septum.

12. Attach a stainless-steel non-coring needle to the nitrogen manifold (or another inert atmosphere source).

13. Insert the purge needle through the rubber septum in test tube B.

14. Immerse test tube B in the chilled water bath to precool for 5 minutes.

15. Add 2.5 mL of DMAEMA to test tube B and carefully vortex to homogenize.

16. Rinse the reduce copper wire with methanol and dry under a stream of nitrogen.

17. Re-coil the copper wire and add to test tube B, ensuring that the copper is fully submersed in liquid.

18. Replace the rubber septum and lower the nitrogen sparge needle to the bottom of the test tube.

19. Insert a disposable 18-gauge hypodermic needle to begin sparging. Inspect for bubbles and replace the needle if N_2 does not bubble properly.

20. Place the test tube into the chilled water bath. Polymerization will run with an apparent rate constant of ca. 0.8 hr^{-1} with respect to monomer (95% conversion at $t = 4$ hr).

21. To terminate polymerization, uncap the test tube and decant the polymer solution into a clean, dry vial. Do not transfer the copper wire.

a. Rinse the test tube and copper wire with fresh Type I ultrapure water to ensure quantitative transfer.

B.2 Procedure for Optimized TPMA & Cu⁰-Mediated ATRP – *pH* 4

The procedure below is outlined as described in Chapter III, with stepwise instructions for greater detail. A representative polymerization is conducted as follows:

1. Place immersion cooling coil in water bath, equipped with magnetic stirrer and temperature probe. Ensure that stir bar and temperature probe are not directly underneath the cooling coil to prevent trapping them in ice.

2. Turn on immersion cooler, ensuring no equipment blocks the intake or outtake manifold.

3. Turn on magnetic stir plate, with stirring rate set to ca. 300 RPM.

    a. Bath will take ca. 30 minutes to cool to equilibrium.

4. Measure and cut a length of copper wire at 33 cm.

    a. Assumes wire with $d = 0.014$" – if using a different gauge wire, adjust length to maintain the surface area of copper as ca. 3.75 cm^2.

5. Coil the copper wire around a ballpoint pen, pencil, etc. and add the coiled wire to a clean, dry test tube (test tube A).

6. Add 3 mL of 36% hydrochloric acid and 3 mL of methanol to the test tube containing the copper wire and cap with a rubber septum. Gently swirl or vortex to homogenize.

7. Let the copper wire sit under the acid-methanol mixture for 15-20 minutes to reduce the oxidized surface and breakdown the protective waxy coating.

8. To a clean, dry test tube (test tube B) add:

    a. 24.8 mg 2-bromoisobutyric acid (BiBA)

b. 17.2 mg tris(2-pyridylmethyl)amine (TPMA)

c. 405 mg sodium chloride

d. 8.0 mg copper(II) chloride

9. In a clean, dry test tube (test tube C) add:

a. 3 mL Type I ultrapure water

b. 1 mL 36% hydrochloric acid

c. 2.5 mL DMAEMA

10. Vortex or gently agitate test tube C to homogenize.

a. This step will liberate a significant amount of heat – place test tube C in a beaker of room temperature water after mixing to mitigate the heating.

11. Adjust test tube C to pH 4 using 1M HCl and 1M NaOH as necessary, recording the total volume added.

12. Add additional Type I ultrapure water to test tube C as needed to bring the total volume to 7.5 mL.

13. Carefully uncap test tube A and decant the liquid to waste. Be careful to not dump the copper wire into waste!

14. With gloved hands, carefully remove the copper wire and wipe dry with a Kimwipe or other low-contamination fabric.

a. Inspect the surface of the wire for residue of the waxy outer coating or any remaining oxidation. The surface should be reflective throughout; if there are visible portions that are matte or still covered by the waxy coating, repeat the acid-methanol wash.

15. Attach a stainless-steel non-coring needle to the nitrogen manifold (or another inert atmosphere source).

16. Carefully transfer the contents of test tube C to test tube B and vortex to homogenize.

17. Insert the purge needle through the rubber septum in test tube B.

18. Immerse test tube B in the chilled water bath to precool for 5 minutes.

19. Rinse the reduce copper wire with methanol and dry under a stream of nitrogen.

20. Re-coil the copper wire and add to test tube B, ensuring that the copper is fully submersed in liquid.

21. Replace the rubber septum and lower the nitrogen sparge needle to the bottom of the test tube.

22. Insert a disposable 18-gauge hypodermic needle to begin sparging. Inspect for bubbles and replace the needle if N_2 does not bubble properly.

23. Place the test tube into the chilled water bath. Polymerization will run with an apparent rate constant of ca. 1.5 hr^{-1} with respect to monomer (98% conversion at $t = 3$ hr).

24. To terminate polymerization, uncap the test tube and decant the polymer solution into a clean, dry vial. Do not transfer the copper wire.

    a. Rinse the test tube and copper wire with fresh Type I ultrapure water to ensure quantitative transfer.

B.3   Procedure for MOEP Purification

The procedure below is outlined as described in Chapter V, with stepwise instructions for greater detail.

1. To a clean, dry 500 mL round bottom flask add:

   a. 25 mL 2-(methacryloyloxy)ethyl phosphate (MOEP)

   b. 25 mL Type I ultrapure water

   c. 100 mL hexanes

   d. Magnetic stir bar

2. Place the round bottom flask over magnetic stirring for one hour.

3. Pour the contents of the round bottom flask into a separatory funnel.

4. Recover the aqueous phase in the round bottom flask. Discard the organic phase.

5. Rotovap the MOEP-water mixture using house vacuum, without heating, for at least one hour to remove residual hexanes.

The monomer should either be used immediately or stored under refrigeration.

B.4 Procedure for Optimized TPMA & Ascorbic Acid-Mediated ATRP of Phosphate Hydrogels

The procedure below is outlined as described in Chapter V, with stepwise instructions for greater detail. A representative polymerization is conducted as follows:

1. To a clean, dry vial add:

    a. 5 mL 2-(methacryloyloxy)ethyl phosphate (MOEP)-water mixture (see section B.3)

    b. 1.3 mg tris(2-pyridylmethyl)amine (TPMA)

    c. 9.4 mg α-bromophenylacetic acid (BPAA)

    d. 1.0 mg copper(II) bromide

    e. 59.5 mg potassium bromide

2. Gently agitate the vial to homogenize.

3. Add 175 μL of 2M sodium ascorbate solution to the vial and gently agitate to homogenize.

4. Using a glass pipette, transfer the reaction mixture to the clean, dry hydrogel mold.

5. Cover the mold with a clean, dry cover slip or glass slide.

6. Place the mold in a sealable container and purge the container with N_2 before sealing.

    a. The container should be sufficiently large to hold the mold, but as small as possible to limit the maximum amount of oxygen present in the container.

7. Place the sealed container on a 40 °C hotplate for 12 hours to polymerize.

8. After polymerization, use a razor blade or other thin tool to carefully lift the edge of the glass cover slide from the mold. Lift the glass slide straight up to extract the hydrogels.

9. If any gels remain in the mold, carefully bend the mold to separate the hydrogel from the surrounding rubber, and use a small, thin spatula to extract the hydrogel as needed.